Development and implementation of a tumor growth simulation tool

Sofie Eikemo Tjensvold

Master thesis in Applied and Computational Mathematics,
Institute of Mathematics,
University of Bergen,
Spring 2023

Abstract

This thesis presents the development and analysis of a mathematical model for avascular tumor growth. The model considers the influence of externally supplied nutrients as growth-promoting factors, growth-inhibiting factors produced by tumor cells during the cell cycle or excreted by necrotic cells, and growth-inhibiting factors produced by the surrounding tissue as a result of the immune system's response to the tumor. The concentrations of these factors are modeled using advection-diffusion partial differential equations. The mathematical model is implemented using forward Euler, backward Euler, and Finite Element methods for discretization. The FEniCS library has been used with respect to the Finite Element method during the implementation. Furthermore, the implementation shows that the mathematical model is in alignment with known tumor evolution. Examinations of various model parameters are conducted, revealing their impact on avascular tumor growth. The examinations showed that alterations in parameters related to nutrients and the internally produced/excreted growth-inhibiting factors had the most significant impact on tumor development. Therefore, it is crucial that these parameters are set to biologically accurate magnitudes to ensure that the simulated tumor development and patterns are qualitatively correct. Additionally, the strong dependency on these parameters suggests that drugs targeting and influencing these parameters have the potential to inhibit tumor growth. Additionally, it was observed that modifications of parameters related to the internally generated or the externally supplied growth-inhibiting factors could significantly alter where quiescent regions formed, and thus result in completely different growth patterns. Furthermore, altering the proportion constituted by the extracellular matrix within the tumor was also observed to significantly influence tumor evolution. Moreover, these findings highlight the potential benefits of developing more detailed models that comprehensively analyze the influence of these parameters. Such models could contribute to the development of experimental approaches and enhance our understanding of tumor evolution.

Acknowledgements

I would like to thank my supervisors Florin Adrian Radu and Erlend Storvik for their guidance and help. I am grateful for everything you have taught me these past years! I am especially grateful for you Florin for always making the time for a "quick question", and to you Erlend for always being just a short zoom-call away whenever I had any coding-related questions.

I would also like to thank my family and friends for always cheering on me. Your support means a lot to me, and it has made it easier to stay motivated throughout this year.

Contents

List of Figures

List of Tables

List of symbols

Symbol	Explanation
sc	Length scaling parameter (e.g., from cm to mm).
T	Time scaling parameter (e.g., from minutes to seconds).
h	Element size.
k	Time step.
n_0	Initial number of cells.
n_{loc}	Number of cells per unit volume.
r_c	Radius of a single cell.
u_N	Nutrient concentration.
u_{G1}	G1 concentration.
u_{G2}	G2 concentration.
$u_{N,0}$	Initial nutrient concentration.
$u_{G1,0}$	Initial G1 concentration.
$u_{G2,0}$	Initial G2 concentration.
D_N	Nutrient diffusion coefficient.
D_{G2}	G2 diffusion coefficient.
D_{G1}	G1 diffusion coefficient.
$\vec{c}_N$	Nutrient velocity field.
$\vec{c}_{G2}$	G2 velocity field.
α_{pro}	Rate of consumption of nutrients in proliferating regions.
α_{qui}	Rate of consumption of nutrients in quiescent regions.
α_{nec}	Rate of consumption of nutrients in necrotic regions.
γ_{proqui}	Rate of consumption of G1 in proliferating and quiescent regions.
γ_{nec}	Rate of consumption of G1 in necrotic regions.
S	Production/excretion of G1.
λ	Parameter scaling the production/excretion of G1.
ξ_{proqui}	Rate of consumption of G2 in proliferating and quiescent regions.
ξ_{nec}	Rate of consumption of G2 in necrotic regions.
κ	Constant supply of nutrients at the boundary.
ψ	Constant supply of G2 at the boundary.
p_{extrm}	Percentage of the tumor volume the extracellular matrix constitute.
m	Mitotic function.
η	Parameter determining the contribution of nutrients to growth.
ν_1	Parameter determining the contribution of G1 to growth.
ν_2	Parameter determining the contribution of G2 to growth.
ρ	Parameter scaling the mitotic value.
θ_N	Nutrient threshold.
θ_G	Growth-inhibitor threshold.
Ω	Domain.
Ω_{pro}	Part of the domain only consisting of proliferating cells.

Introduction

Cancer is a leading cause of death worldwide, with 19.3 million new cases and 9.9 million deaths registered in 2020. It is estimated that by 2040, the number of new cases will increase to approximately 28.9 million, with 16.2 million deaths [1]. Consequently, cancer research is of great importance, as it has the potential to improve existing treatments and hopefully find a cure. There are many types of cancer, and understanding the factors that affect their growth and spreading is complex and comprehensive, making it challenging to gain full overview of the disease.

How can mathematics help with understanding and treating tumors? Developing a mathematical model involves writing a system of equations that describes the dynamics of the tumor and all the factors enabling and preventing its growth. By solving such a model, it is possible to study in detail how a specific factor influences the spatial and temporal behavior of tumor growth. In other words, mathematical models of tumor growth have the potential to be highly useful in cancer research, providing qualitative answers that can be used as guidelines for new experiments, such as indicating what injection rates and injection locations to try.

There are several stages of tumor growth before a tumor becomes large enough to reduce a patients quality of life or cause death. The two main stages are the avascular and vascular phases [2]. An avascular tumor refers to a stage in tumor development where the tumor lacks its own blood supply, particularly before the process of angiogenesis occurs. Angiogenesis is the formation of new blood vessels that supply nutrients and oxygen to the growing tumor [3]. In the early stages of tumor formation, i.e., the avascular phase, it relies on diffusion of nutrients and oxygen from the surrounding tissues to sustain its growth [4]. On the other hand, a vascular tumor is a tumor in which angiogenesis has occurred, meaning that the tumor is connected to the vascular system and has its own blood supply. This allows the tumor to metastasize, i.e., spread, to other parts of the body through the vascular system [2].

In a 1966 paper [5], Burton presented a mathematical model proposing that nutrient consumption could limit tumor growth. The model had the ability to calculate the radius of the tumor's central zone, and the growth curve generated by the model exhibited a good fit with a widely recognized mathematical function called the Gompertzian function [6]. Thereafter, in 1972, Greenspan [7], introduced the first tumor growth model that incorporated distinct layers of proliferative, quiescent, and necrotic cells. The model accounted for the regulation of these cells by mitotic inhibitors and necrotic decomposition. Additionally, the model considered cell adhesion of living cells [6]. Subsequent models introduced various levels of complexity regarding cell movement. Some models assumed convective movement of cells [8, 9, 10, 11, 12],

while others incorporated active diffusion [13, 14, 15, 16, 17] or diffusive/chemotactic behavior [18, 10, 13]. Earlier models primarily considered tumor cell proliferation and death to be influenced by a single generic nutrient. However, more recent models have taken into account additional factors such as growth-inhibiting factors and adhesion forces that can influence cell proliferation and death [2, 19, 20, 21, 22].

This thesis aims to present a model that describes the growth of avascular tumors. The avascular stage is crucial in tumor development as it sets the foundation for subsequent stages. Therefore, studying avascular tumor growth is essential for understanding the early dynamics of tumor formation and identifying factors that contribute to tumor progression. Moreover, avascular tumor growth models offers a significant advantage in terms of mathematical modeling simplicity when compared to vascular tumor growth models, while still encompassing numerous phenomena that need to be addressed in a comprehensive model of vascular tumor growth. Additionally, it is well known that the growth kinetics of spherical *in vitro* tumors are very similar to those of avascular *in vivo* tumors [2]. Consequently, due to the ease and reproducibility of avascular tumors *in vitro*, the quality and accuracy of experiments of avascular tumors exceeds that of vascular tumors.

In the thesis we will explain the development of the mathematical avascular tumor growth model and its assumptions in detail. In contrast to most avascular tumor growth models, this model includes growth-inhibiting factors that are produced both within the tumor and externally supplied through the tumor boundary. Moreover, we will implement the model and perform a sensitivity analysis to ensure that it behaves in accordance with known tumor growth patterns and to explore the impact of various factors on growth.

Outline

Chapter 1 provides the reader with an exposition of the background material upon which the development and implementation of the mathematical model is built. Specifically, Section 1.1 provides information on what a tumor is and the factors that influence its growth. Additionally, the concept of modeling tumor growth is explained in detail. Furthermore, in Section 1.2, the numerical methods used in the implementation will be described, along with derivations and results regarding the accuracy of the methods. Additionally, in Section 1.3, a finite element library named FEniCS [23], which has been used in the implementation, will be explained.

Chapter 2 is dedicated to the mathematical model. In Section 2.1, the mathematical model will be derived, and all the underlying assumptions will be stated and explained. Additionally, there will be a discussion about the expected behavior of the model from a mathematical perspective. Furthermore, in Section 2.2, the model will be discretized. Then, in Section 2.3, the structure of the implementation will be explained, along with a flow chart depicting the main steps of the implementation.

Chapter 3 presents the numerical results obtained from the implementation of the mathematical model, which will be discussed in detail. In Section 3.1 a reference case will be stated,

and numerical results with respect to that case will be displayed. Moreover, in Section 3.2, a sensitivity analysis of the model will be conducted to ensure that it behaves as expected both mathematically and in accordance with known tumor evolution patterns.

Chapter 4 provides a summary of the results and a discussion on their implications for avascular tumor growth. It explores the findings in terms of their qualitative aspects and highlights areas that would be intriguing for future research.

Chapter 5 introduces an extension model that builds upon the model presented and analyzed in the thesis. The chapter describes the development of the extension model, which aims to further investigate and explore certain aspects related to the original model.

Chapter 1

Basic theory & background material

1.1 Tumors

Cancer is a complex and devastating disease that affects millions of people worldwide. Understanding the dynamics of tumor growth is essential for the development of effective treatments. Mathematical models have become an essential tool for studying tumor growth and have the potential to provide valuable insights into the spatial and temporal behavior of cancer. By developing mathematical models, it is possible to study how different factors, such as cell proliferation rates and nutrient diffusion, affect tumor growth.

1.1.1 What is a tumor and what are the main factors of tumor growth?

A tumor is an abnormal mass of tissue that develops due to a malfunction in the process of cell division. In such instances, damaged or abnormal cells exhibit accelerated duplication compared to normal cells, and may also evade programmed cell death. Tumors can be classified as either malignant, commonly referred to as cancerous, or benign, non-cancerous [24][25]. The determination of whether a tumor is cancerous or benign hinges on its potential to spread, metastasize, to other regions of the body.

During the initial stages of tumor development, referred to as the avascular phase, there is no connection between the tumor and the vascular system, specifically the blood vessels. Tumors that remain in this avascular phase are typically benign. However, when tumors establish connections with the vascular system, transitioning into the vascular phase, they become cancerous tumors [25]. This connection to the circulatory system enables the transportation of cancer cells through the vessels to distant parts of the body, where they can give rise to secondary tumors [25].

The following questions naturally arise: What factors contribute to tumor growth? How can we determine if a tumor will be benign or cancerous? These questions are highly complex, and even oncologists do not have definitive answers to them. However, extensive research indicates that nutrient supply and the concentration of growth-inhibitor factors (GIFs) play a crucial role [2, 4, 26, 27, 28]. GIFs are produced by cells during the cell cycle, and the

immune system also produces them in response to tumors [19, 7]. Furthermore, studies have demonstrated that adhesive forces between cells and between cells and the extracellular matrix (referring to all fluids, molecules, etc., surrounding the cells) significantly influence the tumor's ability to maintain its shape and promote growth [20, 21, 22].

1.1.2 Mathematical modeling of tumor growth

To model tumor growth mathematically means to develop a system of equations that describes the physical processes within the tumor, such as proliferation rate and nutrient supply. However, tumor growth is an exceedingly complex phenomenon. It relies on a combination of biological, chemical, and mechanical factors, all of which contribute to its evolving structure [29]. Describing this complexity with equations would result in a massive system, posing significant mathematical challenges in terms of ensuring well-posedness (the existence of a unique and stable solution) and in terms of solving the system effectively. Moreover, incorporating additional phenomena into the model, which requires introducing more equations, also necessitates knowledge of a greater number of physical parameters [29]. Mathematicians rely on the expertise of oncologists to ensure the reasonableness of the chosen parameters. Consequently, the development of better tumor models necessitates enhanced collaboration between mathematicians and oncologists, among other things.

Because of the aforementioned reasons, mathematical models of tumor growth are often much simpler than the *in vivo* tumor growth they represent. Nevertheless, if the models are not overly simplistic, they can still provide valuable qualitative insights. For instance, mathematical modeling can help streamline and optimize experiments [29].

Before constructing the mathematical model we have to decide what type of model it should be. Should it be a continuous or discrete model? Maybe a combination? Moreover, are we sure that the physical parameters are accurate, meaning we can represent them deterministically or should they be represented as stochastic variables, allowing some uncertainty?

Cells exist as discrete entities, suggesting the suitability of a discrete model. However, it is important to note that all cells are immersed in liquids, indicating a continuum phase. Does this imply the need for a continuous model? Furthermore, the cell cycle encompasses stochastic components [29]. To what extent does this randomness impact the overall processes, and would it no longer be sensible to formulate a deterministic model?

Determining a suitable model type is evidently a complex process that heavily relies on the specific problem and desired objectives. For instance, when dealing with a tumor consisting of relatively few cells, a discrete model would be the natural choice. On the other hand, a continuous model with local average values would not be appropriate in this scenario, as the averaged values are derived from data from a relatively small number of cells [29].

As mentioned, mathematical modeling of tumors is mainly divided into discrete and continuous models. Hence, let us take a closer look at what they entail. In the discrete case,

one focuses on individual cells, meaning that one describes single-cell-scale phenomena. This includes describing its position in the cell cycle, its interaction with neighbouring cells and the local biochemical environment, etc. [4]. Then upscaling techniques such as cellular automata and lattice Boltzmann methods are used to obtain information about the large-scale phenomena of tumor growth. In all of the main upscaling approaches, the state of a cell is characterized by a vector $\mathbf{w} = [\mathbf{x}, \mathbf{v}, \mathbf{u}]$, where $\mathbf{x}$ is the position of the cell, $\mathbf{v}$ is the velocity and $\mathbf{u}$ is a vector describing its internal biological state [4].

In continuous models, often the initial shape of the tumor is assumed to be spherical or disk-shaped. The cells are represented through cell densities, meaning that the cells are described in an averaging sense. In most continuum models of avascular tumors, it is assumed that tumor growth is affected by available nutrients and growth-inhibitor factors (GIFs). This is modelled by conservation equations $\frac{\partial C_i}{\partial t} + \nabla \cdot \mathbf{N}_i = P_i$, where C_i denotes the concentration of the i-th species, $\mathbf{N}_i$ denotes the flux of the species inside the spherical tumor and P_i denotes the net rate of consumption/production of the species both by the tumor cells and due to chemical reactions with other species [4]. In some papers with continuous models, the main focus has been on how cell-cell and cell-matrix adhesion forces affect tumor growth [20, 21, 22].

1.2 Numerical methods for solving differential equations

Many differential equations cannot be solved analytically, meaning it is not possible (at least not yet) to solve them using known mathematical rules such as addition, subtraction, associativity, commutativity, etc. Therefore, one has to approximate the solutions using numerical methods. Since the mid-20th century, numerical analysis has been an active research field. The field entails everything from creating methods, analyzing and understanding them, to actually implementing them [30].

The numerical methods used in this thesis are Forward Euler to approximate ordinary differential equations, Backward Euler to approximated time derivatives in partial differential equations, and the Finite Element Method, abbreviated FEM, to discretize the resulting time independent set of equations with respect to space.

1.2.1 Forward Euler

Forward Euler is one of the simplest numerical methods for solving initial value problems, IVPs. Given the general IVP:

$$\frac{dy}{dt} = f(t, y(t)), \quad y(t_0) = y_0 \tag{1.1}$$

where $f(t, y(t))$ is a function depending on t and y, and y_0 denotes the known solution at initial time t_0, the forward Euler method is as follows:

$$y_{n+1} = y_n + \tau f(t_n, y_n). \tag{1.2}$$

The time interval $t \in [t_0, t_{final}]$ has been divided into m discrete times, $m = \frac{t_{final} - t_0}{\tau}$, where τ denotes the distance between two adjacent times, and y_n denotes the approximate solution

at time t_n. From equation (1.2) it is evident that the method only uses known values when computing the next approximation, hence forward Euler is termed an explicit method.

Given the initial value problem

$$\frac{dy}{dt} = ty + t^3, \quad y(0) = 1, \quad t \in [0, 1]. \tag{1.3}$$

The analytic solution and the forward Euler approximation are plotted in Figure 1.1.

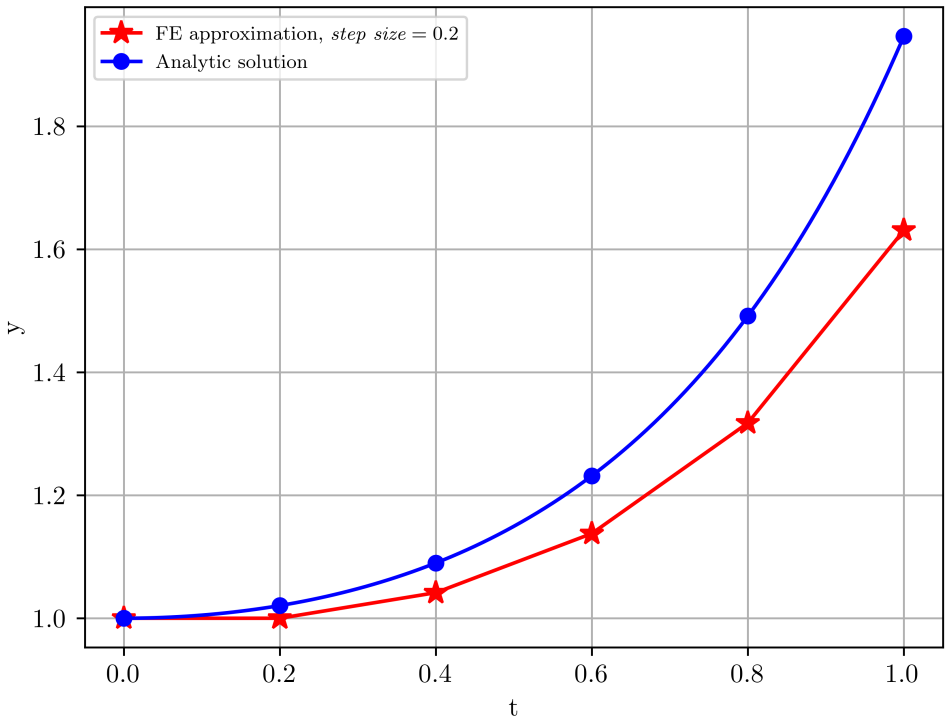

Figure 1.1: Forward Euler approximation and analytic solution

One can think of the initial value problem as giving the slope of the tangent line at specific time. The forward Euler method approximates the solution by moving a short distance along the tangent line and re-evaluating the slope at the stopping point, continuing in this manner until the final time is reached. How good the approximation is depends highly on how often the slope is re-evaluated, and also on how much the slope changes [31].

The error produced in one step of the method is called a local truncation error, e_n. The local error is defined as the absolute value of the difference between the approximation in this step and the analytic solution given the approximation in the previous step as the initial value, that is, $\tilde{y}(t_n) = y_n$, i.e., $e_{n+1} = |y_{n+1} - \tilde{y}(t_{n+1})|$. y_{n+1} denotes the approximate solution, while $\tilde{y}$ denotes the analytic solution. At a specific time, say t_{n+1}, using Taylor expansion one can rewrite the exact solution $\tilde{y}(t_{n+1})$ (assuming it is sufficiently smooth) as

$$\tilde{y}(t_{n+1}) = \tilde{y}(t_n + \tau) = \tilde{y}(t_n) + \tilde{y}'(t_n)\tau + \frac{\tilde{y}''(s)}{2}\tau^2 \tag{1.4}$$

for some $t_n < s < t_{n+1}$. Substituting $\tilde{y}'(t_n)$ with $f(t_n, \tilde{y}(t_n))$ gives

$$\tilde{y}(t_{n+1}) = \tilde{y}(t_n + \tau) = \tilde{y}(t_n) + f(t_n, \tilde{y}(t_n))\tau + \frac{\tilde{y}''(s)}{2}\tau^2. \tag{1.5}$$

Using the expansion in calculating the local truncation error leads to

$$e_{n+1} = |y_{n+1} - \tilde{y}(t_{n+1})| = |y_n + \tau f(t_n, y_n) - (\tilde{y}(t_n) + \tau f(t_n, \tilde{y}(t_n)) + \frac{\tilde{y}''(s)}{2}\tau^2)|. \tag{1.6}$$

Remembering $\tilde{y}(t_n) = y_n$ results in the following expression,

$$e_{n+1} = \frac{|\tilde{y}''(s)|}{2}\tau^2. \tag{1.7}$$

Assuming $|\tilde{y}''(s)|$ has an upper bound M on the interval $[t_n, t_{n+1}]$ we get that

$$e_{n+1} \leq \frac{M}{2}\tau^2. \tag{1.8}$$

Hence, $e_{n+1} = \mathcal{O}(\tau^2)$ and one can conclude that the local truncation error of the forward Euler method is of second order.

The following definition and results are needed to deduce the order of the global error.

Definition 1 (Lipschitz continuous function [31]). *A function $f(t, y)$ is **Lipschitz continuous** in the variable y on a convex set S if there exists a constant L satisfying*

$$|f(t, y_1) - f(t, y_2)| \leq L|y_1 - y_2|$$

$\forall (t, y_1), (t, y_2) \in S$.

Theorem 1.2.1 (Existence and uniqueness of solutions [31]). *Assume that $f(t, y)$ is Lipschitz continuous in the variable y on a convex set S and y_0 is in the y domain of definition. Then there exists a constant c in the t domain of definition such that the initial value problem*

$$y' = f(t, y)$$

$$y(t_0) = y_0$$

for $t \in [t_0, c]$ has exactly one solution. Moreover, if the y domain of definition is $(-\infty, \infty)$, then one knows that there exists exactly one solution given the entire t domain of definition.

Theorem 1.2.2 (Bound on difference between solutions defined on the same set with different initial values [31]). *Assume that $f(t, y)$ is Lipschitz continuous in the variable y on a convex set S. If $Y(t)$ and $Z(t)$ are solutions on S of the differential equation*

$$y' = f(t, y)$$

with initial conditions Y_0 and Z_0 respectively, then

$$|Y(t) - Z(t)| \leq e^{L(t-t_0)}|Y_0 - Z_0|$$

Proof. If $Y_0 = Z_0$ then one knows by Theorem 1.2.1 that there exists only one solution and hence that $Y(t) = Z(t)$. Thus the inequality is satisfied trivially. Now assume that $Y_0 \neq Z_0$. This implies that $Y(t) \neq Z(t)\ \forall t$ in the interval, if not the uniqueness statement is contradicted. Define $u(t) := Y(t) - Z(t)$, which is either strictly positive or strictly negative. The inequality depends on $|u|$ so the sign is not relevant, and one may therefore assume that $u(t) > 0$. Taking the derivative of u results in

$$u'(t) = Y'(t) - Z'(t) = f(t, Y(t)) - f(t, Z(t))$$

using the assumption that u is positive and the definition of Lipschitz continuity gives us

$$u'(t) = |f(t, Y(t)) - f(t, Z(t))| \leq L|Y(t) - Z(t)| = L|u(t)| = Lu(t) \tag{1.9}$$

giving the relation

$$\frac{u'(t)}{u(t)} \leq L.$$

Using the Mean Value Theorem and the fact that $ln(u(t))' = \frac{u'(t)}{u(t)}$ one gets

$$\frac{ln(u(t)) - ln(u(t_0))}{t - t_0} \leq L$$

which simplifies to

$$ln\left(\frac{u(t)}{u(t_0)}\right) \leq L(t - t_0).$$

Adding the exponential function on both sides of the above equation gives the desired result

$$u(t) \leq e^{L(t-t_0)}u(t_0).$$

□

The global error at step n is $g_n = |y_n - y(t_n)|$, which is the difference between the approximate solution and analytic solution at time t_n. In the following y denotes the analytic solution of the initial value problem with initial condition $y(t_i) = y(t_i)$, while $\tilde{y}$ denotes the analytic solution of the same IVP, but with $y(t_i) = y_i$ as the initial condition. At $n = 0$ the global error is $g_0 = |y(t_0) - y(t_0)| = 0$. Thus at $n = 1$ the global error is $g_1 = e_1 = |y_1 - \tilde{y}(t_1)|$. In the next step one will divide the global error into local error and previous global error.

$$g_2 = |y_2 - y(t_2)| = |y_2 - \tilde{y}(t_2) + \tilde{y}(t_2) - y(t_2)| \tag{1.10}$$

$$|y_2 - \tilde{y}(t_2) + \tilde{y}(t_2) - y(t_2)| \leq |y_2 - \tilde{y}(t_2)| + |\tilde{y}(t_2) - y(t_2)|. \tag{1.11}$$

The first term is the local truncation error e_2, the second term is the difference between to solutions of the same IVP but with different initial values, hence we can estimate the difference using theorem 1.2.2.

$$g_2 \leq e_2 + e^{L(t_2-t_1)}|\tilde{y}(t_1) - y(t_1)| = e_2 + e^{L\tau}g_1 = e_2 + e^{L\tau}e_1. \tag{1.12}$$

Doing the same calculations for $n = 3$ results in

$$g_3 \leq e_3 + e^{L\tau}(e_2 + e^{L\tau}e_1) = e_3 + e^{L\tau}e_2 + e^{2L\tau}e_1. \tag{1.13}$$

By using induction, one can show that the $i-th$ global error is bounded in the following way

$$g_i \leq e_i + e^{L\tau}e_{i-1} + e^{2L\tau}e_{i-2} + \cdots + e^{(i-2)L\tau}e_2 + e^{(i-1)L\tau}e_1. \tag{1.14}$$

Due to the local truncation error being of second order, we have that $e_j \leq C\tau^2 \ \ \forall j$. Substituting this relation into the global truncation error estimate results in

$$g_i \leq C\tau^2(1 + e^{L\tau} + \cdots + e^{(i-1)L\tau}) = C\tau^2\frac{e^{iL\tau} - 1}{e^{L\tau} - 1} \tag{1.15}$$

$$\leq C\tau^2\frac{e^{L(t_i - t_0)} - 1}{L\tau} = \frac{C\tau}{L}(e^{L(t_i - t_0)} - 1). \tag{1.16}$$

Therefore, we can conclude that the global truncation error is proportional to τ, implying that the forward Euler method is a first order method.

The advantage of this method is that it is explicit, and thus very easy to implement. A drawback is that the time step has to be sufficiently small, otherwise, the solution will diverge. What is "sufficiently small" depends on the specific problem at hand. The reason why the method diverges for time steps that are not "sufficiently small" is because, in those cases, the method progresses along the tangent lines for too long. As a result, the method fails to detect possible changes in the slope of the analytic solution.

Additionally, it should be mentioned that if forward Euler and a spatial discretization method are used to discretize a PDE, then for the numerical solution to converge, the domain of dependency of the method must include the mathematical domain of dependency [32]. This is a necessary condition for stability of a numerical method and was first described in a 1928 paper by Richard Courant, Kurt Friedrichs, and Hans Lewy [32]. The condition is commonly referred to as the CFL-condition, named after the pioneering work of Courant, Friedrichs, and Lewy.

1.2.2 Backward Euler

Backward Euler is another numerical method for solving initial value problems. It is the simplest implicit method, which means that the method depends on the unknown solution.

Given the general IVP:

$$\frac{dy}{dt} = f(t, y(t)), \quad y(t_0) = y_0 \tag{1.17}$$

where $f(t, y(t))$ is a function depending on t and y, and y_0 denotes the known solution at initial time t_0, the backward Euler method is as follows:

$$y_n = y_{n-1} + \tau f(t_n, y_n). \tag{1.18}$$

The time interval $t \in [t_0, t_{final}]$ has been divided into m discrete times, $m = \frac{t_{final} - t_0}{\tau}$, where τ denotes the distance between two adjacent times, and y_n denotes the approximate solution at t_n.

Given that the method is implicit, it does not provide a formula that can be directly solved for the next approximation. Instead, the equation must be rewritten. If the resulting equation is nonlinear with respect to the unknown, a nonlinear solver method must be used at each time step, in addition to the backward Euler method, to solve the problem. This approach can require a considerable amount of additional work. However, unlike the forward Euler method, this method converges when dealing with stiff problems.

By Taylor expanding y about t the local truncation error of the method can be studied. As stated in the previous section, the local truncation error is the error accumulated by one iteration of the method. That is, $e_n = |y_n - \tilde{y}(t_n)|$ where y_n denotes the approximate solution at time t_n and $\tilde{y}(t_n)$ denotes the analytic solution at time t_n, but with initial condition $\tilde{y}(t_{n-1}) = y_{n-1}$ such that the approximation and analytic solution is equal at the beginning of the iteration. If that was not the case, it would not be possible to solely compute the difference between the solutions at that particular time step, which is the local truncation error.

$$y(t-\tau) = y(t) + y'(t)(t-\tau-t) + \frac{y''(s)}{2}(t-\tau-t)^2 \tag{1.19}$$

for some $s \in \langle t-\tau, t\rangle$. Rewriting the equation yields the following

$$y(t) = y(t-\tau) + y'(t)\tau - \frac{y''(s)}{2}\tau^2. \tag{1.20}$$

Substituting the above equation, (1.20), for the analytic solution and the definition of the numerical method yields the following local truncation estimate

$$e_n = |y_n - \tilde{y}(t_n)| = |y_{n-1} + \tau f(t_n, y_n) - (\tilde{y}(t_{n-1}) + \tau\tilde{y}'(t_n) - \frac{\tilde{y}''(s)}{2}\tau^2)| \tag{1.21}$$

Further using that $\tilde{y}(t_{n-1}) = y_{n-1}$ and $\tilde{y}'(t_n) = f(t_n, \tilde{y}(t_n))$ results in

$$e_n = |y_{n-1} + \tau f(t_n, y_n) - y_{n-1} - \tau f(t_n, \tilde{y}(t_n)) + \frac{\tilde{y}''(s)}{2}\tau^2| \tag{1.22}$$

$$e_n \leq \tau|f(t_n, y_n) - f(t_n, \tilde{y}(t_n))| + |\frac{\tilde{y}''(s)}{2}\tau^2|.$$

Assuming that f is Lipschitz continuous in the second variable, the first term on the left side can be bounded, and as a result, a larger bound can be reached

$$e_n \leq \tau L|y_n - \tilde{y}(t_n)| + |\frac{\tilde{y}''(s)}{2}\tau^2|$$

where L is the Lipschits constant.

$$e_n(1-\tau L) \leq |\frac{\tilde{y}''(s)}{2}\tau^2|$$

$$\implies e_n \leq \frac{\tau^2}{2(1-\tau L)}|\tilde{y}''(s)|$$

Thus, as long as $\tau < \frac{1}{L}$ and $|\tilde{y}''(s)|$ is bounded, the local truncation error has an upper bound. Due to τ^2 the local truncation error is said to be of second order.

There exists a theorem related to one-step ODE solvers that pertains to the order of the global truncation error, which is equivalent to the order of the method. The theorem states that if the local truncation error e_n is proportional to $\mathcal{O}(\tau^{k+1})$, then the global truncation error g_n is proportional to $\mathcal{O}(\tau^k)$ at time t_n. For the Backward Euler Method, this means that the global truncation error is of first order, indicating that the method itself is of first order.

1.2.3 The Finite Element Method (FEM)

The Finite Element Method, FEM, is a numerical method mainly used to discretize a partial differential equation, PDE, with respect to space. The idea of the method is to divide the spacial domain into a finite number of non-overlapping elements, and approximate the solution at each element using local functions. To perform this approximation, one must first rewrite the given problem in its weak form. Next, a finite dimensional space is selected in which to search for solutions, and the weak form is approximated within this space [33]. The finite dimensional problem can be expressed as a system of equations on the form $Ax = b$. Once solved, x represents the vector of solution values at the degrees of freedom of the mesh. To obtain the approximate solution at an element, one interpolates between the computed solution values at its nodes. Repeating this process for all elements while assuming continuity between adjacent elements yields the approximate solution for the entire domain. It is important to note that the choice of a finite dimensional function space greatly influences the accuracy of the method, as well as which known results are applicable. Furthermore, FEM has the advantage that the numerical formulation closely resembles the mathematical weak formulation of a PDE, which has been extensively studied by mathematicians. Consequently, in many cases there are known error estimates available, both *a priori* and *a posteriori* [33].

The following will provide a detailed explanation of how to obtain the weak form of a PDE and how the FEM discretization process operates. Furthermore, results pertaining to the existence and uniqueness of solutions will be presented.

1.2.3.1 Hilbert Spaces

As previously mentioned, the choice of function spaces used in the weak formulation significantly impacts the existence and uniqueness of solutions. Hilbert spaces are a specific class of spaces, that possess several advantageous properties which enable qualitative analysis of the approximate solution. As a result, the function spaces utilized in this thesis are Hilbert spaces. This class of spaces will be examined in greater detail in the following.

Before proceeding with the definition of a Hilbert space, it is important to be acquainted with some preliminary definitions. These will now be presented.

Definition 2 (Real vector space [34])**.** *A real vector space is a triple $(V, +, \cdot)$, in which V is a set, and $+$ and $\cdot$ are binary operations satisfying the following axioms.*

(i) If x and y belong to V then so does $x + y$

(ii) $x + y = y + x$

(iii) $x + (y + z) = (x + y) + z$

(iv) *V contains a unique element, 0, such that* $x + 0 = x$ *for all* x *in* V.

(v) *With each element* x *there is associated a unique element,* $-x$, *such that* $x + (-x) = 0$

(vi) *If* $x \in V$ *and* $\lambda \in \mathbb{R}$, *then* $\lambda \cdot x \in V$

(vii) $\lambda \cdot (x + y) = \lambda \cdot x + \lambda \cdot y, \quad \lambda \in \mathbb{R}$

(viii) $(\lambda + \mu) \cdot x = \lambda \cdot x + \mu \cdot x, \quad \lambda, \mu \in \mathbb{R}$

(ix) $\lambda \cdot (\mu \cdot x) = (\lambda\mu) \cdot x$

(x) $1 \cdot x = x$.

Note that the terms **vector space** and **linear space** are interchangeable.

Definition 3 (Norm [34]). *Given a vector space V, a* ***norm****,* $\|\cdot\|$, *is a function on V with values in the non-negative reals having the following properties:*

(i) $\|v\| \geq 0 \quad \forall v \in V$
$\|v\| = 0 \iff v = 0$

(ii) $\|c \cdot v\| = |c| \cdot \|v\| \quad \forall c \in \mathbb{R}, v \in V$

(iii) $\|v + w\| \leq \|v\| + \|w\| \quad \forall v, w \in V$ *(the triangle inequality)*

Definition 4 (Normed linear space [34]). *A* ***normed linear space*** *is a linear space in which a norm has been introduced.*

Definition 5 (Metric [35]). *A metric,* $d(\cdot, \cdot)$, *is as a distance function on a set X satisfying the following relations for all points* $p, q \in X$

(i) $d(p, q) > 0$, *if* $p \neq q$

(ii) $d(p, p) = 0$

(iii) $d(p, q) = d(q, p)$

(iv) $d(p, q) \leq d(p, r) + d(r, q)$, *for any* $r \in X$

where $d(p, q)$ *is a real number called the distance from* p *to* q.

Note that all norms are metrics. Thus all normed linear spaces can also be termed metric spaces.

Definition 6 (Cauchy sequence [35]). *A sequence* $\{x_j\}$ *in a metric space,* $(X, d(\cdot, \cdot))$, *is said to be a* ***Cauchy sequence*** *if* $\forall \epsilon > 0$ $\exists$ *an integer N such that*

$$d(x_n, x_m) < \epsilon$$

for all $n, m \geq N$.

Definition 7 (Convergence of a sequence [35]). *A sequence $\{x_j\}$ in a metric space, (X,d(·,·)), is said to converge to a point $x \in X$ if $\forall \epsilon > 0$ $\exists$ an integer N such that*

$$d(x_n, x) < \epsilon \quad \forall n \geq N$$

Definition 8 (Complete space [35]). *A metric space (a space endowed with a distance function, e.g., a norm) is termed complete if every Cauchy sequence converges to a point in the space.*

Definition 9 (Inner-product space [36]). *A (real or complex) inner-product space is a (real or complex) vector space V with an inner product specified. An inner product is a rule which, given any $x, y \in V$, specifies a (real or complex) number $\langle x, y\rangle$, called the inner product of x and y, such that*

(i) $\langle x, x\rangle \in \mathbb{R}^+ \quad \forall x \neq 0$

(ii) $\langle 0, 0\rangle = 0$

(iii) $\langle x, y\rangle = \overline{\langle y, x\rangle}$

(iv) $\langle \lambda x, y\rangle = \lambda\langle x, y\rangle$ *for any* $\lambda \in \mathbb{R}$ (*respctively* $\mathbb{C}$) *and* $x, y \in V$

(v) $\langle x, y + z\rangle = \langle x, y\rangle + \langle x, z\rangle, \quad \forall\ x, y, z \in V.$

In an inner-product space, one defines the norm of an element x to be $\|x\| := \sqrt{\langle x, x\rangle}$.

Definition 10 (Hilbert space [34]). *A Hilbert space is a complete inner-product space.*

In the setting of variational formulations, the most usefull Hilbert spaces are those where differentiation can be preformed. These spaces are denoted $H^k(\Omega)$ and are special cases of Sobolov spaces W_p^k, more precisely where $p = 2$.

In order to define $H^k(\Omega)$ and W_p^k, the concepts of L^p-spaces and weak derivatives must be introduced.

Definition 11 (Lebesgue norm [33]). *For $1 \leq p < \infty$, let*

$$\|f\|_{L^p(\Omega)} := \left(\int_\Omega |f(x)|^p dx\right)^{\frac{1}{p}}$$

and for the case $p = \infty$ set

$$\|f\|_{L^\infty(\Omega)} := ess\,sup\{|f(x)| : x \in \Omega\}$$

Definition 12 (Lebesgue spaces [33]).

$$L^p(\Omega) := \{f : \|f\|_{L^p(\Omega)} < \infty\}$$

with two functions f, g identified as equal if $\|f - g\|_{L^p(\Omega)} = 0$, implying that the functions only differ on a set of measure zero. In this context one can consider $L^p(\Omega)$ as a set of equivalence classes of functions with respect to the identification relation.

The multi-index notation is a short-hand notation for calculus partial derivatives. Let α denote a multi-index, which is an n-tuple of non-negative integers, α_i. The length of α is given by

$$|\alpha| = \sum_{i=1}^{n} \alpha_i$$

For $\phi \in C^\infty$ let $D^\alpha \phi$ denote the usual (pointwise) derivatives

$$\left(\frac{\partial}{\partial x_1}\right)^{\alpha_1} \left(\frac{\partial}{\partial x_2}\right)^{\alpha_2} \cdots \left(\frac{\partial}{\partial x_n}\right)^{\alpha_n} \phi = \frac{\partial^{|\alpha|}\phi}{\partial_{x_1}^{\alpha_1} \partial_{x_2}^{\alpha_2} \cdots \partial_{x_n}^{\alpha_n}}$$

The order of the derivative above is given by $|\alpha|$.

Definition 13 (Compact set [34])**.** *A subset K in a normed linear space is said to be **compact** if each sequence in K has a subsequence that converges to a point in K.*

Definition 14 (Support and Compact Support of a function defined on a subdomian of $\mathbb{R}^n$ [36])**.** *Let u be a continuous function. Then the **support** of u is the closure of the (open) set $\{x : u(x) \neq 0\}$. In other words, it is the closure of the set that does not map to zero. If this set is compact (i.e., bounded) and a subset of the interior of a set Ω then we say that u has **compact support** with respect to Ω. Outside the support it is natural to define the function to be zero and thus extend the function to be defined on all of $\mathbb{R}^n$. Hence, if $\Omega \subset \mathbb{R}^n$ and u is a continuous function compactly supported with respect to Ω we say that u vanishes in a neighborhood of $\partial\Omega$.*

Definition 15 ($C^\infty(\Omega)$ [37])**.** *$C^\infty(\Omega)$ is the space of functions that are infinitely many times differentiable. $C_0^\infty(\Omega)$ denotes the set of $C^\infty(\Omega)$ with compact support in Ω.*

Definition 16 (Set of locally integrable functions [33])**.** *Given a domain Ω, the set of **locally integrable** functions is denoted by*

$$L^1_{Loc}(\Omega) := \{f : f \in L^1(K) \quad \forall \, compact \, K \subset \Omega\}$$

Definition 17 (Generalized (weak) derivatives [33])**.** *We say that a given function $f \in L^1_{Loc}$ has a **weak derivative**, $D_w^\alpha f$, provided there exists a function $g \in L^1_{Loc}$ such that*

$$\int_\Omega g(x)\phi(x)dx = (-1)^{|\alpha|} \int_\Omega f(x) D^\alpha \phi(x) dx \quad \forall \phi \in C_0^\infty(\Omega)$$

If such a g exists, we define $D_w^\alpha f = g$.

Sobolev spaces are complete normed linear spaces of weakly differentiable functions. In other words, Sobolev norms and spaces are generalizations of Lebesgue norms and spaces to include derivatives.

Definition 18 (Sobolov norm [33]). *Let k be a non-negative integer, and let $f \in L^1_{Loc}(\Omega)$. Suppose that the weak derivatives $D^\alpha_w f$ exist for all $|\alpha| \leq k$. Define the* ***Sobolev norm***

$$\|f\|_{W^k_p(\Omega)} := \left(\sum_{|\alpha|\leq k} \|D^\alpha_w f\|^p_{L^p(\Omega)} \right)^{\frac{1}{p}} = \left(\sum_{|\alpha|\leq k} \int_\Omega |D^\alpha_w f|^p dx \right)^{\frac{1}{p}} \tag{1.23}$$

for $1 \leq p < \infty$, and in the case $p = \infty$

$$\|f\|_{W^k_\infty(\Omega)} := \max_{|\alpha|\leq k} \|D^\alpha_w f\|_{L^\infty(\Omega)} \tag{1.24}$$

Definition 19 (Sobolov spaces [33]). *For $1 \leq p \leq \infty$ we define the* ***Sobolev space*** *to be*

$$W^k_p(\Omega) := \{f \in L^1_{Loc}(\Omega) : \|f\|_{W^k_p(\Omega)} < \infty\} \tag{1.25}$$

By setting $p = 2$ the resulting norm is induced by an inner-product, and is therefore a Hilbert space. As mentioned earlier these spaces are often termed H^k.

Definition 20 ($H^k(\Omega)$ [33]). $H^k := \{f \in L^2(\Omega) : \|f\|_{W^k_2(\Omega)} < \infty\}$.

In the thesis, the function space used in variational formulations is the Hilbert space

$$H^1_g(\Omega) := \{f \in H^1(\Omega) : trace(f) = g\}.$$

This space requires a function to have existing weak first derivative.

1.2.3.2 Variational Formulation

The Finite Element Method is a numerical method used to approximate the weak solution of a PDE. Therefore, to apply this method, the problem must first be formulated in weak form, also known as variational form. The term "weak" refers to the fact that this formulation relaxes some of the requirements that a solution must satisfy [38]. It is important to note that many PDEs only have weak solutions, not strong ones. Moreover, it is worth mentioning that a strong solution is always a weak solution, but the converse is not necessarily true.

Given the following partial differential equation, the objective is to find its corresponding variational formulation.

Find u satisfying

$$\begin{cases} \nabla \cdot (-D\nabla u + \vec{c}u) = F & \text{for} \quad \mathbf{x} \in \Omega \\ u = 0 & \text{for} \quad \mathbf{x} \in \partial\Omega. \end{cases} \tag{1.26}$$

Note that (1.26) requires the solution, u, to be satisfied at all points of the domain, i.e., in a point-wise sense. Furthermore, in the cases where $u = g$ at $\partial\Omega$ and $g \neq 0$, it is worth noting that the problem can be reformulated to seek a solution $w = u - \tilde{g}$, subject to the boundary condition $w = 0$. Here, $\tilde{g}$ represents a continuous extension of g on the entire domain Ω.

To obtain the variational form, one start by multiplying the equation by a so-called "test

function" v and integrating over the domain. Here, v is an arbitrary function in $H_0^1(\Omega)$. It is important to note that a test function is compactly supported on the parts of the boundary where the solution is known, i.e., at these parts $v \equiv 0$.

$$\int_\Omega \nabla \cdot (-D\nabla u + \vec{c}u)v = \int_\Omega Fv \tag{1.27}$$

By using the method of integration by parts, one can rewrite the integral on the left-hand side in the following way,

$$\begin{aligned} &\int_\Omega \nabla \cdot (-D\nabla u + \vec{c}u)v dx = \\ &\int_\Omega (D\nabla u - \vec{c}u) \cdot \nabla v dx + \int_{\partial\Omega} \vec{n} \cdot (-D\nabla u + \vec{c}u)v ds \end{aligned} \tag{1.28}$$

where $\vec{n}$ denotes the normal outward pointing unit vector on the boundary. Due to the compact support of the test function, i.e., $v \equiv 0$, the boundary term vanishes, leaving us with the following variational formulation,

Find $u \in H_0^1(\Omega)$ that satisfies

$$\int_\Omega (D\nabla u - \vec{c}u) \cdot \nabla v dx = \int_\Omega F v dx \tag{1.29}$$

for all $v \in H_0^1(\Omega)$

By comparing the strong formulation (1.26) with the variational formulation (1.29), it becomes clear that the former requires the solution to be twice continuously differentiable, while the latter only requires it to be one time continuously differentiable. Moreover, in the strong formulation, the solution must be twice continuously differentiable at every point in the domain, whereas in the variational formulation, the solution only needs to satisfy the equality in an integral sense. This means that the variational solution can even be discontinuous, as long as its integral satisfies the equation for all test functions.

Define $a(u, v) := \int_\Omega (D\nabla u - \vec{c}u) \cdot \nabla v dx$ and $L(v) := \int_\Omega F v dx$. Based on the following definitions, it will be shown that $a(u, v)$ and $L(v)$ are bilinear and linear forms, respectively.

Definition 21 (Linear form [34])**.** *A linear form on a vector space X is a linear mapping $f : X \to \mathbb{R}$. I.e., the mapping satisfies*

$$f(\alpha u + \beta v) = \alpha f(u) + \beta f(v)$$

for all $\alpha, \beta \in \mathbb{R}$ and for all $u, v \in X$

Definition 22 (Bilinear form [33])**.** *A bilinear form $a(\cdot, \cdot)$ on a vector space X is a mapping $a : X \times X \to \mathbb{R}$ such that each of the maps $u \mapsto a(u, v)$ and $v \mapsto a(u, v)$ is a linear form on X. It is a symmetric bilinear form if $a(u, v) = a(v, u)$.*

$$\begin{aligned} a(\alpha u + \beta w, v) &= \int_\Omega (D\nabla(\alpha u + \beta w) - \vec{c}(\alpha u + \beta w)) \cdot \nabla v dx \\ &= \int_\Omega (D\nabla\alpha u - \vec{c}\alpha u + D\nabla\beta w - \vec{c}\beta w) \cdot \nabla v dx \\ &= \int_\Omega (\alpha[D\nabla u - \vec{c}u] + \beta[D\nabla w - \vec{c}w]) \cdot \nabla v dx \\ &= \alpha \int_\Omega (D\nabla u - \vec{c}u) \cdot \nabla v dx + \beta \int_\Omega (D\nabla w - \vec{c}w) \cdot \nabla v dx \\ &= \alpha a(u, v) + \beta a(w, v). \end{aligned} \tag{1.30}$$

$$\begin{aligned} a(u, \alpha v + \beta w) &= \int_\Omega (D\nabla u - \vec{c}u) \cdot \nabla(\alpha v + \beta w) dx \\ &= \int_\Omega (D\nabla u - \vec{c}u) \cdot [\nabla\alpha v + \nabla\beta w)] dx \\ &= \int_\Omega (D\nabla u - \vec{c}u) \cdot \nabla\alpha v + (D\nabla u - \vec{c}u) \cdot \nabla\beta w dx \\ &= \alpha \int_\Omega (D\nabla u - \vec{c}u) \cdot \nabla v dx + \beta \int_\Omega (D\nabla u - \vec{c}u) \cdot \nabla w dx \\ &= \alpha a(u, v) + \beta a(u, w). \end{aligned} \tag{1.31}$$

$$\begin{aligned} L(\alpha v + \beta w) = \int_\Omega F(\alpha v + \beta w) dx &= \int_\Omega F\alpha v dx + \int_\Omega F\alpha w dx \\ &= \alpha \int_\Omega F v dx + \alpha \int_\Omega F w dx \\ &= \alpha L(v) + \beta L(w). \end{aligned} \tag{1.32}$$

The above calculations utilized the fact that integrals, dot products, and gradients are linear operators to demonstrate that $a(u, v)$ is a bilinear form and $L(v)$ is a linear form.

1.2.3.3 Discretization

To discretize the variational formulation, the Galerkin method is used. This involves replacing the test and trial function spaces, i.e., the spaces to which u and v belong, with finite-dimensional subspaces and seeking solutions within these spaces. Let $V_N \subset H_0^1(\Omega)$ be a finite N-dimensional subspace of $H_0^1(\Omega)$ with basis functions $\{\phi_1(\mathbf{x}), \phi_2(\mathbf{x}), \ldots, \phi_N(\mathbf{x})\}$. The Galerkin method has several advantages, such as allowing for the use of standard linear algebra techniques to solve the resulting system of equations, and providing a flexible framework for adapting the discretization to the problem at hand. The finite dimensional variational

problem is written in the following way.

Find $u_h \in V_N$ that satisfies

$$\int_\Omega (D\nabla u_h - \vec{c}u_h) \cdot \nabla v_h dx = \int_\Omega F v_h dx \tag{1.33}$$

for all $v_h \in V_N$

Moreover, one defines

$$a(u_h, v) := \int_\Omega (D\nabla u_h - \vec{c}u_h) \cdot \nabla v_h dx \tag{1.34}$$

$$L(v) := \int_\Omega F v_h dx. \tag{1.35}$$

By following the same steps presented in (1.30)-(1.32), one can demonstrate that $a(u_h, v)$ and $L(v)$ are bilinear and linear forms, respectively.

Since u_h and v_h belong to the finite-dimensional subspace V_N, they can be expressed as linear combinations of the basis functions of V_N. Specifically, one can write $u_h = \sum_{i=1}^N \tilde{u}_i \phi_i(\mathbf{x})$ and $v_h = \sum_{j=1}^N \tilde{v}_j \phi_j(\mathbf{x})$, where $\tilde{u}_i$ and $\tilde{v}_j$ are coefficients. Substituting these expressions for u_h and v_h into (1.33), one obtains

$$\int_\Omega (D\nabla(\sum_{i=1}^N \tilde{u}_i\phi_i) - \vec{c}(\sum_{i=1}^N \tilde{u}_i\phi_i)) \cdot \nabla(\sum_{j=1}^N \tilde{v}_j\phi_j) dx = \int_\Omega F(\sum_{j=1}^N \tilde{v}_j\phi_j) dx \tag{1.36}$$

where ϕ_i and ϕ_j are the basis functions of V_N.

Since the coefficients are independent of space and the gradient is a linear operator, one can apply the gradient directly to the basis functions inside the sum. Moreover, $\tilde{u}_i$ is a common factor in the difference term of the first integral, allowing it to be factored out. Additionally, constants can be taken outside of integrals. As noted, (1.36) must hold for all $v_h = \sum_{j=1}^N \tilde{v}_j \phi_j$, and since all v_h are linear combinations of $\{\phi_j\}_{j=1}^N$, it suffices to verify the equation for each basis function. Thus, the problem can be expressed as follows.

$$\sum_{i=1}^N \tilde{u}_i \int_\Omega (D\nabla\phi_i - \vec{c}\phi_i) \cdot \nabla(\phi_j) dx = \int_\Omega F\phi_j dx \quad \text{for} \quad j \in \{1, 2, ..., N\} \tag{1.37}$$

The above system of equations can be written in matrix vector form $A\mathbf{u} = \mathbf{b}$ with

$$A = \left(\int_\Omega (D\nabla\phi_i - \vec{c}\phi_i) \cdot \nabla(\phi_j) dx \right)_{i,j=1}^N \in \mathbb{R}^{N\times N} =$$

$$\begin{bmatrix} \int_\Omega (D\nabla\phi_1 - \vec{c}\phi_1) \cdot \nabla(\phi_1) dx & \int_\Omega (D\nabla\phi_2 - \vec{c}\phi_2) \cdot \nabla(\phi_1) dx & \cdots & \int_\Omega (D\nabla\phi_N - \vec{c}\phi_N) \cdot \nabla(\phi_1) dx \\ \int_\Omega (D\nabla\phi_1 - \vec{c}\phi_1) \cdot \nabla(\phi_2) dx & \int_\Omega (D\nabla\phi_2 - \vec{c}\phi_2) \cdot \nabla(\phi_2) dx & \cdots & \int_\Omega (D\nabla\phi_N - \vec{c}\phi_N) \cdot \nabla(\phi_2) dx \\ \vdots & & \ddots & \\ \int_\Omega (D\nabla\phi_1 - \vec{c}\phi_1) \cdot \nabla(\phi_N) dx & \int_\Omega (D\nabla\phi_2 - \vec{c}\phi_2) \cdot \nabla(\phi_N) dx & \cdots & \int_\Omega (D\nabla\phi_N - \vec{c}\phi_N) \cdot \nabla(\phi_N) dx \end{bmatrix}$$

$$\mathbf{u} = (\tilde{u}_i)_{i=1}^N = \begin{bmatrix} \tilde{u}_1 \\ \tilde{u}_2 \\ \vdots \\ \tilde{u}_N \end{bmatrix} \in \mathbb{R}^N, \quad \mathbf{b} = \left(\int_\Omega F\phi_j dx \right)_{j=1}^N = \begin{bmatrix} \int_\Omega F\phi_1 dx \\ \int_\Omega F\phi_2 dx \\ \vdots \\ \int_\Omega F\phi_N dx \end{bmatrix} \in \mathbb{R}^N$$

It has now been shown that solving (1.33) is equivalent to solving the linear system $A\mathbf{u} = \mathbf{b}$ with $A, \mathbf{u}$ and $\mathbf{b}$ as defined above.

Note that both A and $\mathbf{b}$ only contain known quantities. This means that they can be computed and the system $A\mathbf{u} = \mathbf{b}$ can be solved for $\mathbf{u}$. The discrete solution provides the solution values at the degrees of freedom of the mesh. Then, it only remains to interpolate over each element and assemble the solutions to obtain the solution on the entire domain. Additionally, it is worth noting that many finite element bases result in a significant number of elements in matrix A being equal to zero, leading to a sparse matrix structure. This sparsity property greatly simplifies the process of solving the system of equations, making it computationally easier and more efficient.

1.2.3.4 Results regarding existence and uniqueness, and errors of solutions to variational problems

When solving a mathematical problem, it is desirable to know whether or not the problem has a solution, and if there is only one possible solution or if there are multiple solutions. In the following, a theorem that provides conditions for a unique solution to exist will be presented. Furthermore, a theorem that provides an upper bound on the error of the Galerkin approximation will also be presented.

Theorem 1.2.3 (Lax Milgram [38])**.** *Given a*

- *Hilbert space $(V, (\cdot, \cdot))$*
- *bilinear form $a(\cdot, \cdot)$ satisfying*
  - $|a(v,w)| \leq M\|v\|_V\|w\|_V \quad \forall v, w \in V$ *with $M > 0$ a constant (continuity)*
  - $a(v,v) \geq \alpha\|v\|_V^2 \quad \forall v \in V$ *with $\alpha > 0$ a constant (coercivity)*
- *linear functional $L(\cdot)$ satisfying*
  - $|L(v)| \leq C\|v\|_V \quad \forall v \in V$ *with $C > 0$ a constant. (Continuity)*

then there $\exists!$ $u \in V$ such that

$$a(u,v) = F(v) \quad \forall v \in V.$$

Proof. See for example [33]. □

Lemma 1.2.4 (Céa's lemma [38])**.** *Assume*

1. $|a(u,v)| \leq M\|u\|\|v\|, \quad M > 0, \ \forall u, v \in V$
2. $a(u,u) \geq \alpha\|u\|^2, \quad \alpha > 0,$ *for* $u \in V$

with $\|\cdot\|$ denoting a norm on V. Then the following error estimate for the Galerkin solution holds:

$$\|u - u_h\| \leq \frac{M}{\alpha} min\{\|u - v\| \mid v \in V_h\}. \tag{1.38}$$

Proof. If $\|u - u_h\| = 0$, then the inequality will always hold because all the terms on the right hand side are non-negative, and there is nothing to prove. Therefore, assume $u \neq u_h$. Further assume that $v \in V_h$. One can then write the difference between the continuous variational formulation, i.e., $a(u, v) = b(v)$, and the discrete variational formulation, i.e., $a(u_h, v) = b(v)$, as follows:

$$a(u, v) - a(u_h, v) = b(v) - b(v) = 0 \implies a(u - u_h, v) = 0. \tag{1.39}$$

Note that v is an arbitrary element of V_h, meaning that the relation hold for all elements of V_h.

Due to the second assumption of the lemma one can write

$$\alpha\|u - u_h\|^2 \leq a(u - u_h, u - u_h). \tag{1.40}$$

Since u_h and v are elements of V_h, a linear space, one knows that $u_h - v$ also is contained in V_h. Therefore, one have that $a(u - u_h, u_h - v) = 0$, and one can rewrite as follows:

$$\alpha\|u - u_h\|^2 \leq a(u - u_h, u - u_h) + a(u - u_h, u_h - v). \tag{1.41}$$

Using the fact that $a(\cdot, \cdot)$ is a bilinear form and the first assumption of the lemma one gets the following

$$\begin{aligned}
\alpha\|u - u_h\|^2 &\leq a(u - u_h, u - u_h) + a(u - u_h, u_h - v) \\
&= a(u - u_h, u) - a(u - u_h, u_h) + a(u - u_h, u_h) - a(u - u_h, v) \\
&= a(u - u_h, u) - a(u - u_h, v) = a(u - u_h, u - v) \\
&\leq M\|u - u_h\|\|u - v\|
\end{aligned}$$

$$\implies \|u - u_h\| \leq \frac{M}{\alpha}\|u - v\| \quad v \in V_h$$

Since it holds for all $v \in V_h$, one gets that the smallest upper bound on the error is

$$\|u - u_h\| \leq \frac{M}{\alpha} min\{\|u - v\| \mid v \in V_h\} \tag{1.42}$$

which is the desired result. □

1.3 FEniCS

FEniCS is a powerful open-source finite element library widely used for solving partial differential equations (PDEs). It provides a user-friendly interface and efficient computational capabilities for researchers and practitioners in various scientific and engineering fields [23].

With FEniCS, users can express their PDE problems using a high-level mathematical language, making it easier to translate mathematical formulations into computationally efficient code [23]. The library handles many aspects of finite element computations, such as mesh generation, function space definitions, and variational problem formulations, allowing users to focus on the mathematical and physical aspects of their problems [23].

Chapter 2

The mathematical model

2.1 Derivation of the mathematical model

In this chapter, we will develop a two-dimensional continuous model of avascular tumor growth *in vitro* using deterministic parameters. Afterward, we will discuss the expected behavior of the model before proceeding to discretize it. Finally, we will also discuss the structure of the implementation.

The Mathematical Model
To enhance our understanding of the model and its development, we will begin by examining the underlying assumptions on which it is based.

Assumptions and comments:

- It is assumed that the tumor is comprised of three main components: viable cells (including both proliferating and quiescent cells), dead cells, and the extracellular matrix. The extracellular matrix encompasses all fluids, proteins, molecules, and other substances that surround the cells.

- One assumes that the tumor initially has a circular shape and grows in a radially symmetric manner, maintaining its circular shape over time. Furthermore, any constraints imposed by the surrounding geometry is disregarded.

- Moreover, it is assumed that the volume fraction of the extracellular matrix remains constant throughout the growth process. In other words, the extracellular matrix always constitutes a fixed percentage, denoted as $p\%$, of the total volume. This assumption implies that both living and dead cells, even considering volume loss, maintain a uniform spatial arrangement within the tumor.

- The influence of cell-cell adhesion forces and cell-matrix adhesion forces are neglected in the model.

- Advection-diffusion type of PDEs will be used to model the concentrations of nutrients and growth-inhibitor factors (GIFs) in a tumor. The model will incorporate three growth factors. Firstly, we will consider externally supplied nutrients as growth-promoting

factors. Secondly, we will account for growth-inhibitor factors that are produced by cells within the tumor during the cell cycle or excreted by necrotic cells. Lastly, we will include externally supplied growth-inhibitor factors that represent the immune system's response to the tumor.

  - An advection-diffusion equation will be formulated to represent the nutrient concentration within the tumor. The equation will not include a source term since we assume that nutrients are only externally supplied and not produced within the tumor. However, it will include a sink term to account for the consumption of nutrients by the cells. Furthermore, we will assume that the nutrient level in the surrounding area of the tumor remains fixed, indicating a constant supply of nutrients. This condition will be expressed by a positive Dirichlet boundary data.
  - A diffusion equation will be formulated to represent the growth-inhibitor factors, $G1$, produced or excreted internally by the cells. The PDE is in accordance with the one presented in [2]. The equation incorporates both source and sink terms, representing the production/excretion and consumption of $G1$ within the tumor, respectively. Moreover, we assume that these GIFs do not exist outside the tumor, which is reasonable considering they are a product of the cells specific to the tumor. Hence, we assume no transport of $G1$ across the tumor boundary. This condition will be represented by a homogeneous Neumann boundary condition.
  - We will represent the growth-inhibitor factors, $G2$, produced by the immune system in the surrounding tissue using an advection-diffusion equation. Since $G2$ is not produced within the tumor, the equation will not contain a production term. However, it will include a sink term to account for the cells consumption of $G2$. Additionally, we will assume that the concentration of $G2$ in the tissue surrounding the tumor remains constant. Therefore, the boundary supply of $G2$ will be represented by a positive Dirichlet boundary condition.

- The viable and dead cells will not be explicitly addressed or solved for; instead, they will be implicitly represented by the nutrient and GIF concentrations within the tumor. A GIF threshold will be introduced, denoted as θ_G, which serves as an upper limit for GIF concentration allowing cells to proliferate. If the GIF concentration exceeds θ_G, it will inhibit mitosis, leading to cell quiescence or death, depending on the current nutrient level. Additionally, a nutrient threshold will be defined, denoted as θ_N, as the minimum nutrient concentration required for cell growth. In order for a cell to have the potential to proliferate, the nutrient concentration must surpass θ_N. If the nutrient concentration falls below this threshold, the cell will become quiescent or die. The tumor is divided into proliferating, quiescent, and necrotic cells based on the following criteria

  - **Proliferating** if

$$u_N > \theta_N \quad \text{and} \quad w_1(w_2 u_{G1} + w_3 u_{G2}) < \theta_G \tag{2.1}$$

  - **Quiescent** if

$$u_N > \theta_N \quad \text{and} \quad w_1(w_2 u_{G1} + w_3 u_{G2}) \geq \theta_G \tag{2.2}$$

or

$$u_N \leq \theta_N \quad \text{and} \quad w_1(w_2 u_{G1} + w_3 u_{G2}) < \theta_G, \quad \text{for less than a stated time period} \tag{2.3}$$

– **Necrotic** if

$$u_N \leq \theta_N \quad \text{and} \quad w_1(w_2 u_{G1} + w_3 u_{G2}) < \theta_G \quad \text{for longer than the stated time period} \tag{2.4}$$

or

$$u_N \leq \theta_N \quad \text{and} \quad w_1(w_2 u_{G1} + w_3 u_{G2}) \geq \theta_G \tag{2.5}$$

with $w_1, w_2, w_3 \in \mathbb{R}$ being weights, θ_N, θ_G the threshold values, and u_N the nutrient concentration, u_{G1} the concentration of G1 growth-inhibitor factors and u_{G2} the concentration of G2 growth-inhibitor factors.

- All necrotic cells remain necrotic, even though nutrient diffusion might alter the nutrient concentration such that necrotic cells later will satisfy either quiescent or proliferating criteria.

- We will introduce a function to represent the mitotic rate, which denotes the rate at which a cell divides into two daughter cells. This rate will depend on the nutrient and GIF concentrations.

- The volume of the tumor is determined by the following factors

  – the number of cells in the tumor, assuming that each cell has a constant volume

  – the percentage of the total volume made up by the extracellular matrix (ECM)

  – the assumption that the tumor has a perfectly circular shape, meaning that its volume, due to the model being two-dimensional, can be calculated using the formula $V_T = \pi r_T^2$.

  Let n_c represent the total number of cells, r_c the fixed radius of a single cell, V_T the total volume of the tumor, V_c the total volume of the cells, and $p\%$ the percentage of the total tumor volume that the extracellular matrix constitute. Then the tumor volume can be computed in the following way

$$V_c = n_c \pi r_c^2 \tag{2.6}$$

$$V_T = \frac{1}{1 - \frac{p}{100}} V_c. \tag{2.7}$$

  This indicates that as long as we know the number of cells we can always compute the tumor volume.

- As shown in the bullet point above, this model represents tumor growth through changes in the number of cells. The change in the number of cells is modeled by an ODE that depends on the mitotic rate.

The advection-diffusion equation for **nutrient concentration**, $\boldsymbol{u_N}$, is as follows

$$\partial_t u_N + \nabla \cdot (-D_N \nabla u_N + \vec{c}_N u_N) = \phi(n_{loc}, u_N) \quad \forall \vec{x} \in \Omega. \tag{2.8}$$

In the equation above, u_N represents the nutrient concentration. The equation describes how the nutrient concentration changes over time, $\partial_t u_N$, within the tumor. This change is influenced by both advective forces, $\vec{c}_N u_N$, which represent the transport of nutrients throughout the tumor, and diffusive forces, $-D_N \nabla u_N$, which account for the spreading of nutrients. Furthermore, the sink term, ϕ, represents the consumption of nutrients and contributes to the temporal changes in concentration. The constant diffusion coefficient, D_N, determines the rate at which nutrients diffuse in the direction opposite to the gradient of u_N. The negative gradient, $-\nabla u_N$, always points towards regions of lower nutrient concentration, reflecting the movement of nutrients driven by molecular processes. Lastly, $\vec{c}_N$ denotes the velocity field resulting from the extracellular matrix, indicating the speed and direction of nutrient transport within the tumor facilitated by the ECM.

The sink-term is defined as follows

$$\phi(n_{loc}, u_N) = -\alpha n_{loc} u_N \tag{2.9}$$

with $\alpha \in \mathbb{R}^+$ representing the sink coefficient, u_N denotes the nutrient concentration, and n_{loc} represents the local number of cells, i.e. the number of cells at a given point. However, due to the assumption that the cells are uniformly distributed and comprise a constant percentage of the tumor, the value of n_{loc} remains constant. It can be computed using the formula $n_{loc} = \frac{N_0}{\pi r_0^2}$, where N_0 is the initial number of cells and πr_0^2 corresponds to the initial tumor volume.

The amount of nutrients consumed by a cell depends on its cell type. Proliferating cells, which actively grow and divide, have high nutrient demands. Quiescent cells, while not actively proliferating, are still alive and therefore require nutrients, albeit at a lower rate compared to proliferating cells. On the other hand, necrotic cells are already dead and no longer consume any nutrients. These differences are accounted for in the model by representing the sink coefficient α as a discontinuous function with different constant values for each cell type.

$$\alpha(\vec{x}) = \begin{cases} 0 & \text{if } \vec{x} \in \text{necrotic cell} \\ \alpha_{qui} & \text{if } \vec{x} \in \text{quiescent cell} \\ \alpha_{pro} & \text{if } \vec{x} \in \text{proliferating cell} \end{cases}$$

with $\alpha_{qui}, \alpha_{pro} \in \mathbb{R}^+$ and $\alpha_{qui} << \alpha_{pro}$.

The Dirichlet **boundary condition w.r.t $\boldsymbol{u_N}$** is

$$u_N = \kappa \quad \forall \vec{x} \in \partial\Omega \tag{2.10}$$

where $\kappa > 0$ represents the constant nutrient supply at the boundary.

The diffusion equation for the concentration of **growth-inhibitor factors produced/excreted by the tumor cells, u_{G1}**, is as follows

$$\partial_t u_{G1} + \nabla \cdot (-D_{G1}(x,y)\nabla u_{G1}) = -\gamma u_{G1} + \lambda S(x,y) \quad \forall \vec{x} \in \Omega. \tag{2.11}$$

In the above equation, u_{G1} represents the concentration of growth-inhibitor factors produced/excreted by the cells within the tumor. The equation describes how the concentration changes over time, $\partial_t u_{G1}$, taking into account the diffusion of the factors, which refers to their spreading through molecular movements. The equation also considers a sink term that represents the consumption of the factors and a production term that represents their generation/excretion within the tumor. The parameters $\gamma \in \mathbb{R}^+$ and $\lambda \in \mathbb{R}^+$ are fixed constants. The decay constant γ determines the rate at which the concentration of G1 is consumed, while the production constant λ controls the rate at which the factors are produced/excreted within the tumor.

In this PDE, the diffusion coefficient is not constant but rather a monotonically decreasing function, denoted as $D_{G1}(x,y) = 5 \times 10^{-7}(1 - 0.2(x^2 + y^2))$. By incorporating a space-dependent nonlinear function for D_{G1}, the model takes into account the possibility of varying or disrupted intercellular signals caused by the cellular heterogeneity within the tumor [2]. The diffusion coefficient is highest at the center of the tumor and decreases as one moves away from the center, for tumors with radii less than $\sqrt{5}$. Figure 2.1(a) illustrates this diffusion pattern.

Furthermore, the source function $S(x,y) = 1 - \frac{(x^2+y^2)}{R^2}$, with R being the radius of the tumor, describes the distribution of G1 production/excretion within the tumor [2]. The function is space-dependent and indicates that G1 production/excretion is highest at the center and gradually decreases towards zero as one approaches the boundary of the tumor. S is chosen to be space-dependent to account for cellular heterogeneity within the tumor [2]. Refer to Figure 2.1(b) for a visual representation of this source function.

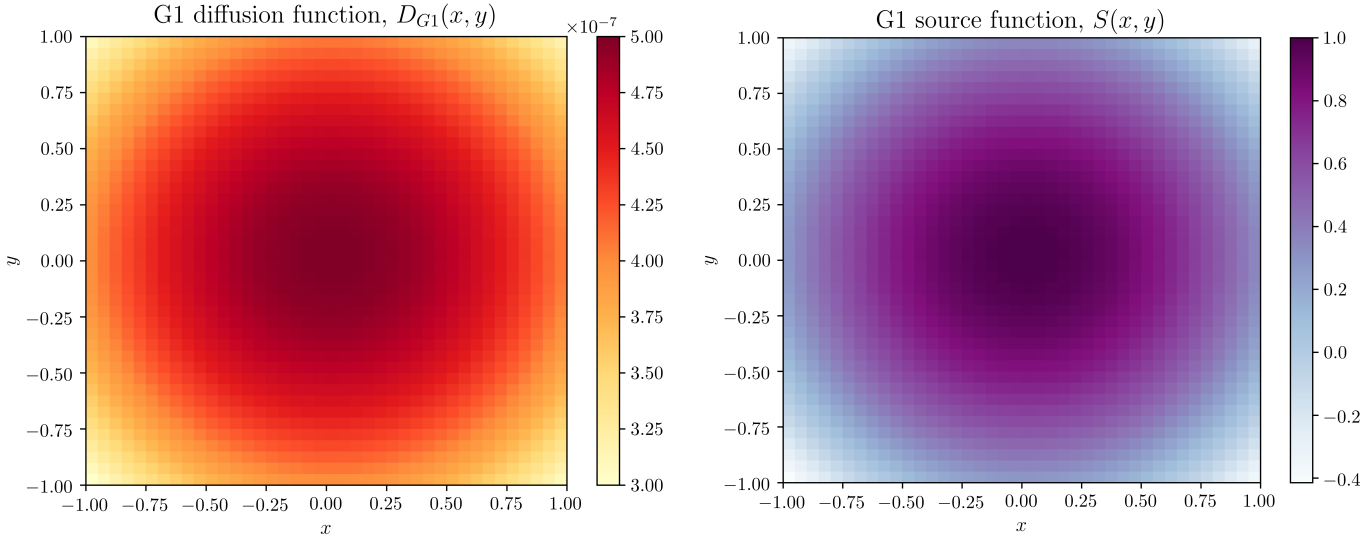

(a) The diffusion equation, $D_{G1}(x,y)$.

(b) The source function, $S(x,y)$.

Figure 2.1: Displaying the diffusion and production/excretion functions in the G1 PDE.

As mentioned, different types of cells consume factors at different rates. In the case of the growth-inhibiting factors G1, they are consumed at an equal rate by proliferating and quiescent cells, while necrotic cells do not consume them at all. Therefore, the decay constant γ must be represented as a discontinuous function that reflects these consumption rates. It can be expressed in the following form

$$\gamma(\vec{x}) = \begin{cases} 0 & \text{if } \vec{x} \in \text{necrotic cell} \\ \gamma_{proqui} & \text{if } \vec{x} \in \text{quiescent cell or proliferating cell} \end{cases}$$

with $\gamma_{proqui} \in \mathbb{R}^+$.

The Neumann **boundary condition w.r.t. u_{G1}** is

$$\vec{n} \cdot (-D_{G1}(x,y)\nabla u_{G1}) = 0 \quad \forall \vec{x} \in \partial\Omega \tag{2.12}$$

with $\vec{n}$ being the outward pointing unit normal vector at the boundary. This boundary condition ensures that there is no diffusion of u_{G1} across the boundary.

The advection-diffusion equation for the **growth-inhibitor factor concentration produced by the immune system, u_{G2}**, is as follows

$$\partial_t u_{G2} + \nabla \cdot (-D_{G2}\nabla u_{G2} + \vec{c}_{G2} u_{G2}) = -\xi n_{loc} u_{G2} \quad \forall \vec{x} \in \Omega. \tag{2.13}$$

In the equation above, u_{G2} denotes the concentration of growth-inhibitor factors produced by the immune system in response to the presence of the tumor. The equation states that the change of u_{G2} with respect to time within the tumor, i.e., $\partial_t u_{G2}$, is related to the diffusion, $-D_{G2}\nabla u_{G2}$, of u_{G2} due to molecular movements and to how the factors are being transported by the velocity field $\vec{c}_{G2}$ induced by the extracellular matrix. Moreover, the consumption of G2 by the cells also contributes to altering u_{G2} over time. Furthermore, $\xi \in \mathbb{R}^+$ is the decay constant of G2. As G2 is consumed at an equal rate by proliferating and quiescent cells, while no factors are consumed by necrotic cells, ξ has to be represented as a constant discontinuous function, as follows

$$\xi(\vec{x}) = \begin{cases} 0 & \text{if } \vec{x} \in \text{necrotic cell} \\ \xi_{proqui} & \text{if } \vec{x} \in \text{quiescent cell or proliferating cell} \end{cases}$$

with $\xi_{proqui} \in \mathbb{R}^+$.

The Dirichlet **boundary condition w.r.t. u_{G2}** is

$$u_{G2} = \psi \quad \forall \vec{x} \in \partial\Omega \tag{2.14}$$

with $\psi \in \mathbb{R}^+$ denoting the constant non-negative u_{G2} supply at the boundary.

The **mitotic function** states the rate at which mitosis occurs. Mitosis is the biological process of a cell dividing into two identical daughter cells. The rate is dependent on the concentrations of growth-promoting and growth-inhibiting factors.

$$m(u_N, u_{G1}, u_{G2}) = \begin{cases} 0 & \text{if } \vec{x} \in \text{necrotic cell} \\ 0 & \text{if } \vec{x} \in \text{quiescent cell} \\ \rho[-\nu_1 u_{G1} - \nu_2 u_{G2} + \eta u_N] & \text{if } \vec{x} \in \text{proliferating cell} \end{cases} \tag{2.15}$$

with $\rho, \nu_1, \nu_2, \eta \in \mathbb{R}^+$ representing weights and u_{G1}, u_{G2}, u_N representing the growth-inhibiting and growth-promoting factor concentrations.

The ODE governing the **change of number of cells** is as follows

$$\frac{dn_c}{dt} = n_{loc} \int_\Omega m dx. \tag{2.16}$$

The equation above indicates that the rate of change in the number of cells is directly influenced by the mitotic function, which represents the rate at which cells are proliferating. As mentioned previously, quiescent and necrotic cells do not undergo growth, resulting in a mitotic function of zero in these regions. Therefore, when integrating over the entire tumor, the integral simplifies to the integral over the proliferating cells only. Thus, the ordinary differential equation (ODE) can be expressed as follows.

$$\frac{dn_c}{dt} = n_{loc} \int_{\Omega_{pro}} m dx = n_{loc} \int_{\Omega_{pro}} \rho[-\nu_1 u_{G1} - \nu_2 u_{G2} + \eta u_N] dx \tag{2.17}$$

n_c represents the total number of cells in the tumor, and $\rho, \nu_1, \nu_2, \eta \in \mathbb{R}^+$ are mitotic weights. u_{G1}, u_{G2}, u_N represent, as always, the growth factor concentrations. The term n_{loc} represents the constant number of cells per unit volume of the tumor, and Ω_{pro} denotes the areas of the tumor consisting exclusively of proliferating cells.

A summary of all the equations and cell type requirements
Find u_N, u_{G1}, u_{G2} and n_c such that the following equations are satisfied

$$\partial_t u_N + \nabla \cdot (-D_N \nabla u_N + \vec{c}_N u_N) = -\alpha n_{loc} u_N \quad \forall \vec{x} \in \Omega \tag{2.18}$$

$$\alpha(\vec{x}) = \begin{cases} 0 & \text{if } \vec{x} \in \text{necrotic cell} \\ \alpha_{qui} & \text{if } \vec{x} \in \text{quiescent cell} \\ \alpha_{pro} & \text{if } \vec{x} \in \text{proliferating cell} \end{cases}$$

$$u_N = \kappa \quad \forall \vec{x} \in \partial\Omega \tag{2.19}$$

$$\partial_t u_{G1} + \nabla \cdot (-D_{G1}(x,y) \nabla u_{G1}) = -\gamma u_{G1} + \lambda S(x,y) \quad \forall \vec{x} \in \Omega \tag{2.20}$$

$$D_{G1}(x,y) = 5 \times 10^{-7}(1 - 0.2(x^2 + y^2)), \quad S(x,y) = 1 - \frac{(x^2 + y^2)}{R^2}$$

$$\gamma(\vec{x}) = \begin{cases} 0 & \text{if } \vec{x} \in \text{necrotic cell} \\ \gamma_{proqui} & \text{if } \vec{x} \in \text{quiescent cell or proliferating cell} \end{cases}$$

$$\vec{n} \cdot (-D_{G1}(x,y) \nabla u_{G1}) = 0 \quad \forall \vec{x} \in \partial\Omega \tag{2.21}$$

$$\partial_t u_{G2} + \nabla \cdot (-D_{G2} \nabla u_{G2} + \vec{c}_{G2} u_{G2}) = -\xi n_{loc} u_{G2} \quad \forall \vec{x} \in \Omega \tag{2.22}$$

$$\xi(\vec{x}) = \begin{cases} 0 & \text{if } \vec{x} \in \text{necrotic cell} \\ \xi_{proqui} & \text{if } \vec{x} \in \text{quiescent cell or proliferating cell} \end{cases}$$

$$u_{G2} = \psi \quad \forall \vec{x} \in \partial\Omega \tag{2.23}$$

$$m(u_N, u_{G1}, u_{G2}) = \begin{cases} 0 & \text{if } \vec{x} \in \text{necrotic cell} \\ 0 & \text{if } \vec{x} \in \text{quiescent cell} \\ \rho[-\nu_1 u_{G1} - \nu_2 u_{G2} + \eta u_N] & \text{if } \vec{x} \in \text{proliferating cell} \end{cases} \tag{2.24}$$

$$\frac{dn_c}{dt} = n_{loc} \int_{\Omega_{pro}} \rho[-\nu_1 u_{G1} - \nu_2 u_{G2} + \eta u_N] dx \tag{2.25}$$

- **Proliferating** if

$$u_N > \theta_N \quad \text{and} \quad w_1(w_2 u_{G1} + w_3 u_{G2}) < \theta_G \tag{2.26}$$

- **Quiescent** if

$$u_N > \theta_N \quad \text{and} \quad w_1(w_2 u_{G1} + w_3 u_{G2}) \geq \theta_G \tag{2.27}$$

or

$$u_N \leq \theta_N \quad \text{and} \quad w_1(w_2 u_{G1} + w_3 u_{G2}) < \theta_G, \quad \text{for less than a stated time period} \tag{2.28}$$

- **Necrotic** if

$$u_N \leq \theta_N \quad \text{and} \quad w_1(w_2 u_{G1} + w_3 u_{G2}) < \theta_G \quad \text{for longer than the stated time period} \tag{2.29}$$

or

$$u_N \leq \theta_N \quad \text{and} \quad w_1(w_2 u_{G1} + w_3 u_{G2}) \geq \theta_G \tag{2.30}$$

with $w_1, w_2, w_3 \in \mathbb{R}$ being weights, θ_N, θ_G the threshold values, and u_N the nutrient concentration, u_{G1} the concentration of G1 growth-inhibitor factors and u_{G2} the concentration of G2 growth-inhibitor factors.

Furthermore, note that all necrotic cells remain necrotic, even though nutrient diffusion might alter the nutrient concentration such that the necrotic cells later will satisfy either quiescent or proliferating criteria.

2.1.1 What type of behavior to expect from the model

Initially, the entire tumor is composed of proliferating cells. However, as the tumor grows, there will be a point/region inside the tumor where one or both of the thresholds θ_N and θ_G are reached. The specific location within the tumor where this occurs, as well as which threshold is reached first, or if they are reached simultaneously, is influenced by various parameters.

For instance, the difference between the initial concentrations and threshold values plays a significant role in determining the duration of tumor growth. If an initial condition is close to its respective threshold value, it will not take long before the threshold is reached, leading

to the formation of quiescent and necrotic regions within the tumor. Conversely, if there is a substantial difference between the initial concentrations and their respective threshold values, the tumor will continue proliferating for a longer period of time before reaching the thresholds.

Additionally, the diffusion coefficients have a substantial impact on tumor growth dynamics. A high nutrient diffusion coefficient facilitates faster transport of nutrients from the boundary towards the center of the tumor. As a result, the tumor would need to grow larger before the nutrient supply at the center falls below the nutrient threshold. Conversely, a low nutrient diffusion coefficient leads to a slower distribution of nutrients from the boundary throughout the tumor domain. With a growing tumor, it becomes increasingly challenging for nutrients to reach the center, and as a consequence, the nutrient threshold is reached sooner. Thus, the diffusion coefficients directly affect the nutrient availability and can influence the tumor's size and nutrient supply dynamics.

In the model, the presence of both internally generated and externally supplied growth-inhibitor factors introduces additional complexity to the formation of GIF quiescent regions within the tumor. The locations within the tumor where the weighted sum of these two concentrations reaches the GIF-threshold can vary significantly based on changes in the distribution of either type of growth-inhibitor factors. Consequently, the initial time of formation of GIF quiescent regions and the locations are highly dependent on the diffusion coefficients and decay constants of $G1$ and $G2$, and also on the production/excretion constant of $G1$. These parameters directly influence the distribution of the growth-inhibiting concentrations within the tumor. Moreover, it's important to note that the comparison to the GIF-threshold is done using a weighted sum of the concentrations. Therefore, the weights assigned to each concentration also play a crucial role. By adjusting the weights, one can control the relative importance of each growth-inhibitor factor concentration in determining the location and extent of the quiescent regions.

In the equation for $G1$, the difference between the sink and production/excretion coefficients has a significant impact on whether the concentration of G1 will increase or decrease over time. In [2], the production/excretion coefficient is much larger than the sink coefficient, therefore in the reference problem used in the sensitivity analysis in the next chapter this relation will be maintained. Furthermore, suppose that $u_{G1} > u_{G2}$. If u_{G1} is so large that u_{G2} becomes negligible in the weighted sum, the GIF quiescent region will be a disk in the center. If the concentrations are of the same order and both contribute to the weighted sum, then the threshold will be reached in an annulus shape somewhere inside the tumor. The location highly depends on both diffusion coefficients. On the contrary, if $u_{G1} < u_{G2}$ and u_{G2} is the only significant contributor in the weighted sum, it will take a significant amount of time before the GIF-threshold is reached because u_{G2} is only being consumed within the tumor. Therefore, one would have to wait until u_{G1} becomes so large that the threshold is reached.

In addition to all the aforementioned factors, the variation in decay constants across different regions also affects tumor evolution. These decay constants are zero in necrotic regions, small in quiescent regions, and larger in proliferating regions. The diffusion coefficients, however, remain constant. This means that in necrotic regions, nutrients are still diffused into the regions even though there is no consumption. Similarly, in quiescent regions, some nutri-

ents are consumed, but not to the same extent as in proliferating regions. As a result, the concentration of nutrients increases in quiescent and necrotic regions. Consequently, after a certain period of time, the nutrient concentration may actually exceed the nutrient threshold. Therefore, it is possible for quiescent cells due to nutrient deficiency to become proliferating again. On the other hand, the necrotic cells remain necrotic, as this is explicitly stated as a part of the model. Hence, modifying the nutrient diffusion coefficient and decay constant will affect the extent to which nutrient-deficient cells can regain their proliferative capacity.

Some possible combinations of regions are shown below. Blue regions represent proliferating areas, red regions represent quiescent areas (both types), and black regions represent necrotic areas.

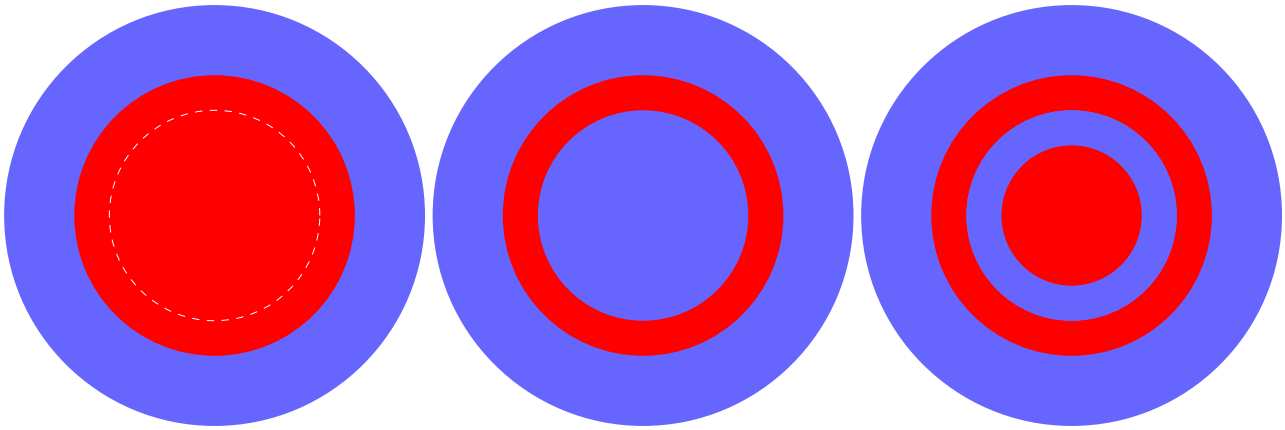

Figure 2.2: Possible quiescent regions

Figure 2.2 shows three possible combinations of proliferating and quiescent regions. In Figure 2.2(a), there is an outer annulus-shaped proliferating region, while the center consists of quiescent cells. The entire quiescent region may be composed of either only GIF quiescent cells or only nutrient-deprived quiescent cells. There is also a third option where the quiescent annulus outside the white stapled circle is composed of GIF quiescent cells, while the inner disk is composed of nutrient-deprived cells. This third option is related to the distribution in Figure 2.2(c), where the annulus-shaped quiescent region consists of GIF quiescent cells and the inner quiescent disk of nutrient-deprived cells. However, note that the quiescent regions are smaller in this case, and there is a proliferating region in between them. In Figure 2.2(b), there are no nutrient-deprived regions, only an annulus-shaped region where the GIF concentrations have surpassed θ_G.

Figure 2.3 displays two possible combinations of all three types of regions. The distribution in Figure 2.3(a) can occur if the previous combination of just proliferating and quiescent regions were distributed as in Figure 2.2(a), when both quiescent cell types were present, or equivalently as in Figure 2.2(c). The distribution in Figure 2.3(a) occurs if either the nutrient-

deprived area and/or the GIF quiescent area has grown such that these two regions overlap. When this happens, the cells in the overlapping area will have GIF concentrations above θ_G and nutrient levels below θ_N, and therefore become necrotic. Another possibility is that the previous quiescent region consisted entirely of nutrient-deprived cells, and then a GIF quiescent annulus-shaped region formed within this disk. This would cause the cells in the annulus to become necrotic.

The distribution in Figure 2.3(b) can result from several different cell type combinations. One possibility is that the entire center was previously quiescent due to high GIF levels, and when an inner part of the center was deprived of nutrients, the necrotic region formed. Another possibility is that the quiescent region initially was a disk-shaped region consisting solely of nutrient-deprived cells, and when the GIF concentrations became too high it happened in the center, and therefore the necrotic region formed in the center. Or the cells in the center had been deprived of nutrients for too long, that would also lead to a necrotic center. A third possibility is that the quiescent region consisted of an annulus-shaped region of GIF cells with an inner disk of nutrient-deprived cells. If the cells closest to the center were deprived of nutrients for too long, a necrotic disk would form, with an adjacent annulus-shaped region of quiescent nutrient-deprived cells, which, in turn, is adjacent to a GIF quiescent region displayed by the white stapled line in Figure 2.3(b).

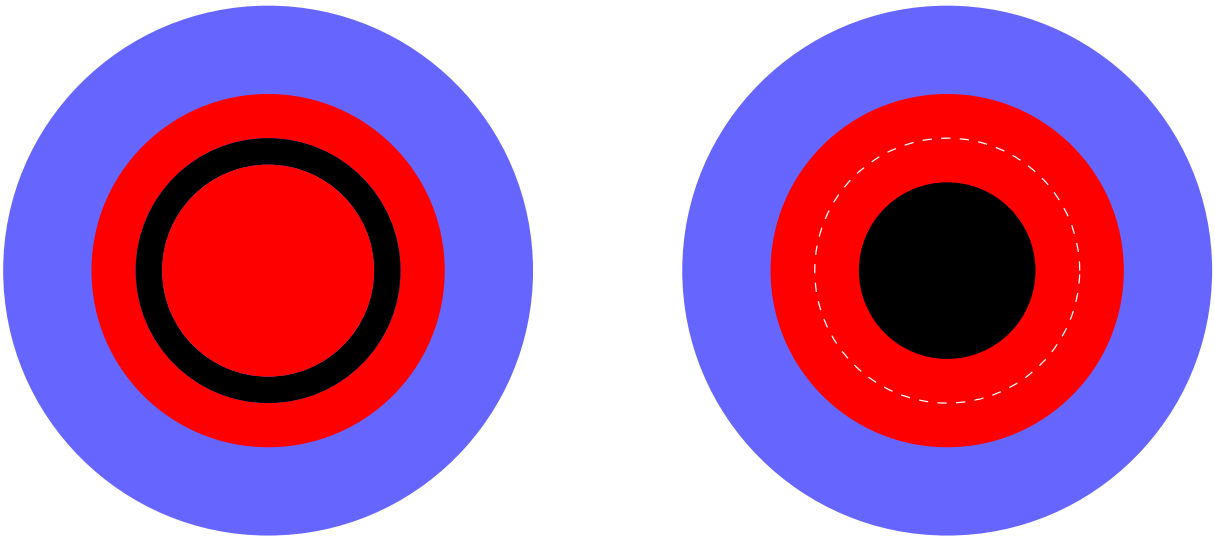

(a) (b)

Figure 2.3: Possible necrotic regions

2.2 Discretization of the mathematical model

In this section, we will discretize the model with respect to time and obtain the variational formulations.

The ODE representing the **change in number of cells** in the tumor is discretized using the forward Euler method. The ODE is as follows

$$\frac{dn_c}{dt} = n_{loc} \int_{\Omega_{pro}} \rho[-\nu_1 u_{G1} - \nu_2 u_{G2} + \eta u_N] dx \tag{2.31}$$

and the resulting discretized equation is

$$n_c^{new} = n_c^{previously} + \tau n_{loc} \int_{\Omega_{pro}} \rho[-\nu_1 u_{G1} - \nu_2 u_{G2} + \eta u_N] dx \tag{2.32}$$

where τ represents the time step and $n_c^{previously}$ denotes the number of cells the tumor was comprised of at the previous time.

The PDE representing the **evolution of nutrient concentration** is given by

$$\partial_t u_N + \nabla \cdot (-D_N \nabla u_N + \vec{c}_N u_N) = -\alpha n_{loc} u_N. \tag{2.33}$$

To discretize the PDE, we start by approximating the time derivative using the backward Euler method, resulting in the following equation

$$u_N^n + \tau \nabla \cdot (-D_N \nabla u_N^n + \vec{c}_N u_N^n) = -\tau \alpha n_{loc} u_N^n + u_N^{n-1}. \tag{2.34}$$

Proceeding to discretize with respect to space, we will use the Finite Element method with P1 elements. To obtain the finite dimensional variational formulation, we multiply the equation by a test function, v_N^n and integrate over the domain. Moreover, gathering all terms containing the unknown u_N^n on the left side results in

$$\int_\Omega u_N^n v_N^n + \tau \alpha n_{loc} u_N^n v_N^n \, dx + \int_\Omega \tau \nabla \cdot (-D_N \nabla u_N^n + \vec{c}_N u_N^n) v_N^n \, dx = \int_\Omega u_N^{n-1} v_N^n \, dx. \tag{2.35}$$

Furthermore, by applying integration by parts to the second term on the left-hand side, we can rewrite the term as follows

$$\int_\Omega \tau \nabla \cdot (-D_N \nabla u_N^n + \vec{c}_N u_N^n) v_N^n \, dx = \tag{2.36}$$

$$-\tau \int_\Omega (-D_N \nabla u_N^n + \vec{c}_N u_N^n) \cdot \nabla v_N^n \, dx + \tau \int_{\partial\Omega} \nu \cdot (-D_N \nabla u_N^n + \vec{c}_N u_N^n) v_N^n \, ds \tag{2.37}$$

where ν denotes the outward pointing unit normal vector at the boundary. Due to v_N^n having compact support on the boundary, v_N^n is equal to zero at the boundary. Thus, we are left with the following equality.

$$\int_\Omega \tau \nabla \cdot (-D_N \nabla u_N^n + \vec{c}_N u_N^n) v_N^n \, dx = \tau \int_\Omega (D_N \nabla u_N^n - \vec{c}_N u_N^n) \cdot \nabla v_N^n \, dx. \tag{2.38}$$

The resulting finite dimensional variational formulation is

$$\int_\Omega u_N^n v_N^n + \tau\alpha n_{loc} u_N^n v_N^n \, dx + \tau \int_\Omega (D_N \nabla u_N^n - \vec{c}_N u_N^n) \cdot \nabla v_N^n \, dx = \int_\Omega u_N^{n-1} v_N^n \, dx. \tag{2.39}$$

The bilinear form is

$$a_N(u_N^n, v_N^n) := \int_\Omega u_N^n v_N^n + \tau\alpha n_{loc} u_N^n v_N^n \, dx + \tau \int_\Omega (D_N \nabla u_N^n - \vec{c}_N u_N^n) \cdot \nabla v_N^n \, dx \tag{2.40}$$

and the linear form is

$$L_N(v_N^n) := \int_\Omega u_N^{n-1} v_N^n \, dx. \tag{2.41}$$

The PDE representing the **evolution of *G2* concentration** is as follows

$$\partial_t u_{G2} + \nabla \cdot (-D_{G2} \nabla u_{G2} + \vec{c}_{G2} u_{G2}) = -\xi n_{loc} u_{G2}. \tag{2.42}$$

By following the exact same steps as when discretizing the nutrient PDE, we obtain the finite dimensional variation formulation for G2, which is as follows

$$\int_\Omega u_{G2}^n v_{G2}^n + \tau\xi n_{loc} u_{G2}^n v_{G2}^n \, dx + \tau \int_\Omega (D_{G2} \nabla u_{G2}^n - \vec{c}_{G2} u_{G2}^n) \cdot \nabla v_{G2}^n \, dx = \int_\Omega u_{G2}^{n-1} v_{G2}^n \, dx. \tag{2.43}$$

With the bilinear form

$$a_{G2}(u_{G2}^n, v_{G2}^n) := \int_\Omega u_{G2}^n v_{G2}^n + \tau\xi n_{loc} u_{G2}^n v_{G2}^n \, dx + \tau \int_\Omega (D_{G2} \nabla u_{G2}^n - \vec{c}_{G2} u_{G2}^n) \cdot \nabla v_{G2}^n \, dx \tag{2.44}$$

and linear form

$$L_{G2}(v_{G2}^n) := \int_\Omega u_{G2}^{n-1} v_{G2}^n \, dx. \tag{2.45}$$

Regarding the discretization of the ***G1* PDE**, it should be noted that the boundary condition is of Neumann type. This implies that the value of u_{G1} is not known on the boundary. Consequently, a test function v_{G1} will not have compact support at the boundary.

The G1 PDE is as follows

$$\partial_t u_{G1} + \nabla \cdot (-D_{G1}(x, y) \nabla u_{G1}) = -\gamma u_{G1} + \lambda S(x, y). \tag{2.46}$$

Following the same approach as used for the other two PDEs, we will discretize the time derivative using the backward Euler method for this PDE as well. This leads to the following time-discrete, space-continuous equation,

$$u_{G1}^n + \tau \nabla \cdot (-D_{G1} \nabla u_{G1}^n) = -\tau\gamma u_{G1}^n + \tau\lambda S + u_{G1}^{n-1}. \tag{2.47}$$

To discretize the equation with respect to space, we multiply the preceding equation by a test function v_{G1}^n and integrate it over the domain.

$$\int_\Omega u_{G1}^n v_{G1}^n \, dx + \int_\Omega \tau\gamma u_{G1}^n v_{G1}^n \, dx + \int_\Omega \tau \nabla \cdot (-D_{G1} \nabla u_{G1}^n) v_{G1}^n \, dx = \int_\Omega \tau\lambda S \, dx + \int_\Omega u_{G1}^{n-1} v_{G1}^n \, dx. \tag{2.48}$$

Applying integration by parts to the third term on the left-hand side results in the following equality.

$$\int_\Omega \tau\nabla\cdot(-D_{G1}\nabla u_{G1}^n)v_{G1}^n dx = -\tau\int_\Omega(-D_{G1}\nabla u_{G1}^n)\cdot\nabla v_{G1}^n dx+\tau\int_{\partial\Omega}\vec{n}\cdot(-D_{G1}\nabla u_{G1}^n)v_{G1}^n ds \quad (2.49)$$

where $\vec{n}$ denotes the outward pointing unit normal vector at the boundary. The Neumann boundary condition states that $\vec{n}\cdot(-D_{G1}\nabla u_{G1}^n)=0$. Therefore, the preceding equality simplifies to

$$\int_\Omega \tau\nabla\cdot(-D_{G1}\nabla u_{G1}^n)v_{G1}^n\,dx = \tau\int_\Omega(D_{G1}\nabla u_{G1}^n)\cdot\nabla v_{G1}^n\,dx. \quad (2.50)$$

The resulting finite dimensional variational problem is

$$\int_\Omega u_{G1}^n v_{G1}^n dx+\int_\Omega \tau\gamma u_{G1}^n v_{G1}^n dx+\tau\int_\Omega(D_{G1}\nabla u_{G1}^n)\cdot\nabla v_{G1}^n dx = \int_\Omega \tau\lambda S dx+\int_\Omega u_{G1}^{n-1}v_{G1}^n dx \quad (2.51)$$

where the bilinear from is

$$a_{G1}(u_{G1}^n, v_{G1}^n) := \int_\Omega u_{G1}^n v_{G1}^n\,dx + \int_\Omega \tau\gamma u_{G1}^n v_{G1}^n\,dx + \tau\int_\Omega(D_{G1}\nabla u_{G1}^n)\cdot\nabla v_{G1}^n\,dx \quad (2.52)$$

and the linear form is

$$L_{G1}(v_{G1}) := \int_\Omega \tau\lambda S\,dx + \int_\Omega u_{G1}^{n-1}v_{G1}^n\,dx. \quad (2.53)$$

Summary of the discretized equations

$$n_c^{new} = n_c^{previously} + \tau n_{loc}\int_{\Omega_{pro}}\rho[-\nu_1 u_{G1}-\nu_2 u_{G2}+\eta u_N]dx. \quad (2.54)$$

$$a_N(u_N^n, v_N^n) := \int_\Omega u_N^n v_N^n + \tau\alpha n_{loc}u_N^n v_N^n\,dx + \tau\int_\Omega(D_N\nabla u_N^n - \vec{c}_N u_N^n)\cdot\nabla v_N^n\,dx. \quad (2.55)$$

$$L_N(v_N^n) := \int_\Omega u_N^{n-1}v_N^n\,dx. \quad (2.56)$$

$$a_{G2}(u_{G2}^n, v_{G2}^n) := \int_\Omega u_{G2}^n v_{G2}^n + \tau\xi n_{loc}u_{G2}^n v_{G2}^n\,dx + \tau\int_\Omega(D_{G2}\nabla u_{G2}^n - \vec{c}_{G2}u_{G2}^n)\cdot\nabla v_{G2}^n\,dx. \quad (2.57)$$

$$L_{G2}(v_{G2}^n) := \int_\Omega u_{G2}^{n-1}v_{G2}^n\,dx. \quad (2.58)$$

$$a_{G1}(u_{G1}^n, v_{G1}^n) := \int_\Omega u_{G1}^n v_{G1}^n\,dx + \int_\Omega \tau\gamma u_{G1}^n v_{G1}^n\,dx + \tau\int_\Omega(D_{G1}\nabla u_{G1}^n)\cdot\nabla v_{G1}^n\,dx. \quad (2.59)$$

$$L_{G1}(v_{G1}^n) := \int_\Omega \tau\lambda S\,dx + \int_\Omega u_{G1}^{n-1}v_{G1}^n\,dx. \quad (2.60)$$

2.3 Implementation of the mathematical model

The implementation has been written in Visual Studio Code (VS Code) using the Python programming language. VS Code is deployed within a Docker container. For the finite element method, the FEniCS library has been utilized. This library enables writing a substantial portion of the code in a way that closely resembles the notation used in finite element theory. For instance, the library handles the generation of the function space, requiring the coder only to specify the desired space. As a result, FEniCS greatly simplifies the process of solving partial differential equations using the finite element method.

The code structure
To begin with, one needs to choose parameter values and define the functions that form the partial differential equations. Additionally, decisions must be made regarding the initial number of cells, the size of each cell, the percentage of extracellular matrix within the tumor, the size of triangular elements, the time step, boundary data, initial values, threshold values, and unit conversions. Although the code represents time and length dependent variables in seconds and centimeters, it allows for easy modification of values to accommodate different units (e.g., from seconds to minutes or centimeters to millimeters).

Given the initial number of cells, the size of each cell, and the percentage of extracellular matrix, the radius of the assumed circular domain can be computed. Furthermore, by specifying an element size, the initial mesh can be generated using FEniCS. The mesh generation process involves defining a domain object and utilizing a built-in mesh generation function, which takes the domain and the desired number of elements as input. In addition, one defines the function space over the triangular elements, known as P1-elements, using the newly created mesh. FEniCS provides a built-in function space class that facilitates this process, requiring the mesh, function type, and function degree as inputs. This stage of the implementation closely follows the notation used in finite element theory. Furthermore, boundary and initial data are connected to the mesh using FEniCS built-in functions and classes.

With all the necessary components in place, it is time to start solving the growth problem. The code performs the following calculations at each time step until all proliferating regions have vanished, i.e., the tumor has stopped growing. First, the vertices of the mesh are classified into proliferating, quiescent, or necrotic regions. To accomplish this, a function has been implemented to take the current mesh (i.e., the vertices), concentration solutions, and threshold values as input. It evaluates the concentration values at each vertex against the cell-type criteria, and ensures that all necrotic vertices remain necrotic. Utilizing the functionality provided by FEniCS, the mesh is divided into subdomains based on the coordinates of these vertices. The subdomains represent proliferating regions, quiescent regions due to high growth-inhibitor concentrations, quiescent regions due to nutrient deficiency, and necrotic regions.

Once the proliferating regions are identified, the growth of the tumor can be calculated, which means to calculate the new number of cells. The number of cells is determined by solving an ordinary differential equation (ODE) using the forward Euler method. The mitotic function,

which is non-zero only in proliferating regions, contributes to the cell count calculation. The next step involves computing the new tumor radius using the previously mentioned function, which depends on the number of cells, the radius of a single cell, and the percentage of extracellular matrix. Subsequently, the corresponding new mesh and P1-elements are defined using FEniCS functions and classes. Furthermore, the concentrations obtained from the previous step, when the mesh was smaller, need to be extrapolated onto the new mesh. While extrapolation can be challenging, FEniCS provides a built-in mechanism to handle this, simplifying the process.

With the concentrations defined on the mesh, the next step involves redefining the mesh to include proliferating, quiescent, and necrotic subdomains. This is done by following the same procedure as described above. Using FEniCS functionality the boundary data and other space-dependent parameters are adjusted to be valid on the new mesh. Additionally, trial, test, and solution functions are defined with respect to the new mesh.

Having the new mesh and the previous concentrations defined on it, one can proceed to solve the equations and obtain solutions at the current time. This involves solving the variational problems of the partial differential equations, where the time derivatives have been discretized using the backward Euler method. A class has been implemented to generate the necessary bilinear and linear forms for the variational problem. This class takes all region-dependent variables as input and utilizes FEniCS functionality to define the respective bilinear and linear forms.

To solve the variational problems, the built-in solver in FEniCS is utilized. In this case, a Multifrontal Massively Parallel Sparse direct Solver (MUMPS) is used. The equations are solved in the following order: first, the nutrient equation, then the first growth-inhibitor equation, and finally the second growth-inhibitor PDE.

After solving the equations, the process continues to the next time step, repeating the classification of mesh vertices based on the new solutions, and assessing the tumor's growth. The iteration continues until there are no more proliferating regions, indicating that the tumor has ceased growing.

The structure of the code is schematized in the flow chart below.

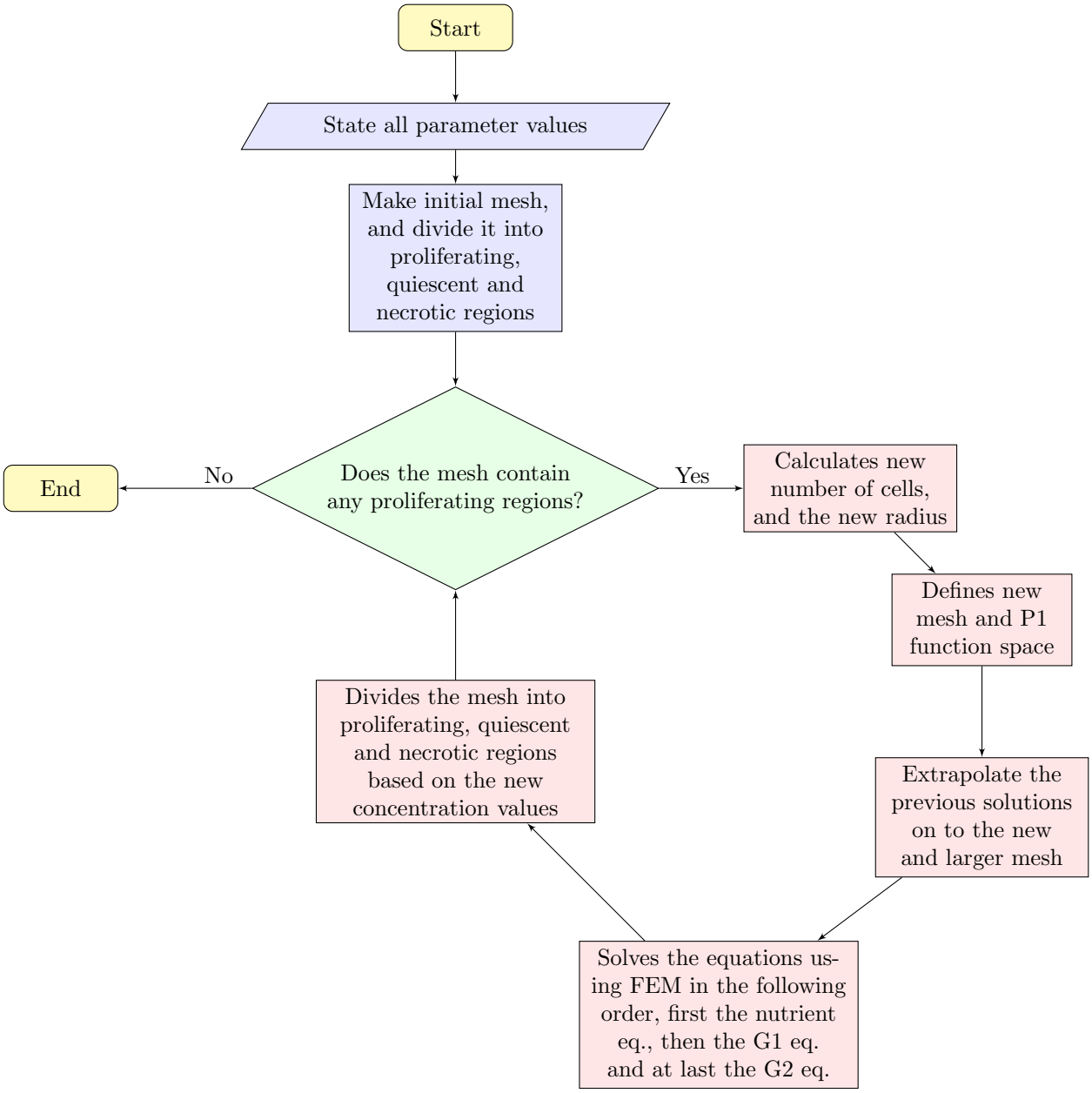

Figure 2.4: Flow chart of the code structure.

Chapter 3

Numerical results

In this chapter, numerical results produced by the mathematical model will be presented. First, we will define and examine the reference solution, followed by an exploration of how modifying parameters affect tumor growth.

3.1 The reference solution

The reference case was chosen such that the initial tumor is classified as a small tumor. The size is defined as the longest length of the tumor, which is the distance between the two points farthest from one another [39]. Given that avascular tumors usually do not become particularly large, this is a reasonable initial size. The initial radius is 0.5677 mm meaning the size, which is the diameter due to the model assumption that a tumor is perfectly circular, is 1.1354 mm. Initially, the tumor is fully proliferating, but after 630 minutes, a disk in the center of the tumor has insufficient nutrients to sustain proliferation and becomes quiescent. As a result, only a smaller part of the tumor continues to proliferate, leading to slower growth. Thus, it is possible for enough nutrients to diffuse into the quiescent region and cause cells to proliferate again. This cycle of alternating proliferation and quiescence continues until the tumor becomes so large that nutrient-deficient regions persist. In addition, after 780 minutes the growth-inhibitor concentrations have increased enough to surpass the growth-inhibitor threshold, θ_G, causing a larger portion of the tumor to become quiescent. Ten minutes later, the center of the tumor experiences both growth-inhibitor concentrations above θ_G and nutrient concentration below θ_N, leading to cell death and the formation of a necrotic region. After 1780 minutes, approximately 29 hours, all cells have become quiescent or necrotic, and tumor evolution ceases.

In Figure 3.1, we can observe the changes in radius over time, while Figure 3.2 displays the variations in the number of cells. It is evident that the curves in both figures exhibit similar shapes. This is because there is a linear relationship between a tumor's radius and the number of cells comprising the tumor. From both figures, we can see that the tumor grows fastest in the beginning, which makes sense because then the entire tumor is fully proliferating. After approximately 800 minutes, the growth slows down, which is when the quiescent

regions have become significantly large, and necrotic regions form. From there on the growth rate decreases until the entire tumor stops growing.

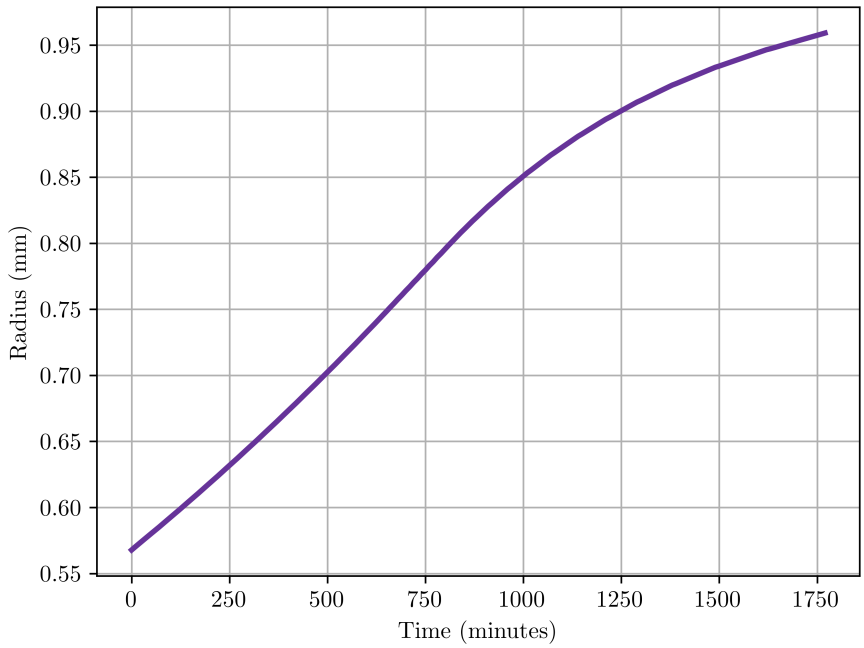

Figure 3.1: Radius vs time, reference solution

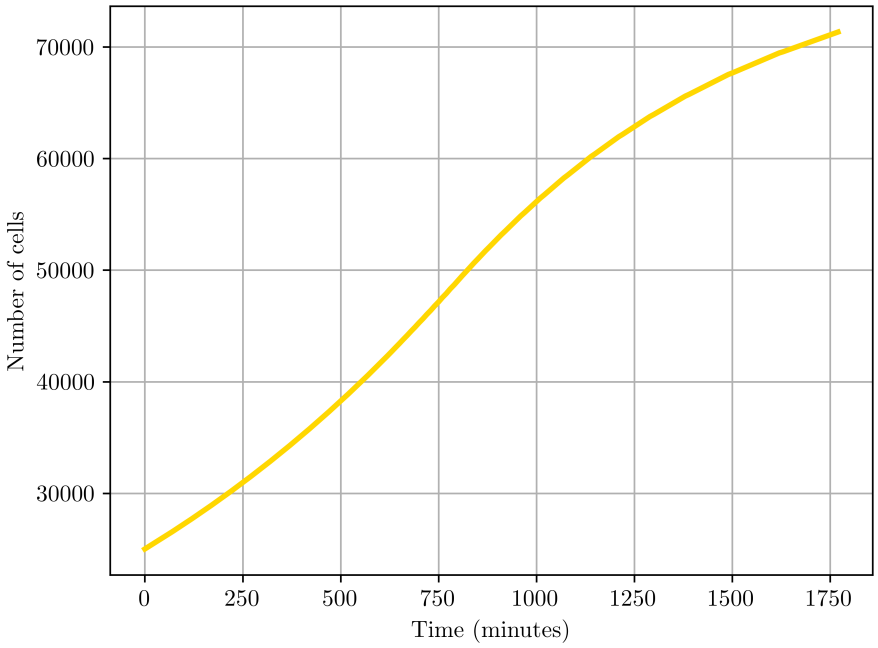

Figure 3.2: Number of cells vs time, reference solution

In Figure 3.3 we can see how the tumor has grown, and also how the cell type distribution has altered. The light brown regions represent proliferating cells, the blue regions represent quiescent cells, and the red regions represent necrotic cells.

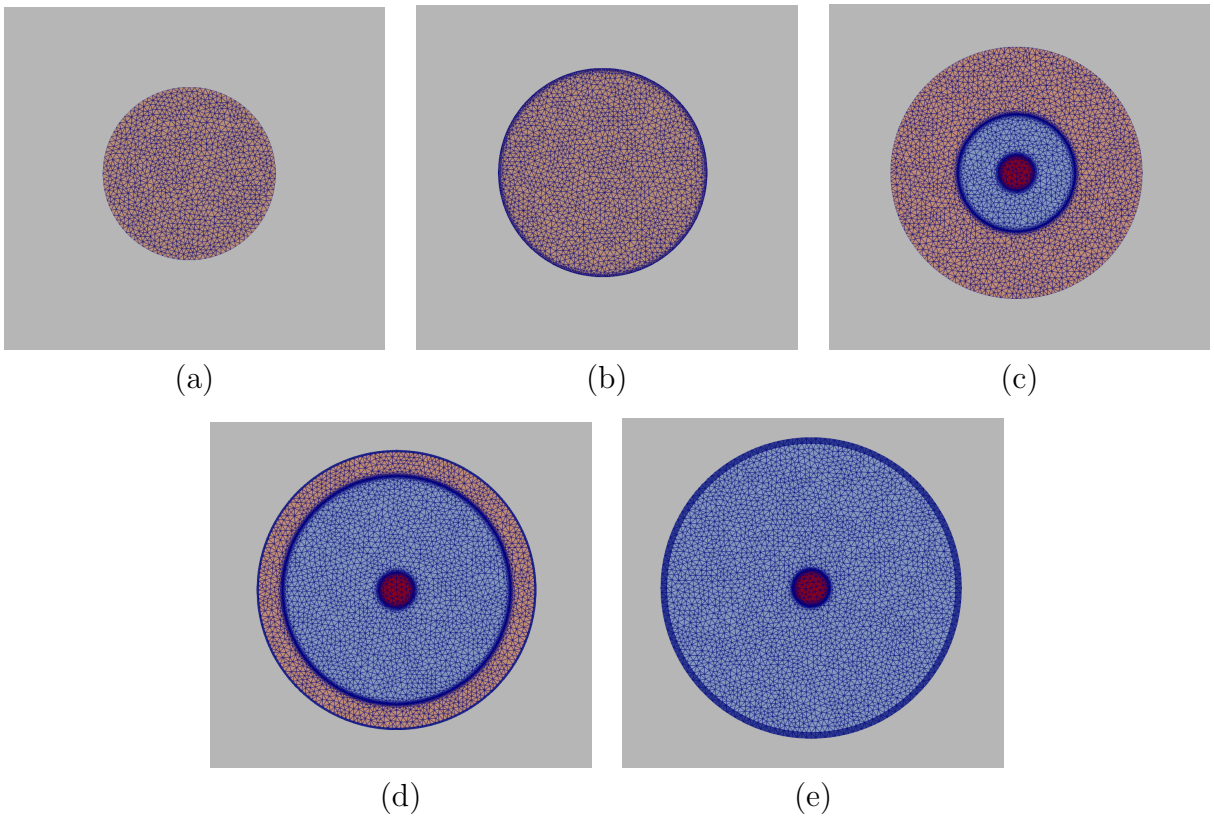

Figure 3.3: (a) Initial cell distribution (b) The cell distribution after 445 minutes (c) The cell distribution after 890 minutes (d) The cell distribution after 1330 minutes (e) The final cell distribution. In the transition between subdomains, FEniCS has significantly refined the mesh to ensure an accurate approximation in these regions where the cell types alters.

From Figure 3.3(a), we observe that the tumor was initially in a state of full proliferation. Furthermore, Figure 3.3(b) illustrates that after 445 minutes the tumor has grown and remains fully proliferating. By the 890th minute, as shown in Figure 3.3(c), both quiescent and necrotic regions have emerged in the central area. In Figure 3.3(d), we can see a significant growth of the quiescent region, with only a small annulus-shaped proliferating region remaining. The necrotic region appears to have undergone minimal changes. Additionally, Figure 3.3(e) portrays the cell distribution at the point where tumor growth ceased, consisting exclusively of quiescent and necrotic cells.

Parameter		**Value**
sc		10
T		60
n_0		25000
r_c	$[mm]$	$sc \times 3.5 \times 10^{-4}$
p_{extrm}		0.05
h	$[mm^2]$	0.05
k	$[min]$	10
α_{pro}	$[\frac{mm^2}{min}]$	$T \times sc^2 \times 10^{-8}$
α_{qui}	$[\frac{mm^2}{min}]$	$T \times sc^2 \times 0.5 \times 10^{-8}$
α_{nec}	$[\frac{mm^2}{min}]$	0
γ_{proqui}	$[min^{-1}]$	$T \times 5 \times 10^{-5}$
γ_{nec}	$[min^{-1}]$	0
λ	$[mm^{-2}min^{-1}]$	$\frac{T}{sc^2} \times 0.00325$
ξ_{proqui}	$[\frac{mm^2}{min}]$	$T \times sc^2 \times 10^{-8}$
ξ_{nec}	$[\frac{mm^2}{min}]$	0
κ		3
ψ		0.1
η	$[\frac{mm^2}{min}]$	$T \times sc^2 \times 10^{-6}$
ν_1	$[\frac{mm^2}{min}]$	$T \times sc^2 \times 10^{-7}$
ν_2	$[\frac{mm^2}{min}]$	$T \times sc^2 \times 10^{-7}$
ρ	$[mm^2]$	$sc^2 \times 0.5 \times 10^{-3}$
D_N	$[\frac{mm^2}{min}]$	$T \times sc^2 \times 5 \times 10^{-4}$
D_{G2}	$[\frac{mm^2}{min}]$	$T \times sc^2 \times 5 \times 10^{-4}$
$D_{G1}(x, y)$	$[\frac{mm^2}{min}]$	$T \times sc^2 \times 5 \times 10^{-7} \times (1 - 0.2(x^2 + y^2))$
$\vec{c}_N$	$[\frac{mm}{min}]$	$[T \times sc \times 10^{-5}, 0]$
$\vec{c}_{G2}$	$[\frac{mm}{min}]$	$[T \times sc \times 10^{-5}, 0]$
$u_{G1,0}$		0.1
$u_{G2,0}$		0
$u_{N,0}$		3
θ_N		2.81
θ_G		0.416
Nutrient deprivation time		6 hours

Table 3.1: Reference values.

3.2 Sensitivity analysis

The purpose of conducting a sensitivity analysis is to determine the extent to which a parameter affects the growth and how it influences it. Furthermore, the sensitivity analysis allows us to assess whether the mathematical model aligns with the expected tumor evolution and conforms to physical and biological principles. Throughout the remaining chapters, all results will be compared to the reference solution, see Table 3.1 for the reference values, unless

otherwise specified.

3.2.1 Diffusion coefficients

In this section, we will explore how altering the diffusion coefficients, one at a time, will affect the growth. Remember that, with respect to the mathematical model, the diffusion coefficients determine the rate at which their respective concentrations diffuse. That is, they govern how fast a substance move from an area of high concentration to an area of low concentration. For the nutrients and G2 concentrations, diffusion leads to a flow directed inwards towards the center of the tumor. This is because they are supplied at the boundary, thus having the highest concentration there, and are only consumed inside, resulting in the lowest concentration at the center, farthest from the boundary. On the other hand, G1 is produced/excreted inside the tumor with the highest production/excretion level at the center, gradually decreasing towards zero at the boundary. In other words, the G1 concentration is highest in the center and lowest at the boundary, indicating that diffusion will induce a flow from the center towards the boundary in this case.

Figures 3.4 and 3.5, and Table 3.2 show the impact of the nutrient diffusion coefficient on tumor growth. It is important to note that nutrients are only supplied at the boundary and consumed inside the tumor. When the diffusion coefficient is small, the nutrients supplied at the boundary move slowly inwards. Consequently, the tumor in this case has a lower nutrient concentration at the center compared to the reference solution. The lower nutrient concentration leads to earlier formation of quiescent regions, where cells become dormant due to a lack of nutrients. This phenomenon is evident in Table 3.2, specifically in the fifth column for sensitivity cases (i), (ii), (iii), and (iv). Once quiescent regions have formed, only a smaller portion of the tumor remains actively proliferating, resulting in slower growth. Due to the slow growth, it is possible for nutrients to diffuse into the quiescent regions and transition the cells back to proliferative state. This is particularly likely immediately after the initial formation of nutrient-deprived quiescent regions when these regions are small. Although this alternating cycle between fully proliferating and partially proliferating inhibits growth, its impact is not significant.

Nutrient diffusion coefficient	$\boldsymbol{D_N}$ $(T \times sc^2)$	Final radius (mm)	Quiescent, GIF's	Quiescent, lack of nutrients	Necrotic	Stop time (minutes)
The reference case	5.000×10^{-4}	0.9591	780	630	790	1780
(i)	3.000×10^{-4}	0.7903	830	160	790	930
(ii)	3.500×10^{-4}	0.8121	810	240	790	980
(iii)	4.000×10^{-4}	0.8228	790	380	780	990
(iv)	4.500×10^{-4}	0.8456	780	530	790	1070
(v)	5.500×10^{-4}	0.9602	780	750	790	1790
(vi)	6.000×10^{-4}	1.2640	780	-	2130	3260
(vii)	6.500×10^{-4}	1.3292	780	-	2320	3580
$(viii)$	7.000×10^{-4}	1.3800	780	-	2510	3620

Table 3.2: Tumor evolution, altered D_N.

Regarding the formation of growth-inhibitor quiescent regions, one should note that the G1 concentration is the main contributor in reaching the GIF threshold, θ_G. Furthermore, it should be noted that the source term of G1 is space dependent, with highest production/excretion in the center and decreasing towards zero at the boundary. Hence, the larger the domain, the higher the G1 production/excretion is within a given area. In cases with smaller nutrient diffusion coefficients, the growth of the tumor will be slightly smaller compared to the reference case due to the earlier formation of quiescent regions caused by nutrient deprivation. Therefore, in these cases, since the tumor sizes are smaller, one would expect the formation of quiescent regions due to high growth-inhibitor concentrations to occur later than in the reference case. This is evident in Table 3.2, specifically in the fourth column for sensitivity cases (i)-(iii). For sensitivity case (iv), the diffusion coefficient has been reduced, but apparently not enough to substantially alter the concentrations of growth-inhibitors. As a result, in this case, the formation of growth-inhibitor-induced quiescent regions occurred at the same time as in the reference solution.

Necrotic regions can form as a result of either a lack of nutrients for more than 6 hours or a combination of nutrient deficiency and high growth-inhibitor (GIF) concentrations. In Table 3.2, for sensitivity cases (i)-(iv) the formation time of necrotic regions for decreased nutrient diffusion coefficients can be observed in the sixth column. Since the timing of necrotic region formation is quite similar across all cases and considering that nutrient-deprived cells alternate between dormant and proliferating states, it is reasonable to conclude that necrotic cells are a result of high GIF concentrations and nutrient deficiency.

As mentioned, the early onset of nutrient-deprived quiescent cells leads to a smaller proliferating area earlier than in the reference problem, resulting in smaller growth. The necrotic regions are thus formed in a smaller tumor compared to the reference case, leading to an overall smaller growth and growth period. This trend can be observed in Table 3.2, specifically in the third and seventh columns for sensitivity cases (i)-(iv), respectively. The same pattern is visualized in Figure 3.4, where the radius at each time step is plotted for all the different cases. The four lower graphs represent the cases where the nutrient diffusion coefficient has decreased. It can be observed that these cases grow for approximately 1000 minutes before ceasing to grow, and their growth is always below the reference graph, indicating a smaller radius.

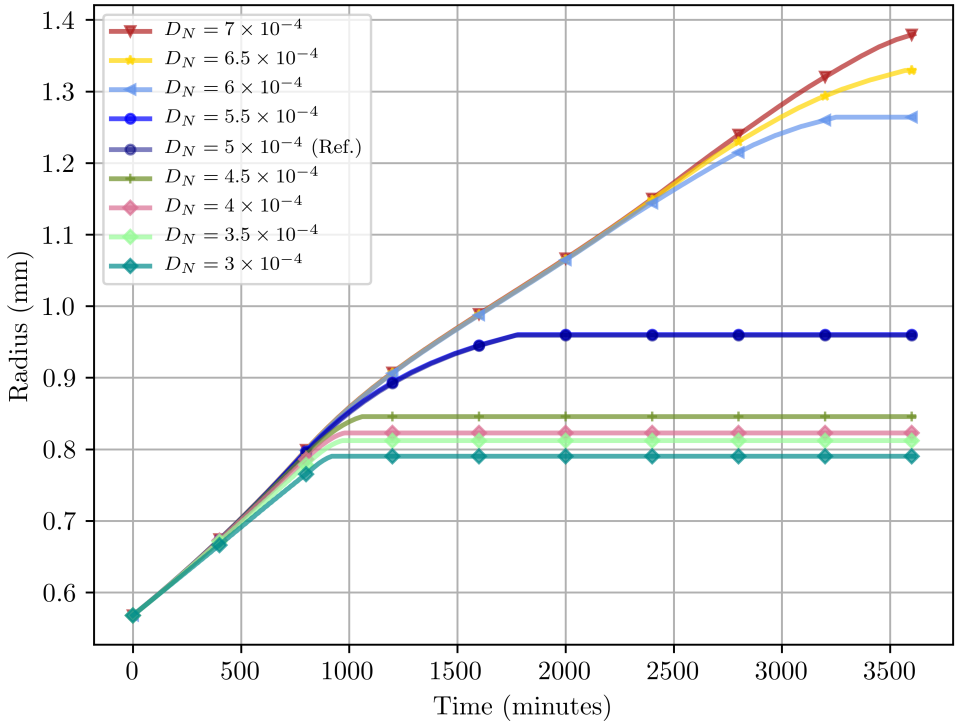

Figure 3.4: Radius vs time, altered D_N.

In the lower half of Table 3.2, the nutrient diffusion coefficients have increased compared to the reference coefficient. A higher diffusion coefficient means that nutrients supplied at the boundary are transported faster towards the center, where the concentration is lowest. Consequently, the tumor center in these cases has a higher nutrient concentration compared to the reference case. A higher nutrient concentration implies that it takes more time before nutrient-deprived quiescent regions form. Furthermore, it is possible that the diffusion is so high that quiescent regions due to excessive growth-inhibitor concentrations have already formed and are large enough that when the nutrient level drops below the threshold, necrotic regions immediately form. This was observed in the three cases with the highest nutrient diffusion coefficients analyzed. From the onset of necrosis, it is evident that it took a long time for the nutrient concentration to decrease enough to reach the threshold, as shown in Table 3.2, column 6, for sensitivity cases (vi)-$(viii)$. Regarding sensitivity case (v), a nutrient-deprived quiescent region formed, but much later compared to the reference solution, as expected. In this case, the necrotic region formed immediately after the GIF quiescent region formed. It can be seen from Table 3.2 that in these cases with high diffusion coefficients, quiescent regions due to excessive growth-inhibitors formed at the same time as in the reference case. Therefore, the increase in growth rate is not significant enough to result in earlier formation of quiescent regions due to excessive growth-inhibitors.

In all these cases with high diffusion coefficients, the tumor remains fully proliferating for a longer period of time compared to the reference case. Additionally, the nutrient concentration is more evenly distributed, leading to increased growth at each time step. Therefore, one would expect these tumors to grow for a longer duration and reach larger sizes than the reference tumor. Figure 3.4 clearly shows that the cases with increased nutrient diffusion

coefficients grow for a longer period of time than the reference case, and that their final radii are larger (as indicated by the curves being above the reference curve). In Figure 3.5, the final radii is plotted against the respective nutrient diffusion coefficient values. It demonstrates that increasing the diffusion coefficient results in a larger final radius, while decreasing the nutrient coefficient leads to smaller growth. It is evident, expect for small alterations in D_N, that increasing the nutrient diffusion coefficient has a greater impact on growth compared to decreasing it.

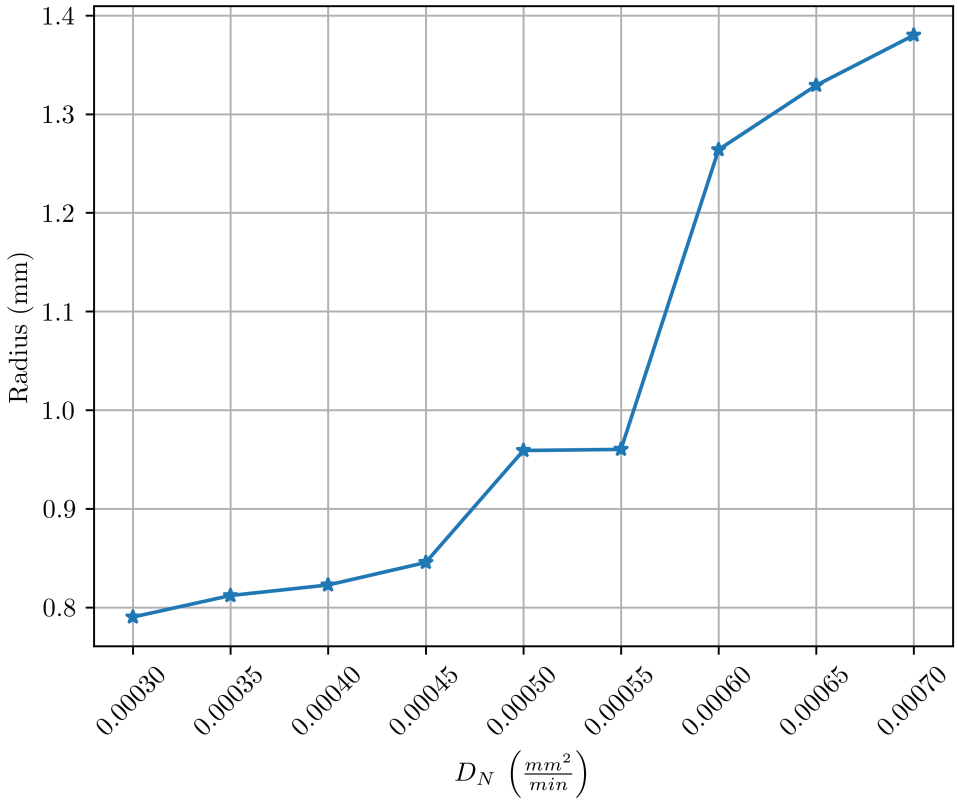

Figure 3.5: Final radius vs D_N.

Before proceeding to analyze the results obtained by modifying the diffusion coefficient for the second growth-inhibitor factor, G2, it is important to note that G2 is externally supplied and is only consumed within the tumor. Additionally, it is worth noting that G2 is combined with internally produced/excreted G1 in a weighted sum, which is then compared to the GIF threshold, θ_G. However, it is observed that the G1 concentration surpasses the G2 concentration relatively quickly, making G1 the primary contributor to reaching θ_G. Consequently, any changes in the G2 diffusion coefficient would not be expected to significantly alter tumor growth. In fact, when examining all the cases tested in Table 3.3, it is evident that the occurrence of different types of regions happens at the same time as in the reference case. This indicates that the overall tumor evolution has not been significantly affected. The formation of GIF quiescent regions consistently occurs after 780 minutes, nutrient-lacking quiescent regions after 630 minutes, and necrotic regions after 790 minutes.

Altering the diffusion coefficient influences how fast G2 is transported towards the center

of the tumor where the concentration is smallest. When the diffusion coefficient is small, one would expect the quiescent region to either appear as an annulus closer to the boundary compared to the initial quiescent region in the reference case, or alternatively as a disk with larger radius compared to the initial quiescent region in the reference case. This is because smaller diffusion coefficients result in lower G2 concentrations in the center, requiring one to move closer to the boundary for the G2 concentration to be high enough for θ_G to be reached. Furthermore, it's worth noting that since G1 is produced/excreted within the tumor and has the highest production/excretion level in the center, the annular quiescent region will soon become disk-shaped. Consequently, in cases with decreased G2 diffusion coefficients, the quiescent regions covers a larger portion of the tumor. As a result, one would expect the final tumor size to be smaller compared to the reference case.

On the other hand, when the diffusion coefficient increases, the supply of G2 at the boundary is transported faster towards the center. In these cases, the G2 concentration in the center will be higher compared to the G2 concentration in the center of the reference case. Therefore, one would expect the initial quiescent region to appear closer to the center compared to the reference solution. As a result, the tumor should grow faster, due to a larger part of the tumor remaining proliferating, and lead to a larger final size compared to the reference solution. It is also possible that the diffusion coefficient becomes so high that the G2 concentration becomes evenly distributed, resulting in minimal difference between the concentration at the boundary and the concentration at the center. In such cases, one would expect the initial quiescent region to be disk-shaped with a larger radius than the initial quiescent region in the reference case. Consequently, the tumor would experience slower growth and reach a smaller final size.

Second growth-inhibitor factor diffusion coefficient	$\boldsymbol{D_{G2}}$ $(T \times sc^2)$	Final radius (mm)	Stop time (minutes)
The reference case	5.000×10^{-4}	0.9591	1780
(i)	3.000×10^{-4}	0.9543	1760
(ii)	3.500×10^{-4}	0.9555	1790
(iii)	4.000×10^{-4}	0.9552	1740
(iv)	4.500×10^{-4}	0.9558	1790
(v)	5.500×10^{-4}	0.9660	1910
(vi)	6.000×10^{-4}	0.9730	1970
(vii)	6.500×10^{-4}	0.9843	2110
$(viii)$	7.000×10^{-4}	0.9723	1950
(ix)	7.500×10^{-4}	0.9695	1940
(x)	8.000×10^{-4}	0.9578	1790
(xi)	8.500×10^{-4}	0.9531	1740

Table 3.3: Tumor evolution, altered D_{G2}.

For sensitivity cases (i)-(iv) of Table 3.3 the diffusion coefficient is reduced compared to the reference case. As expected, all final radii are slightly smaller than the reference radius. However, when comparing the final radii and total growth time for the cases with smaller D_{G2}, it

becomes clear that they are not strictly decreasing. This is because the evolution of the tumor is influenced by the shape of the initial quiescent region. If it is annulus-shaped, the remaining proliferating region is larger for a short period until the quiescent region becomes disk-shaped. Consequently, the tumor grows at a higher rate for a short period of time, and as a result, achieves a slightly larger final tumor size compared to cases where the initial quiescent region is disk-shaped. Furthermore, the reason why one can have an increase in growth time, even though the total growth is smaller, is because when the growth rate decreases so does the production/excretion of G1. In other words, the quiescent GIF region will grow slower.

In Figure 3.6, the relationship between final radii and diffusion coefficients is plotted. It is evident that when the diffusion coefficient is reduced compared to the reference case, the final radius also decreases relative to the reference end radius. However, perhaps the most important observation is that decreasing D_{G2}, relative to the reference case, only has a minor effect on growth.

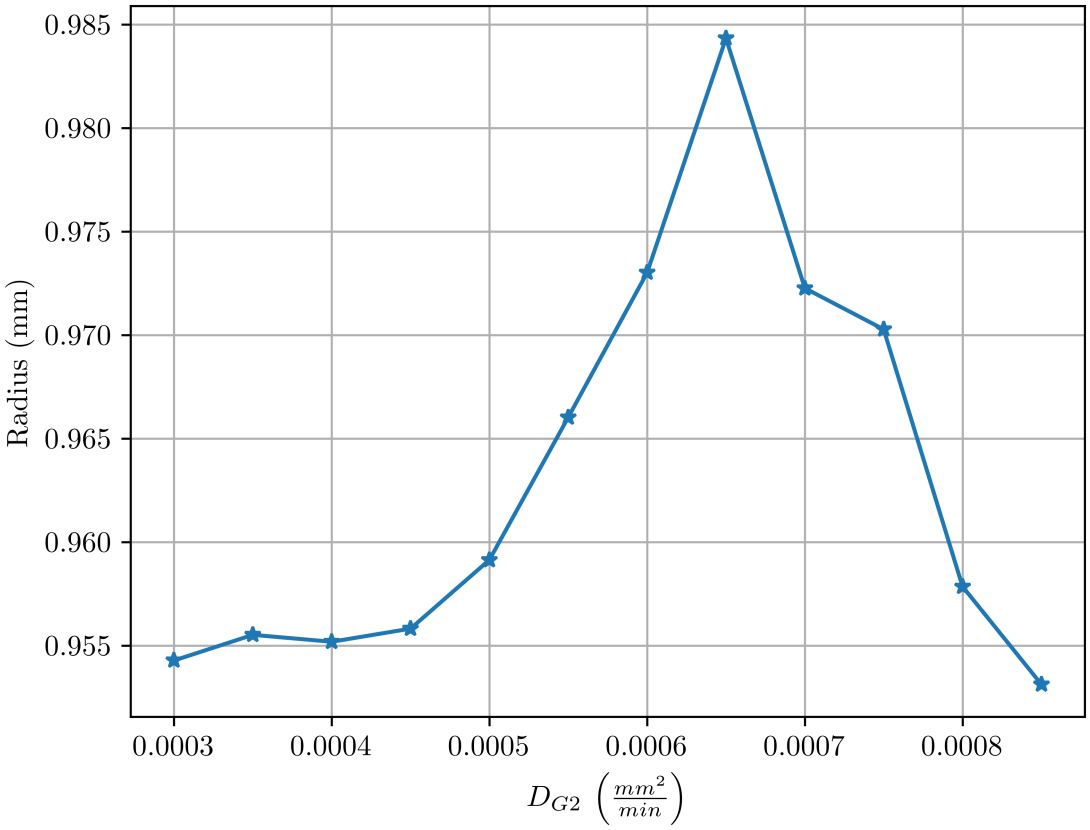

Figure 3.6: Final radius vs D_{G2}.

For the sensitivity cases (v)-(xi) in Table 3.3, the diffusion coefficient D_{G2} has been increased relative to the reference case. By examining the column listing the final radii and referring to Figure 3.6, where final radii have been plotted against their respective diffusion coefficient values, it becomes apparent that a slight increase in the diffusion coefficient leads to larger growth. However, as the increase becomes more significant, the growth also increases but to a lesser extent, and after further increasing D_{G2} the growth actually starts to decrease.

This aligns with the expected behavior discussed earlier. Nevertheless, the changes resulting from altering the G2 diffusion coefficient are relatively minor. This is clearly demonstrated in Figure 3.7, where the radius at each time step is plotted for all the cases. It can be observed that all the curves are closely aligned, with only slight variations towards the end. This implies that modifications in D_{G2} do not have a significant impact on the growth, as anticipated.

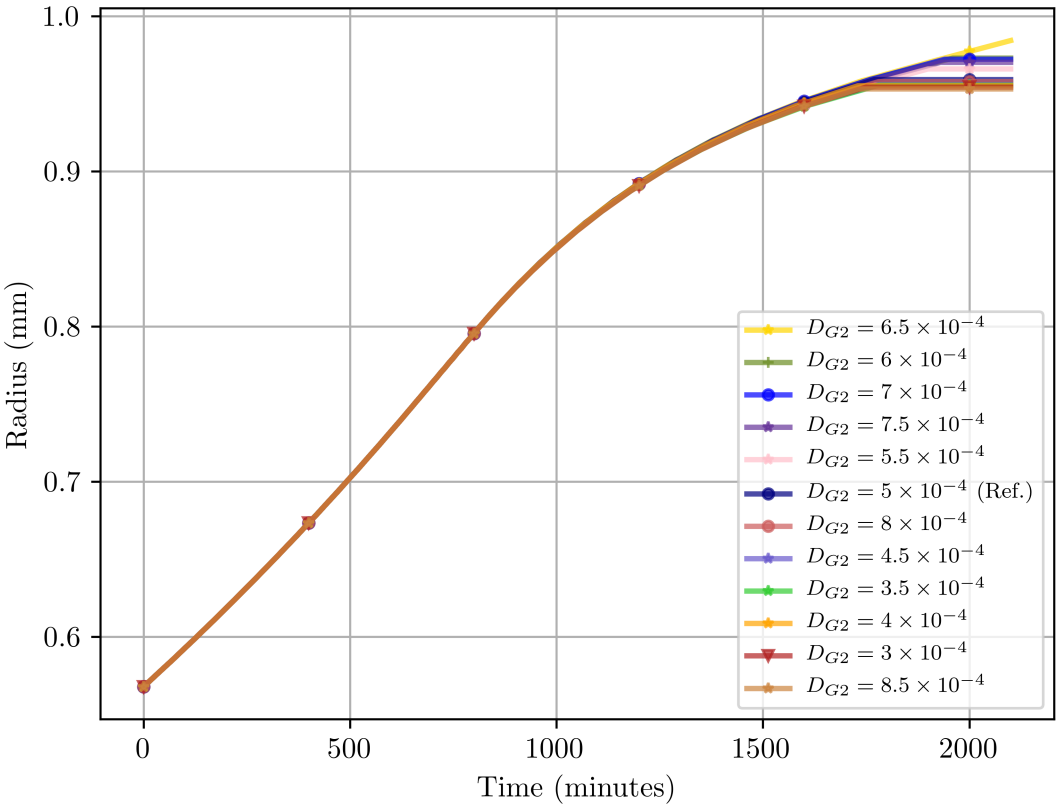

Figure 3.7: Radius vs time, altered D_{G2}.

As mentioned previously, G1 plays a significant role in reaching and surpassing the threshold θ_G. Therefore, it is reasonable to expect that modifying its distribution within the tumor would impact its growth. Additionally, since G1 is produced/excreted internally and has the highest production/excretion rate in the center, diffusion processes contribute to transporting G1 away from the center and towards the boundary.

First growth-inhibitor factor diffusion coefficient	$\boldsymbol{D_{G1}}$ $(T \times sc^2)$	Final radius (mm)	Quiescent, GIF's	Necrotic	Stop time (minutes)
The reference case	5.000×10^{-7}	0.9591	780	790	1780
(i)	3.500×10^{-7}	1.1521	720	730	2960
(ii)	4.000×10^{-7}	1.1141	740	750	2680
(iii)	4.500×10^{-7}	1.0906	760	770	2660
(iv)	5.500×10^{-7}	0.9064	800	810	1400
(v)	6.000×10^{-7}	0.8832	820	810	1220
(vi)	6.500×10^{-7}	0.8528	840	830	1060

Table 3.4: Tumor evolution, altered D_{G1}.

When the diffusion coefficient is reduced compared to the reference case, the transportation of G1 concentration towards the boundary slows down, resulting in higher G1 concentration in the center. Consequently, the quiescent region is expected to form based solely on the elevated G1 concentration in the center, as G2 is only consumed within the tumor and will therefore never reach the threshold on its own. Due to the increased G1 concentration, the quiescent regions form earlier compared to the reference case and take on a disk-shaped form. However, the disk will be relatively small due to the proximity of the high G1 concentration to the center, caused by the limited diffusion. Additionally, the reduced diffusion also slows down the evolution of the quiescent regions. As a result, a larger portion of the tumor remains proliferating, leading to faster and prolonged growth. This ultimately results in a larger final radius.

For the sensitivity cases (i)-(iii) in Table 3.4, where D_{G1} has decreased compared to the reference case, one can observe the expected growth patterns based on the columns displaying the final radius and total growth time. These trends are also evident in Figure 3.8, where the radius at each time step is plotted for all the cases. The tumor growth becomes more significant as D_{G1} becomes smaller. Furthermore, it should be noted that the quiescent region due to nutrient deprivation appeared at the same time, that is, after 630 minutes, for all the cases in Table 3.4. Since GIF quiescent regions appear after nutrient deprived quiescent regions have formed, necrotic regions form immediately afterwards.

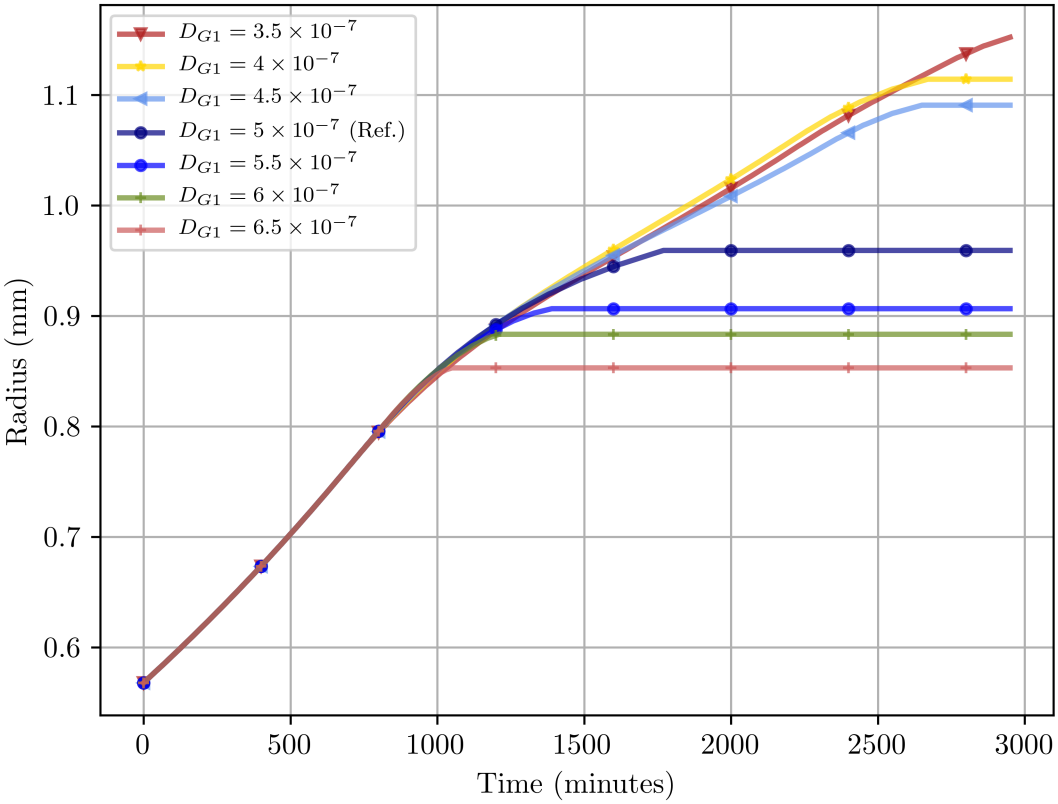

Figure 3.8: Radius vs time, altered D_{G1}.

With increased diffusion coefficients, G1 is transported faster towards the boundary. Therefore, one would anticipate the boundary of the GIF quiescent region (which is now determined by the weighted sum of G1 and G2) to be closer to the tumor boundary, but formed at a later time. This is because, despite the higher G1 concentration towards the boundary, it still takes a longer time for the concentration to reach a level high enough, due to the increased distance from the center compared to the reference case, for the weighted sum to surpass the threshold θ_G. However, once the threshold is initially reached, the evolution of the quiescent region progresses rapidly due to the fast supply of G1 from the center, facilitated by the increased diffusion coefficient. Furthermore, the proximity of the quiescent region to the boundary indicates that a smaller portion of the tumor is actively proliferating compared to the reference case. Consequently, one should expect smaller growth and a shorter growth period. In Table 3.4, it can be observed that for the sensitivity cases (iv)-(vi) where the diffusion coefficient has increased compared to the reference case, both the final radii and the growth period have decreased as expected. This trend is also clearly observed in Figure 3.8.

We have now observed the effects of altering the diffusion coefficients on tumor growth. Among the factors we considered, changing the nutrient diffusion coefficient has the most significant impact on the growth, resulting in both the largest and smallest sizes observed. Furthermore, we found that modifying the G1 diffusion coefficient had a greater impact on growth than altering the G2 diffusion coefficient. Interestingly, we discovered that increasing D_{G2} did not always lead to the same growth pattern.

3.2.2 Sink and source coefficients

In this section, we will examine how modifying the sink and source coefficients for different concentrations impacts tumor evolution. The sink coefficients represent constants that determine the rate at which concentrations are consumed, while the source coefficient scales the source function, thereby determining the amount of a growth factor generated.

It is important to note that different cell types do not necessarily consume the same quantity of each concentration. Proliferating cells have a high nutrient consumption rate, while quiescent cells consume nutrients at a lower rate. On the other hand, necrotic cells do not consume any nutrients. Regarding the growth-inhibitor factors, both proliferating and quiescent cells consume the same amount, whereas necrotic cells do not consume any. Additionally, it should be emphasized that G1 is the only factor produced/excreted within the tumor, and thus it is the only factor associated with a source coefficient.

The nutrient sink coefficient in the proliferating region, denoted by α_{pro}, states the rate at which nutrients are consumed in this region.

Nutrient sink coefficient in proliferating regions	$\boldsymbol{\alpha_{pro}}$ $(T \times sc^2)$	Final radius (mm)	Quiescent, GIF's	Quiescent, lack of nutrients	Necrotic	Stop time (minutes)
The reference case	1.000×10^{-8}	0.9591	780	630	790	1780
(i)	1.400×10^{-8}	0.8173	790	240	800	990
(ii)	1.200×10^{-8}	0.8430	780	430	790	1080
(iii)	0.800×10^{-8}	1.1051	780	-	1730	2380
(iv)	0.600×10^{-8}	1.1331	780	-	1870	2490

Table 3.5: Tumor evolution, altered α_{pro}.

If the sink coefficient in the proliferating regions increases, more nutrients are consumed, leading to lower concentration in these regions. Thus θ_N will sooner be reached, and as a result quiescent regions due to lack of nutrients will form earlier on. These quiescent regions form when the tumor is relatively small, and it is likely that they will transition back to proliferating regions as nutrients diffuse into the area. This transition causes the tumor to grow more rapidly compared to the previous time step. The new tumor will be large enough such that diffusion no longer is enough to keep the entire region proliferating, and a nutrient lacking quiescent region will form again. This cyclic process of quiescent and proliferating regions continues until the tumor becomes large enough such that nutrient lacking cells remain nutrient deprived. When the quiescent regions are present the proliferating regions become smaller, and therefore the growth rate decreases. As a result of the transition between fully proliferating and partially proliferating states from an early stage, one should anticipate that

the overall growth will be smaller compared to the reference case. For sensitivity cases (i) and (ii), where α_{pro} has increased, the expected growth tendency can be observed in Table 3.5 and Figure 3.9.

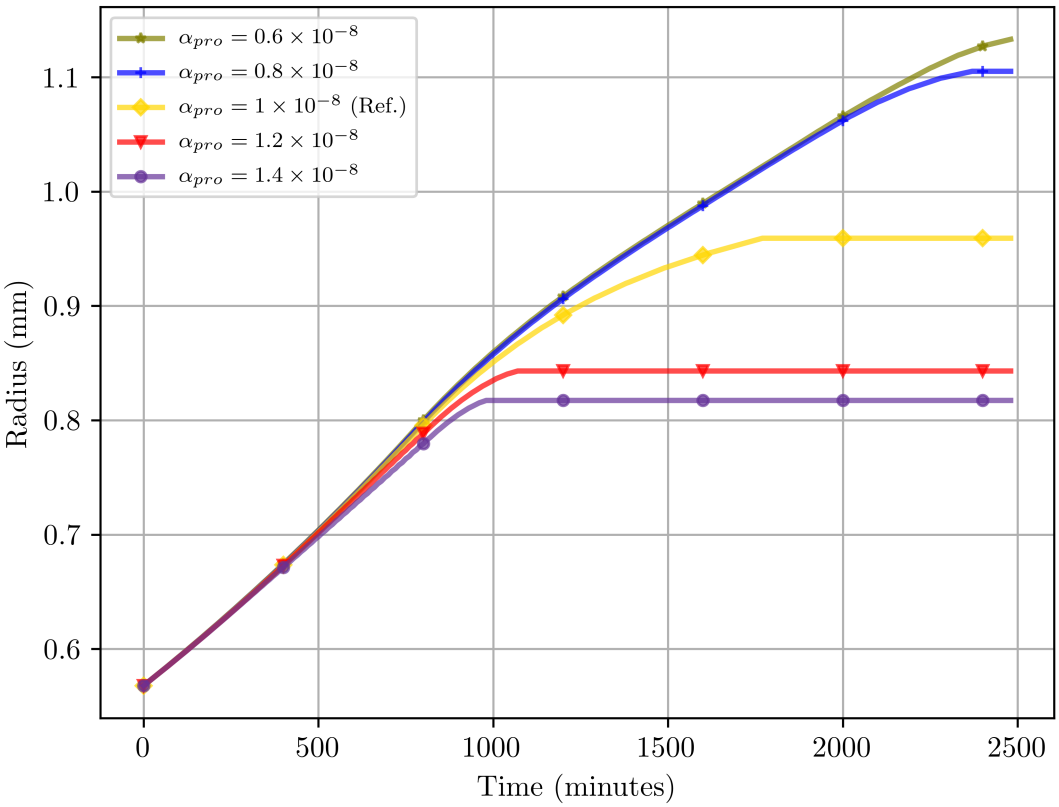

Figure 3.9: Radius vs time, altered α_{pro}.

Conversely, if the sink coefficient in the proliferating regions decreases, it results in a higher nutrient concentration in these regions. Consequently, proliferating areas with reduced sink coefficients exhibit larger growth compared to the equivalent regions in the reference case. It also takes a longer time before any cells become nutrient deprived. Therefore, one can expect the formation of nutrient-deprived quiescent regions and necrotic regions to occur much later than in the reference case. This is seen to be the case in Table 3.5, for the sensitivity cases (iii) and (iv) where α_{pro} is decreased. As a result, one should anticipate a larger final size and an extended growth period. Figure 3.9, which plots the radius at each time step for all cases, confirms that decreasing α_{pro} indeed leads to increased growth and a longer growth period.

Now we will proceed to analyze how modifications in the nutrient sink coefficient in the quiescent regions, denoted by α_{qui}, impact tumor growth. Note that α_{qui} states the rate at which nutrients are consumed in the quiescent regions. Furthermore, note that α_{qui} does not affect the growth until a quiescent region is formed. Therefore, until that happens the tumor evolution should be identical with the evolution in the reference case. In all the cases analyzed the first quiescent region that appeared was the nutrient-deprived quiescent region after 630 minutes. Which coincides with the first quiescent region formed in the reference case.

Nutrient sink coefficient in quiescent regions	$\boldsymbol{\alpha_{qui}}$ $(T \times sc^2)$	Final radius (mm)	Quiescent, GIF's	Necrotic	Stop time (minutes)
The reference case	0.500×10^{-8}	0.9591	780	790	1780
(i)	0.100×10^{-8}	0.9716	780	790	1920
(ii)	0.300×10^{-8}	0.9695	780	790	1910
(iii)	0.700×10^{-8}	0.9070	800	780	1400
(iv)	0.900×10^{-8}	0.8676	800	780	1170

Table 3.6: Tumor evolution, altered α_{qui}.

When the sink coefficient in the quiescent regions is increased, a greater amount of nutrients is consumed, resulting in a decrease in nutrient concentration. This creates a more pronounced nutrient gradient between the proliferating and quiescent regions, leading to increased transport of nutrients from the proliferating to the quiescent regions. As a consequence, the proliferating regions experience a slightly lower nutrient concentration and exhibits reduced growth compared to the reference case. Moreover, the lower nutrient concentration in the quiescent regions makes it more challenging for a nutrient-deprived quiescent region to transition back to a proliferating state. Therefore, it can be expected that the overall growth will be smaller compared to the reference case, as observed in Table 3.6 and depicted in Figure 3.10 for the sensitivity cases (iii) and (iv) where α_{qui} is increased.

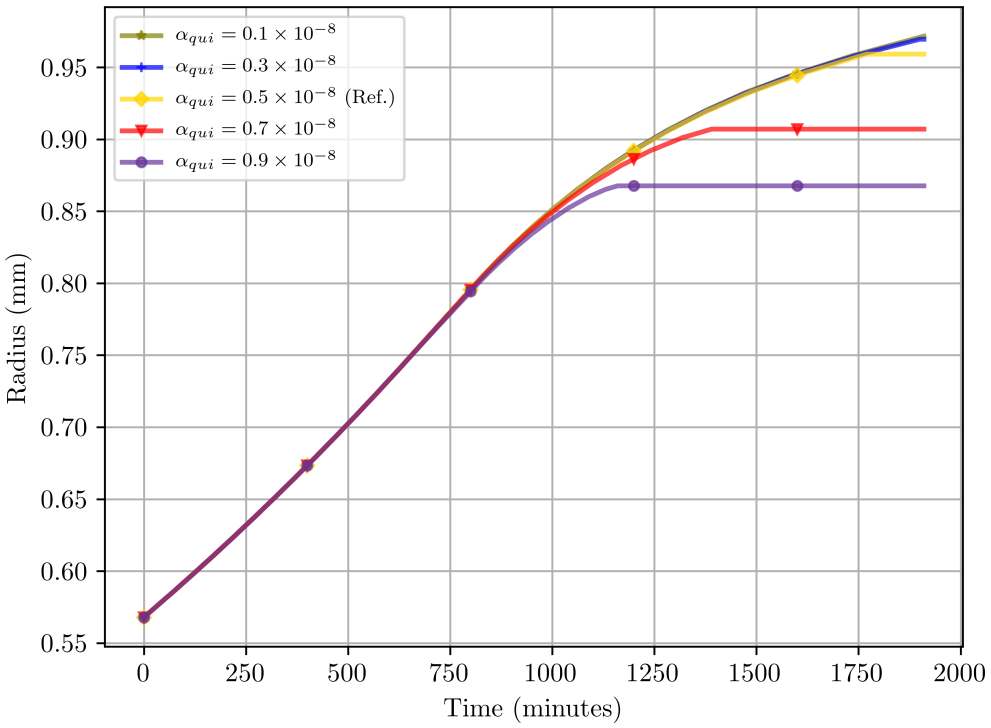

Figure 3.10: Radius vs time, altered α_{qui}.

On the contrary, if the sink coefficient in the quiescent regions decreases, fewer nutrients are consumed, resulting in an increase in nutrient concentration. As a result, the nutrient gradient between proliferating and quiescent regions becomes less steep, and the transport of nutrients from the proliferating to the quiescent regions decreases. Consequently, the proliferating region has a slightly higher nutrient concentration, which should lead to a larger tumor size. Additionally, with a lower consumption of nutrients, it becomes easier for nutrient-deprived quiescent regions to transition back into proliferating regions. As a result one should expect longer growth periods and larger final radii. This expectation is supported by the observed longer growth period and larger final radii, compared to the reference case, for sensitivity cases (i) and (ii) of Table 3.6, and illustrated in Figure 3.10. Moreover, it is evident that increasing α_{qui} has a more significant effect on the growth compared to decreasing α_{qui}.

Now we will proceed to analyze how modifications in the G2 sink coefficient, denoted by ξ_{proqui}, in both proliferating and quiescent regions affect tumor growth. The sink coefficient ξ_{proqui} determines the rate at which G2 is consumed in these regions. As mentioned earlier, G2 is not the main factor contributing to reaching the threshold θ_G. Therefore, changes in ξ_{proqui} are not expected to have a significant impact on the initial formation of the quiescent GIF regions. In fact, in all the cases analyzed, the different regions appeared initially at the same time as in the reference case. Specifically, the initial GIF quiescent region formed after 780 minutes, the nutrient-deprived quiescent region after 630 minutes, and the necrotic region after 790 minutes.

G2 sink coefficient in proliferating and quiescent regions	$\boldsymbol{\xi_{proqui}}$ $(T \times sc^2)$	Final radius (mm)	Stop time (minutes)
The reference case	5.000×10^{-8}	0.9591	1780
(i)	4.600×10^{-8}	0.9582	1810
(ii)	4.800×10^{-8}	0.9745	1940
(iii)	5.200×10^{-8}	0.9709	1940
(iv)	5.400×10^{-8}	0.9849	2160

Table 3.7: Tumor evolution, altered ξ_{proqui}.

If the sink coefficient ξ_{proqui} decreases, it implies that less G2 is consumed, leading to an increase in the G2 concentration. When ξ_{proqui} becomes slightly smaller than the reference case, as in sensitivity case (ii) of Table 3.7, one would expect the formation of the quiescent region (due to high GIF) to occur closer to the center compared to the reference case, due to the slight increase in G2 concentration. Since this region forms closer to the center, simultaneously with the reference case, the proliferating region will be larger. Consequently, one can anticipate slightly faster growth and a slightly larger final radius. However, if the sink coefficient decreases more significantly, it would result in a larger initial GIF quiescent region compared to the reference case. This is because with minimal G2 consumption, the G2 concentration becomes more evenly distributed within the tumor, leading to an enlarged GIF quiescent region. As a consequence, the proliferating regions would be smaller. Consequently, one would observe slower growth, and due to the spatial dependency of G1 production/excretion, there would

also be a decrease in G1 generation, resulting in smaller overall growth but a prolonged growth period. This trend is clearly seen for sensitivity case (i) in Table 3.7 and is illustrated in Figure 3.11, which display the radius at each time step for all the cases.

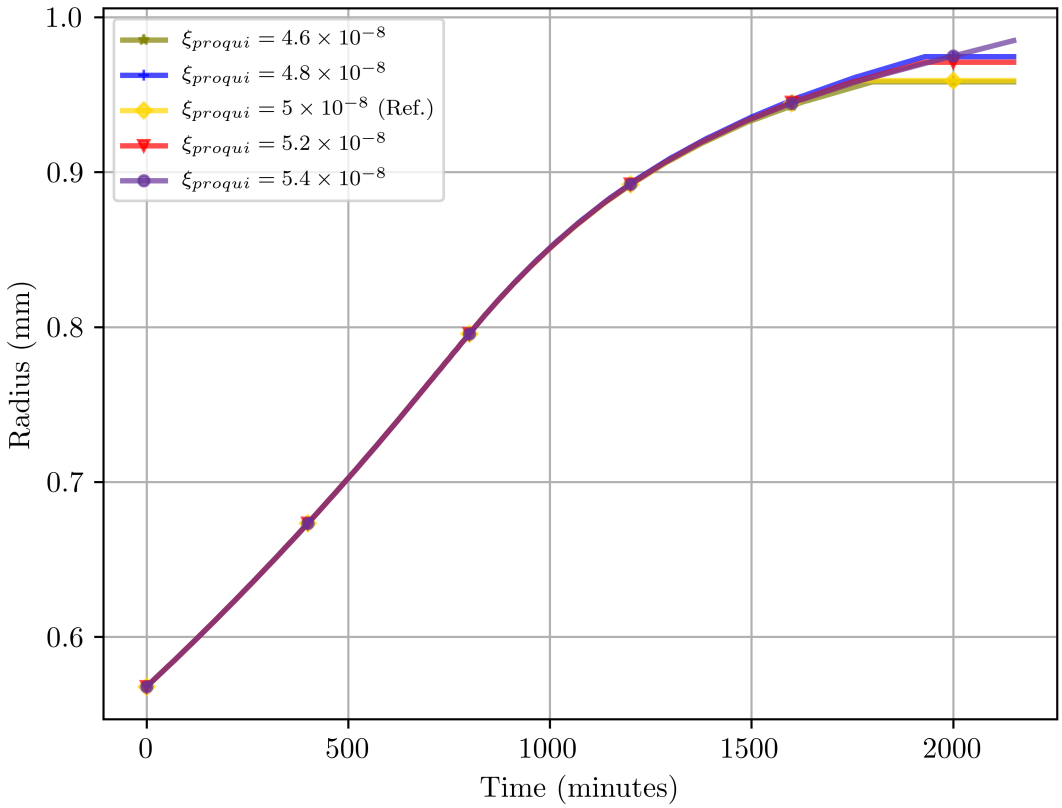

Figure 3.11: Radius vs time, altered ξ_{proqui}.

On the contrary, if the G2 sink coefficient is increased, more G2 is consumed, resulting in a decrease in its concentration. As a result, the GIF quiescent region is more likely to be formed solely based on G1, causing it to be located closer to the center of the tumor. Consequently, a larger portion of the tumor remains in proliferating state, contributing to its growth. Moreover, the reduced concentration of G2 implies a lower presence of growth-inhibiting factors in the proliferating regions, further enhancing the growth. Therefore, when the ξ_{proqui} value is increased, one can expect a larger final radius and a longer growth period. These trends can be observed in Table 3.7.

Now we will analyze the impact of modifying the G1 sink coefficient, denoted by γ_{proqui}, on tumor growth. γ_{proqui} determines the amount of G1 that will be consumed in proliferating and quiescent regions. As mentioned earlier, G1 plays a crucial role in reaching the threshold θ_G and forming GIF quiescent regions. Therefore, it is expected that altering γ_{proqui} will significantly affect the growth dynamics.

G1 sink coefficient in quiescent regions	γ_{proqui} (T)	Final radius (mm)	Quiescent, GIF's	Quiescent, lack of nutrients	Necrotic	Stop time (minutes)
The reference case	5.000×10^{-5}	0.9591	780	630	790	1780
(i)	4.600×10^{-5}	0.7782	610	-	620	820
(ii)	4.800×10^{-5}	0.8128	680	630	690	950
(iii)	5.200×10^{-5}	0.9796	940	630	930	1680
(iv)	5.400×10^{-5}	1.0473	1220	630	1190	1790

Table 3.8: Tumor evolution, altered γ_{proqui}.

If the G1 sink coefficient is increased in both proliferating and quiescent regions, the concentration of G1 will decrease. As a result, it will take longer time for the threshold θ_G to be reached, leading to a delayed formation of GIF quiescent regions within the tumor. Additionally, with lower G1 concentration, there will be fewer growth-inhibiting factors in the proliferating regions. Consequently, for sensitivity cases (iii) and (iv), one can anticipate that the tumor will grow larger, as it will experience more significant growth at each time step compared to the reference case. The accelerated tumor growth should also lead to an increase in G1 production/excretion. Therefore, the overall growth period may not differ significantly from the reference growth time. Table 3.8 and Figure 3.12 illustrate the expected tumor evolution when the G1 sink coefficient, γ_{proqui}, is increased.

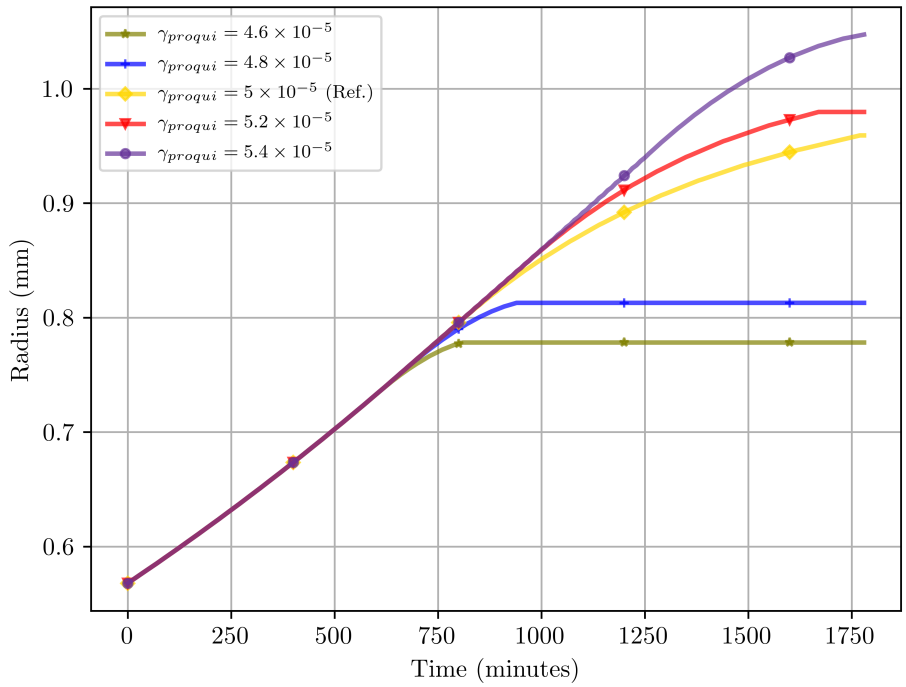

Figure 3.12: Radius vs time, altered γ_{proqui}.

On the contrary, if the G1 sink coefficient decreases, less G1 will be consumed, leading to an increase in G1 concentration. The elevated concentration of G1 will cause θ_G to be reached earlier and potentially cover a larger area within the domain. Since G1 plays a crucial role in reaching the threshold θ_G, this reduction in sink coefficient is expected to substantially shorten the growth period and result in a smaller final radius. This trend is clearly observed comparing sensitivity cases (i) and (ii) to the reference case in Table 3.8 and is illustrated in Figure 3.12 where the tumor evolution aligns with the expected outcomes.

Now, we will examine how modification of the G1 source coefficient, denoted by λ, affects tumor growth. The value of λ determines the scale of G1 generation. A higher value of λ leads to a greater production/excretion of G1, while a smaller value results in less G1 production/excretion. Since G1 plays a crucial role in reaching the threshold θ_G, any alterations in its generation are expected to have a substantial impact on tumor growth.

G1 source coefficient	$\boldsymbol{\lambda}$ $(\frac{T}{sc^2})$	Final radius (mm)	Quiescent, GIF's	Quiescent, lack of nutrients	Necrotic	Stop time (minutes)
The reference case	0.00325	0.9591	780	630	790	1780
(i)	0.00305	1.2561	1160	630	1160	3040
(ii)	0.00315	1.1851	940	630	930	3090
(iii)	0.00335	0.8202	680	630	690	990
(iv)	0.00345	0.7881	610	-	-	880

Table 3.9: Tumor evolution, altered λ.

As mentioned earlier, when the G1 source coefficient increases, more G1 is produced/excreted, leading to an increase in its concentration. Consequently, the threshold θ_G is reached sooner and covers a larger area of the tumor. Moreover, there will be a higher presence of growth-inhibiting factors in the proliferating regions throughout the growth process. Therefore, one should expect an earlier onset of GIF quiescent regions and a reduced growth rate at each time step. Ultimately, this should result in smaller final radii and shorter growth periods. These expectations align with the observations in Figure 3.13 and Table 3.9, and in particular when comparing the sensitivity cases (iii)-(iv) with the reference case.

If the source coefficient decreases the G1 concentration will be smaller and thus it will take longer time before a GIF quiescent region is formed. In other words, the tumor will remain fully proliferating for a longer period of time, and grow more at each time step because there are less growth-inhibiting factors present. Additionally, when GIF quiescent regions eventually form, they will exhibit slower growth. Therefore, one can expect both the growth period and the final radius of the tumor to significantly increase. These observations are consistent with the findings in Figure 3.13 and Table 3.9, and in particular when comparing sensitivity cases (i) and (ii) with the reference case.

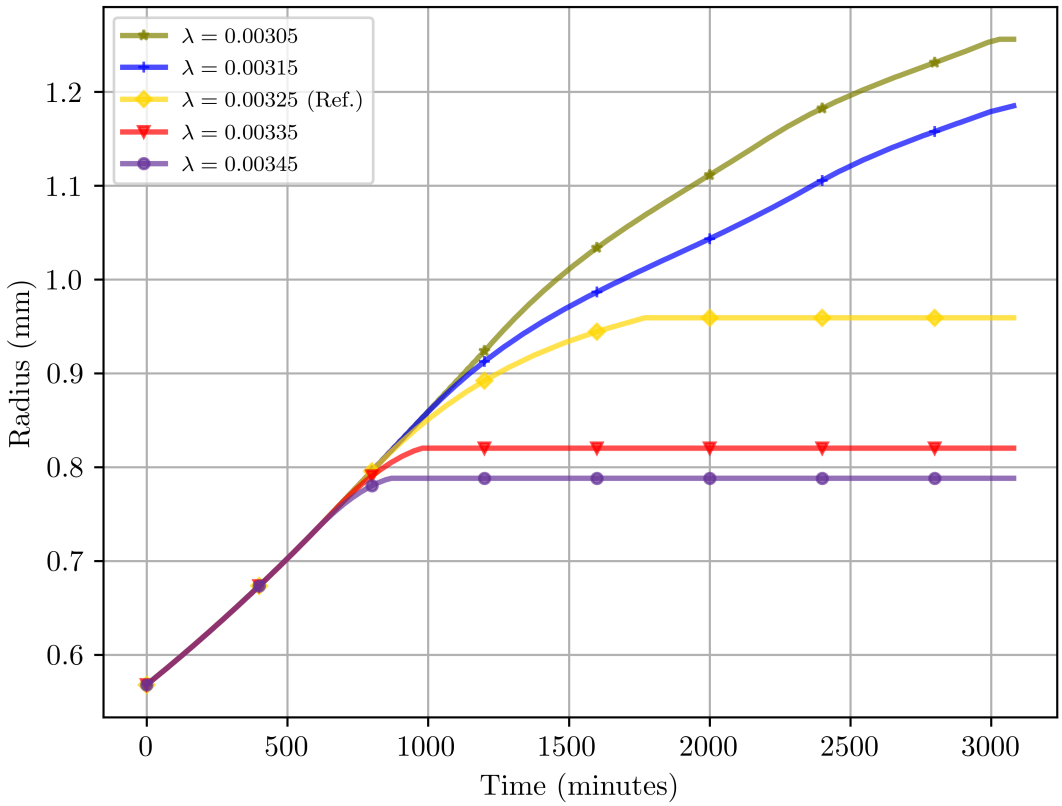

Figure 3.13: Radius vs time, altered λ.

Now we have observed how altering the sink and source parameters affect tumor evolution. Modifying the production/excretion coefficient λ for the G1 factor has the most significant impact on growth, resulting in the largest and second smallest sizes observed. Among the sink coefficients, it was observed that altering α_{pro} and γ_{proqui} have the most significant impact on tumor evolution. This is reasonable because α_{pro} alters the nutrient concentration in the proliferating regions, which is directly connected to the growth calculations. Meanwhile, γ_{proqui} affects the concentration of the main contributor to the formation of GIF quiescent regions, so one should expect a significant alteration in growth. Changes to α_{qui} also affected the growth, but on a much smaller scale compared to α_{pro}. This is reasonable as the alterations do not affect the growth until quiescent regions form. Additionally, it was observed that alterations to ξ_{proqui} only led to minor changes in growth, as expected since $G2$ is a secondary contributor to the formation of GIF quiescent regions.

3.2.3 Boundary data

In this section, we will investigate the impact of modifying the Dirichlet boundary data on tumor evolution. Specifically, we will examine how changes in the supply of nutrients, denoted by κ, and G2, denoted by ψ, at the boundary influence the tumor's development. It is important to note that both nutrients and G2 are constantly provided across the entire boundary.

Nutrient boundary data	κ	Final radius (mm)	Quiescent, GIF's	Quiescent, lack of nutrients	Necrotic	Stop time (minutes)
The reference case	3.000	0.9591	780	630	790	1780
(i)	2.950	0.8238	800	290	790	1030
(ii)	2.975	0.8440	780	490	790	1080
(iii)	3.025	1.1573	800	780	780	3370
(iv)	3.050	1.3172	780	-	2180	3500

Table 3.10: Tumor evolution, altered κ.

As previously mentioned, κ represents the constant supply of nutrients at the boundary. Within the tumor, nutrients are solely consumed, highlighting the significant impact of the boundary's nutrient supply on the concentration level. When the supply decreases, fewer nutrients are transported into the tumor, resulting in a lower nutrient concentration. Consequently, θ_N will be reached earlier, inhibiting growth. Consequently, one should expect an earlier onset of nutrient-deficient quiescent regions. Additionally, the proliferating regions will experience reduced growth at each time step due to the lower nutrient concentration. Therefore, if the nutrient supply at the boundary is decreased, one can expect a shorter growth period and a smaller final size. The anticipated growth pattern can be observed in Table 3.10, in particular when comparing sensitivity cases (i) and (ii) to the reference case, as well as in Figure 3.14, which depicts the radius at each time step for all the analyzed cases.

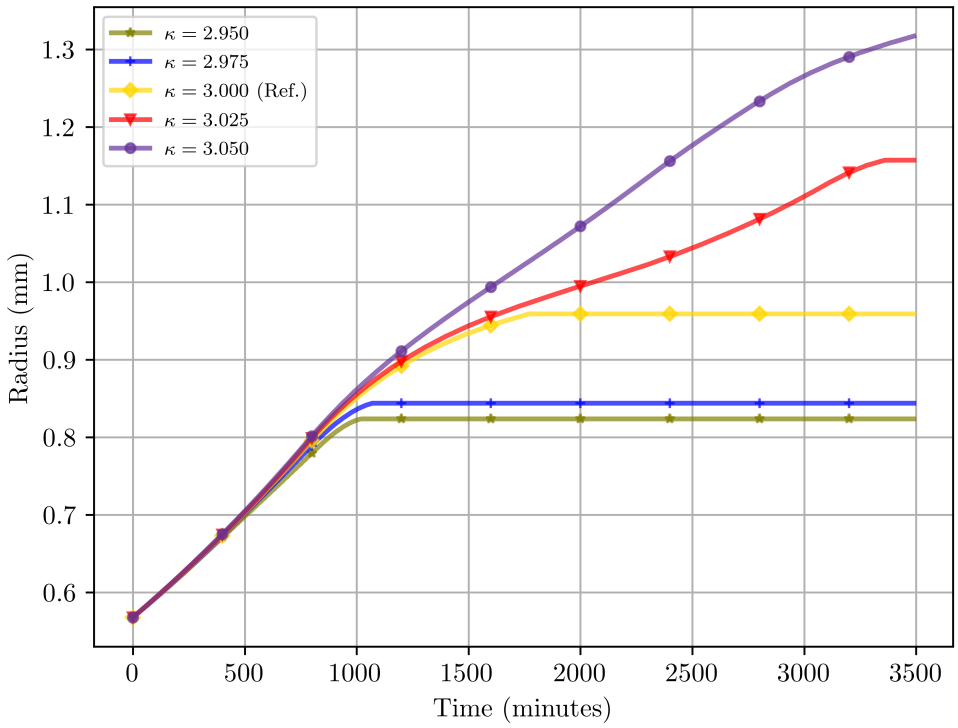

Figure 3.14: Radius vs time, altered κ.

On the contrary, if the nutrient supply at the boundary increases, the concentration within the tumor will also increase. Consequently, the proliferating regions will experience enhanced growth at each iteration due to the generally higher nutrient concentration. Moreover, it will take a longer time for the nutrient concentration to decrease to the level of θ_N. As a result, the formation of nutrient-deficient quiescent regions will occur later compared to the reference case. Therefore, when κ is increased compared to the reference case, one can expect the tumor to exhibit faster and prolonged growth compared to the reference scenario. The expected growth trend can be observed in Figure 3.14 and Table 3.10, in particular when sensitivity cases (iii)-(iv) are compared to the reference case.

Now, we will analyze the impact of modifying the constant supply of G2 at the boundary, denoted as ψ, on the growth. It is important to note that G2 is solely consumed within the tumor, and ψ represents the only source of G2. Therefore, altering ψ is expected to have an effect on the tumor's evolution.

G2 boundary data	$\boldsymbol{\psi}$	Final radius (mm)	Quiescent, GIF's	Necrotic	Stop time (minutes)
The reference case	0.1000	0.9591	780	790	1780
(i)	0.0960	1.1315	840	830	2680
(ii)	0.0975	1.0979	820	810	3100
(iii)	0.1025	0.8626	760	750	1170
(iv)	0.1040	0.8516	740	750	1130

Table 3.11: Tumor evolution, altered ψ.

If ψ decreases, the G2 concentration will also decrease. As a result, it will take longer time for θ_G to be reached, and the formation of GIF quiescent regions will be delayed. Moreover, there will be fewer growth-inhibiting factors in the proliferating regions, leading to larger growth at each time step. Therefore, one can expect a larger final tumor size and longer growth period. This growth tendency is observed in Table 3.11, in particular when comparing sensitivity cases (i)-(ii) with the reference case, and in Figure 3.15, which depicts the radius at each time step for all the analyzed cases. Furthermore, it is important to note that modifying the G2 supply does not impact the nutrient supply. Therefore, in all the analyzed cases, the formation of nutrient-deficient quiescent regions occurred at the same time as in the reference case, which was after 630 minutes.

On the contrary, if the supply of G2 increases, the G2 concentration will also increase. Consequently, GIF quiescent regions will form at an earlier stage. Furthermore, higher G2 concentration implies the presence of more growth-inhibiting factors in the proliferating regions, leading to reduced growth at each time step compared to the reference case. Therefore, one can expect both the tumor size and growth period to be smaller than in the reference scenario. This is evident from comparing sensitivity cases (iii) and (iv) with the reference case in Table 3.11, and also in Figure 3.15.

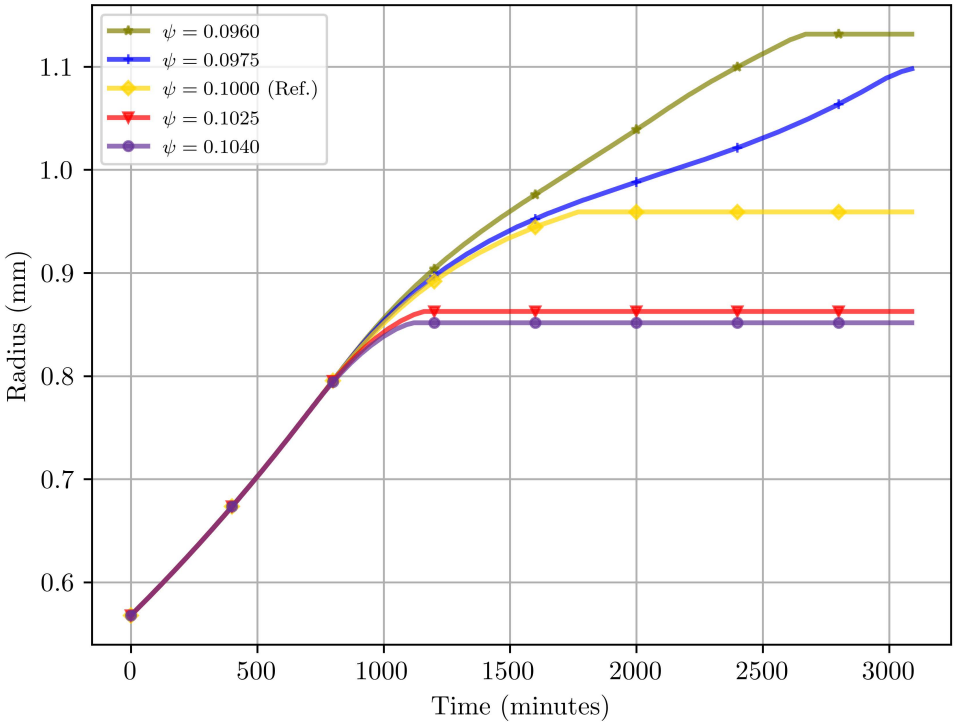

Figure 3.15: Radius vs time, altered ψ.

We have now examined the effects of modifying the constant supplies of nutrients and G2 at the boundary on tumor evolution. Since the supplies at the boundary are the sole sources of nutrients and G2, altering them has a significant impact on the concentration levels within the tumor. Increasing the nutrient supply, κ, resulted in increased growth, whereas increasing the G2 supply, ψ, inhibited growth and led to smaller growth. Conversely, decreasing κ resulted in smaller growth, while decreasing ψ resulted in larger growth.

3.2.4 The weights in the mitotic function

The equation that calculates the new number of cells, equation (2.25), in other words, the growth, depends on the mitotic function, equation (2.24). Therefore, altering the parameters in the mitotic function is expected to influence the growth.

The parameter ρ represents the weight that scales the entire mitotic function. When ρ increases, the number of cells produced at each time step will also increase. Conversely, if ρ decreases, fewer cells will be generated at each time step. Figure 3.16 illustrates the relative differences in the number of cells for each sensitivity case compared to the reference solution. The relative difference is calculated as $\frac{nc - nc_{\text{ref}}}{nc_{\text{ref}}}$, the difference in number of cells divided by the reference number of cells.

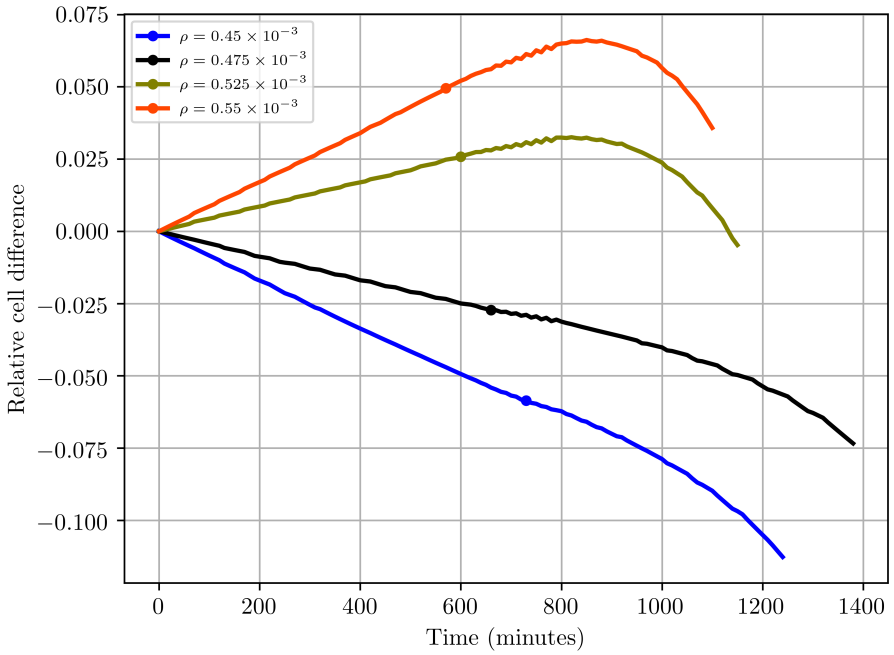

Figure 3.16: Relative difference in number of cells vs time, altered ρ. The dots denote when nutrient lacking quiescent regions initially occurred.

In Figure 3.16, we can observe that when ρ increases compared to the reference case (indicated by the red and green curves), the cell difference becomes positive, as expected. Initially, the difference increases as one would anticipate due to the heightened mitotic function. However, after a certain period, the difference plateaus and eventually decreases. This phenomenon occurs because nutrient-deficient regions form earlier compared to the reference case, and additionally, GIF quiescent regions cover a larger portion of the tumor due to increased G1 production/excretion resulting from rapid growth. The decrease in cell difference can be attributed to the earlier formation of quiescent regions, leading to a shorter overall growth period compared to the reference case. Table 3.12 and Figure 3.17 demonstrate that an increase in ρ results in a smaller final size and a shorter growth period when compared to the reference case.

ρ, weighting m	**ρ (sc^2)**	Final radius (mm)	Quiescent, GIF's	Quiescent, lack of nutrients	Necrotic	Stop time (minutes)
The reference case	0.500×10^{-3}	0.9591	780	630	790	1780
(i)	0.450×10^{-3}	0.8465	800	730	790	1250
(ii)	0.475×10^{-3}	0.8853	790	660	800	1390
(iii)	0.525×10^{-3}	0.8807	790	600	790	1160
(iv)	0.550×10^{-3}	0.8883	770	570	780	1110

Table 3.12: Tumor evolution, altered ρ.

Figure 3.16 shows that decreasing ρ also leads to the anticipated decrease in new cells at each time step. Additionally, Table 3.12 demonstrates that quiescent regions due to nutrient deficiency form later on in these cases, primarily due to the slow increase and the time required for the tumor to become large enough for the center to be deprived of nutrients. Consequently, these tumors remain fully proliferating for an extended period. Therefore, decreasing ρ results in longer growth periods compared to increasing ρ. As seen in Figure 3.16, for decreased ρ, the cell difference becomes increasingly negative towards the end of the growth period. This occurs because in the case of decreased ρ, the tumor ceases to grow earlier than the reference case, i.e., fewer new cells are produced. This is due to the formation of GIF quiescent and necrotic regions, which occur almost simultaneously as in the reference case but in a much smaller tumor size. Hence, it takes less time for the entire tumor to become quiescent and/or necrotic. Therefore, one should expect the final radius to be smaller and the growth period to be shorter compared to the reference case. The anticipated growth tendency is observed in Figure 3.17 and in Table 3.12 when comparing sensitivity cases (i) and (ii) with the reference case.

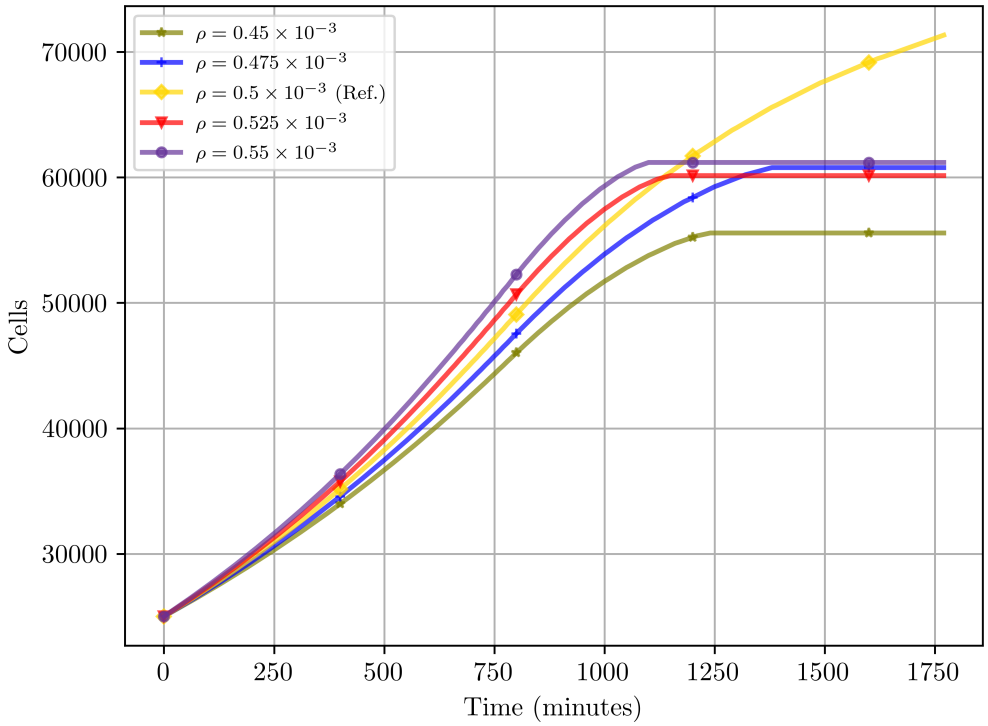

Figure 3.17: Number of cells vs time, altered ρ. The dots denote when nutrient lacking quiescent regions initially occurred.

Now, let us analyze the impact of modifying η, which is the parameter that determines how much the nutrient concentration contributes to the mitotic rate. Nutrients are growth-promoting factors, so if η is increased, one would anticipate a higher production of new cells at each time step. Conversely, if η decreases, fewer new cells should be produced at each time step.

By examining Figure 3.18, which illustrates the relative cell difference at each time step for all the analyzed cases, it becomes evident that increasing η results in a higher production of new

cells at each time step. However, as shown in Table 3.13 and Figure 3.19, increasing η leads to a shorter growth period and a smaller final radius. This is due to the rapid growth of the tumor, which causes quiescent nutrient-deficient regions to appear earlier and cover a larger portion of the tumor. Furthermore, in rapidly growing tumors, the production/excretion rate of $G1$ increases, leading to faster evolution of the GIF quiescent region. Comparing sensitivity cases (iii) and (iv) in Table 3.13, it is observed, as expected, that the case with the highest η value (sensitivity case (iv)) exhibits the shortest growth period and the earliest formation of nutrient-lacking quiescent regions.

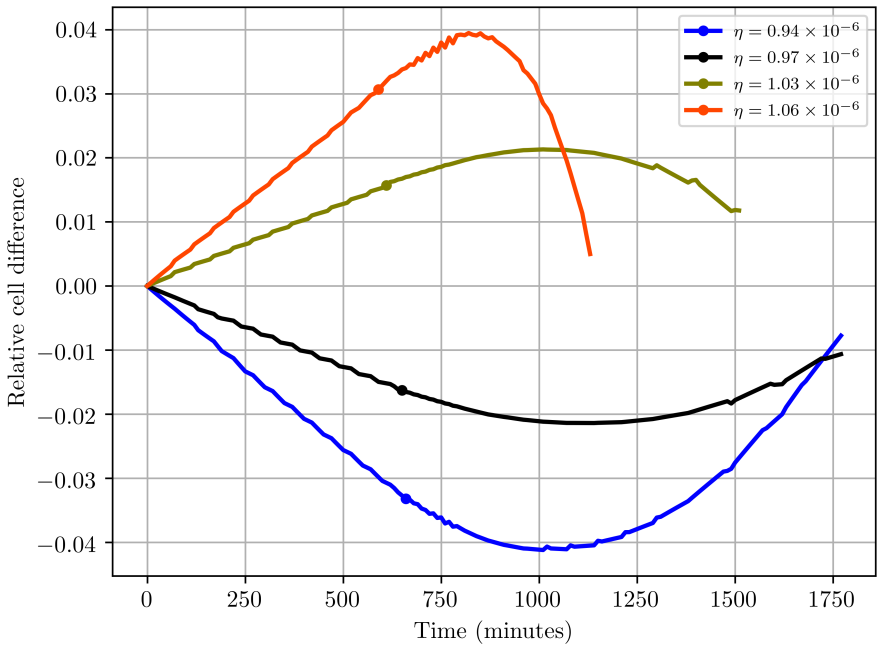

Figure 3.18: Relative difference in number of cells vs time, altered η. The dots denote when nutrient lacking quiescent regions initially occurred.

η, weighting the nutrient concentration	**η $(T \times sc^2)$**	Final radius (mm)	Quiescent, GIF's	Quiescent, lack of nutrients	Necrotic	Stop time (minutes)
The reference case	1.000×10^{-6}	0.9591	780	630	790	1780
(i)	0.940×10^{-6}	1.0824	800	660	790	2890
(ii)	0.970×10^{-6}	1.0837	800	650	790	3130
(iii)	1.030×10^{-6}	0.9407	780	610	790	1520
(iv)	1.060×10^{-6}	0.8812	790	590	780	1140

Table 3.13: Tumor evolution, altered η.

Figure 3.18 also demonstrates that decreasing η, compared to the reference case, leads to the expected reduction in the production of new cells at each time step. Additionally, Figure 3.19 reveals that decreasing η results in a fundamentally different growth pattern for the tumor compared to the cases where η is increased. The decrease in cell production, or slower growth, should correspondingly lead to the formation of nutrient-deprived quiescent regions at a later stage. As a result, the tumor should continue its fully proliferating state for a longer duration. Furthermore, slower growth implies less production/excretion of $G1$ compared to the reference case. However, it is noteworthy that the case with the largest decreased η (sensitivity case (ii) in Table 3.13) exhibits the greatest overall growth. This occurs because, over time, the quiescent and necrotic regions in sensitivity case (ii) of Table 3.13 become sufficiently large, causing the remaining proliferating region to be so small that the increase in cell count becomes smaller than in sensitivity case (i), despite the higher value of η in sensitivity case (ii). Consequently, sensitivity case (ii) can sustain a longer growth period.

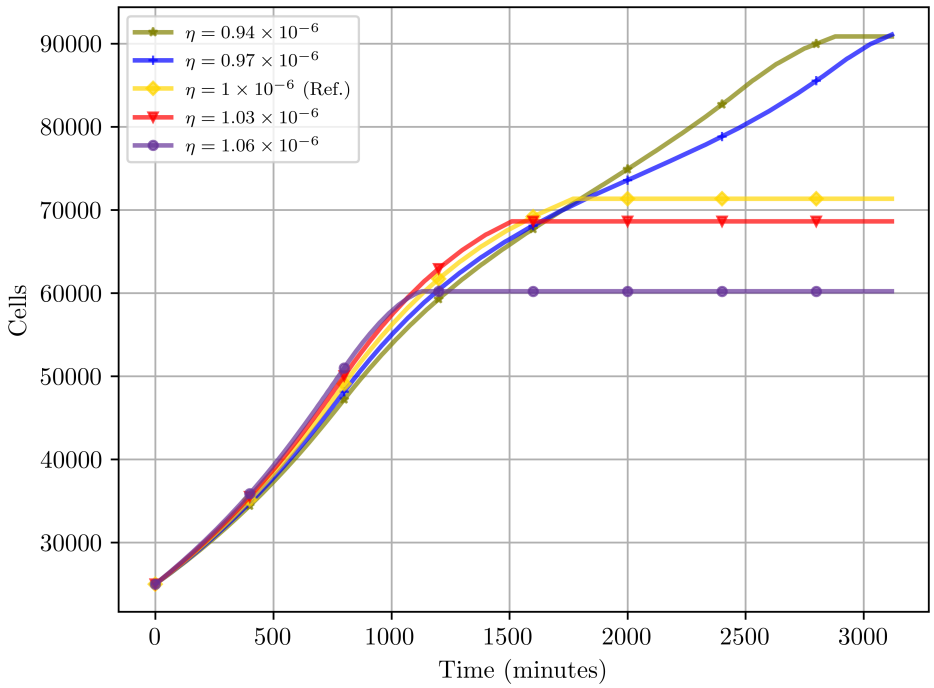

Figure 3.19: Number of cells vs time, altered η. The dots denote when nutrient lacking quiescent regions initially occurred.

The curvature observed in the curves of Figure 3.18, which occurs after the formation of non-proliferating regions, can be attributed to the significantly different growth periods compared to the reference case. For $\eta = 1.03 \times 10^{-6}$ and $\eta = 1.06 \times 10^{-6}$, the growth periods are shorter, causing the rate of cell increase to slow down towards the end. In contrast, the reference case continues to grow, resulting in a decrease in the difference in the number of cells for the red and green curves. On the other hand, for $\eta = 0.94 \times 10^{-6}$ and $\eta = 0.97 \times 10^{-6}$, the growth period is extended. Therefore, when the reference case reduces cell production, these cases continue with the same cell production. As a result, the difference in cell count decreases, as observed in the plot for the black and blue curves.

Now we will analyze the effect of modifying the parameter ν_1, which determines how much the G1 concentration contributes to the mitotic rate. Since G1 is a growth-inhibiting factor, increasing ν_1 should lead to a lower production of new cells at each time step, whereas decreasing ν_1 should result in a higher production of cells at each time step. However, it should be noted that at the beginning of the simulation, the concentration of G1 is very small, so changes in ν_1 are not expected to substantially alter growth.

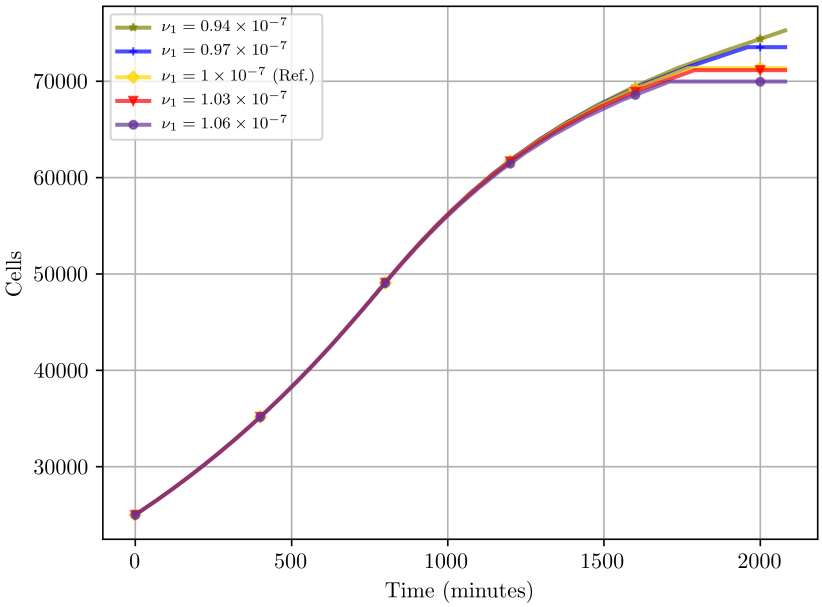

Figure 3.20: Number of cells vs time, altered ν_1.

From Figures 3.20 and 3.21, it becomes apparent that initially changes in ν_1 have a negligible effect. It is only after a certain period, coinciding with the onset of necrosis, that the G1 concentration becomes sufficiently large to impact mitosis. Figure 3.21 clearly demonstrates that increasing ν_1 results in a tendency of fewer new cells being produced at each time step. Conversely, an increasing trend in cell production is observed for decreased ν_1. (The small oscillations are assumed to be caused by rounding errors.)

ν_1, weighting the G1 concentration	**ν_1** $(T \times sc^2)$	Final radius (mm)	Stop time (minutes)
The reference case	1.000×10^{-7}	0.9591	1780
(i)	0.940×10^{-7}	0.9850	2090
(ii)	0.970×10^{-7}	0.9736	1970
(iii)	1.030×10^{-7}	0.9577	1800
(iv)	1.060×10^{-7}	0.9497	1720

Table 3.14: Tumor evolution, altered ν_1.

Table 3.14 and Figure 3.20 indicate that the overall impact of modifying ν_1 has had minimal effect on the growth. The formation of quiescent and necrotic regions occurred at the same

time as in the reference case. It was only after the formation of these regions that altering ν_1 began to have an impact on the growth.

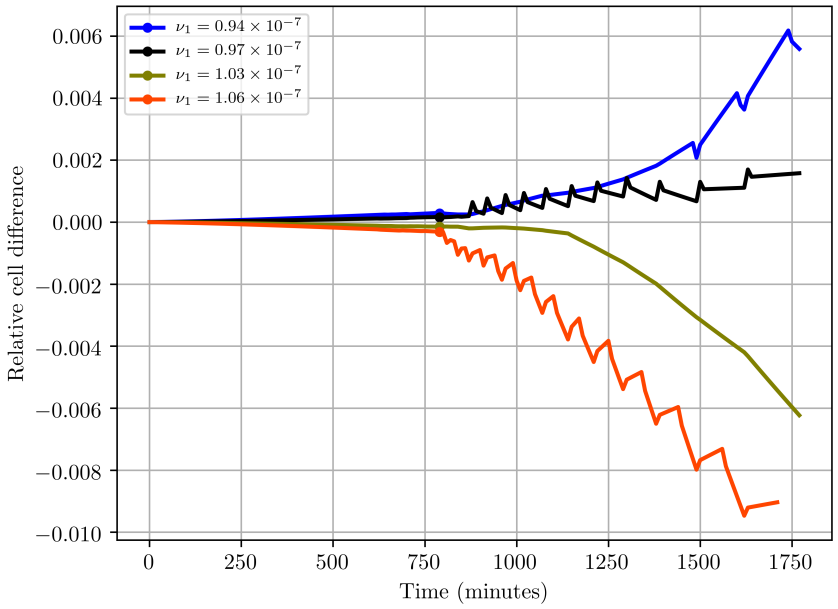

Figure 3.21: Relative difference in cells vs time, altered ν_1. The dots denote the initial formation of necrotic regions.

Now we will analyze the impact of modifying ν_2, which determines the contribution of G2 to the mitotic rate. Since G2 is a growth-inhibiting factor, increasing ν_2 should result in a decrease in cell production at each time step. Conversely, decreasing ν_2 should lead to an increase in cell production at each time step. However, it is important to note that the concentration of G2, except during the initial stages of growth, is much lower compared to the nutrient and G1 concentrations. Therefore, altering ν_2 is not expected to have a significant effect on the overall growth. Actually, for all the cases analysed the quiescent and necrotic regions formed at the same time as in the reference case.

ν_2, weighting the G2 concentration	**ν_2** $(T \times sc^2)$	Final radius (mm)	Stop time (minutes)
The reference case	1.000×10^{-7}	0.9591	1780
(i)	0.850×10^{-7}	0.9784	2000
(ii)	0.900×10^{-7}	0.9716	1920
(iii)	1.100×10^{-7}	0.9557	1800
(iv)	1.150×10^{-7}	0.9489	1690

Table 3.15: Tumor evolution, altered ν_2.

From Table 3.15 and Figure 3.22, it is evident that increasing ν_2 leads to a slightly smaller final size, whereas decreasing ν_2 results in a slightly larger final size, as anticipated.

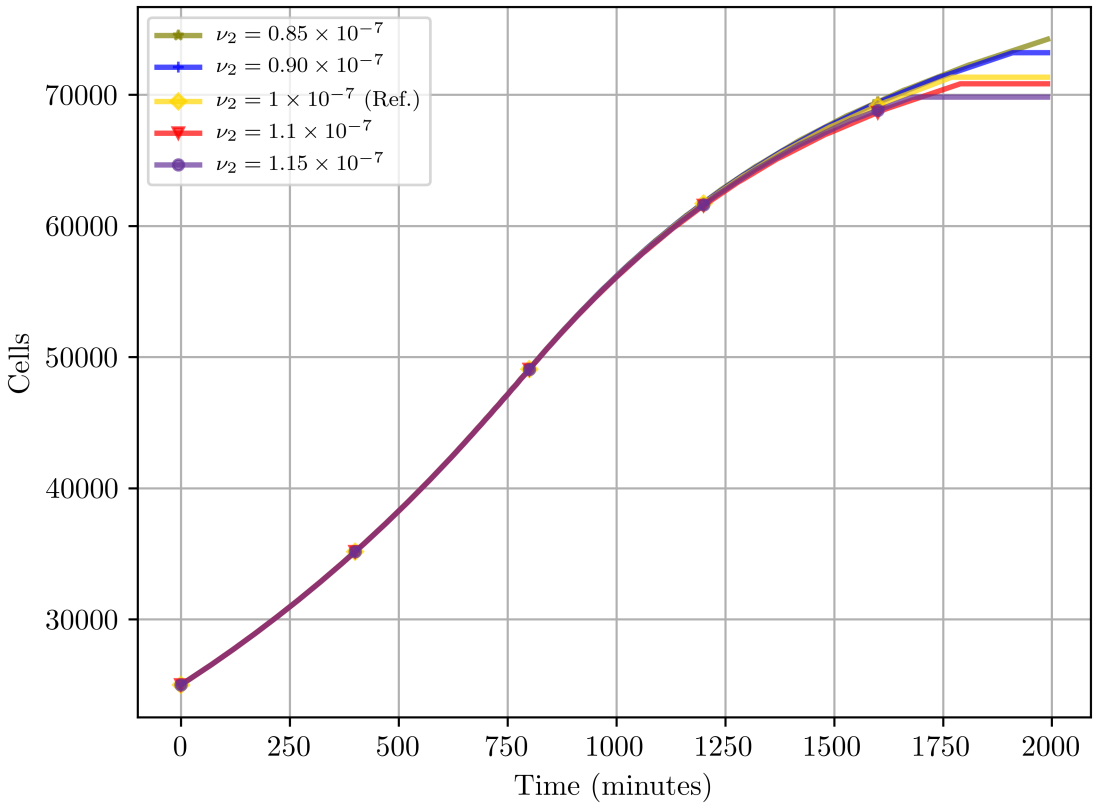

Figure 3.22: Number of cells vs time, altered ν_2.

From Figure 3.23, it is apparent that changes in ν_2 do not significantly affect the growth until after the formation of necrotic regions. However, we can observe that prior to the formation of necrotic regions, an increase in ν_2 leads to a lower production of new cells, while a decrease in ν_2 results in a higher production of new cells. This aligns with our expectations.

As the proliferating regions become smaller, the contribution of G2 in the mitotic function becomes more pronounced, as shown in Figure 3.23. The reason why the red curve representing $\nu_2 = 1.15 \times 10^{-7}$ is above the green curve representing $\nu_2 = 1.1 \times 10^{-7}$, despite $1.15 \times 10^{-7} > 1.1 \times 10^{-7}$, is because the necrotic region in sensitivity case $\nu_2 = 1.15 \times 10^{-7}$ is smaller than the necrotic region in sensitivity case $\nu_2 = 1.1 \times 10^{-7}$. Consequently, there are more proliferating regions in the $\nu_2 = 1.15 \times 10^{-7}$ case, and at a certain point, they become large enough to produce more new cells compared to the $\nu_2 = 1.1 \times 10^{-7}$ case, even though the mitotic function in the $\nu_2 = 1.15 \times 10^{-7}$ case generates fewer cells at each time step.

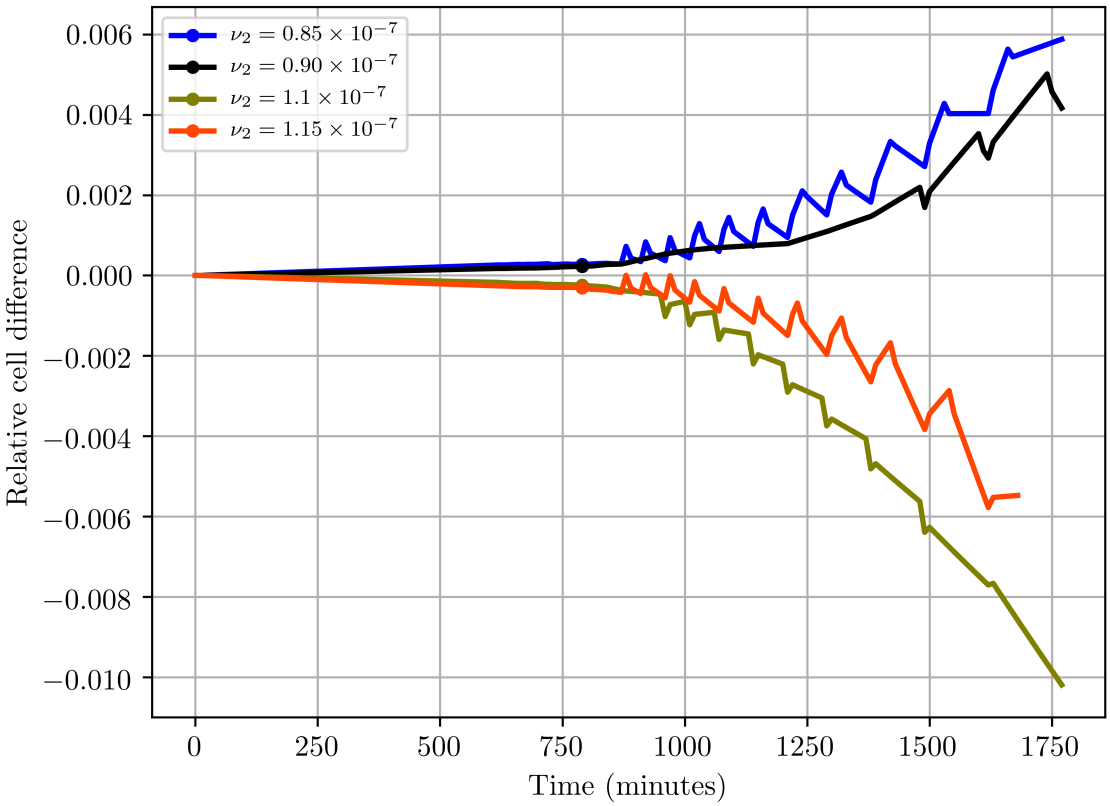

Figure 3.23: Relative difference in cells vs time, altered ν_2. The dots mark initial formation of necrotic regions. (The oscillations are due to rounding errors.)

Now that we have analyzed how modifying the parameters in the mitotic function affects tumor evolution, we can conclude that altering η had the most significant effect on growth, resulting in both the largest and smallest sizes observed. We also observed significant alterations in growth when changing ρ, whereas modifications to ν_1 and ν_2 only had minor effects on growth.

3.2.5 The extracellular matrix

The extracellular matrix comprises all the fluids and molecules present in the tumor that are not part of the cells. In this model, the proportion of the tumor occupied by the extracellular matrix remains constant. The new radius is related to the percentage of extracellular matrix, denoted as p_{extrm}, according to the following relationship:

$$r_{new} = \sqrt{\frac{1}{(1 - p_{extrm})} n_c r_c^2}. \tag{3.1}$$

Here, n_c represents the number of cells and r_c represents the radius of a single cell. Equation (3.1) illustrates that when the extracellular matrix occupies a larger percentage of the tumor, compared to the reference case, one can expect the radius to increase more at each time step relative to the reference case. This is because the fraction becomes larger. Conversely, if the percentage is decreased, the fraction becomes smaller, leading to a smaller new radius at each time step.

The ECM percentage of the tumor.	p_{extrm}	Final radius (mm)	Quiescent, GIF's	Quiescent, lack of nutrients	Necrotic	Stop time (minutes)
The reference case	0.0500	0.9591	780	630	790	1780
(i)	0.0400	1.0792	780	630	790	2850
(ii)	0.0450	0.9700	780	630	790	1940
(iii)	0.0550	0.9409	780	630	790	1610
(iv)	0.0600	0.9052	800	620	780	1350

Table 3.16: Tumor evolution, altered p_{extrm}.

From Table 3.16 and Figure 3.24, it is evident that increasing the percentage of extracellular matrix leads to a shorter growth period and smaller tumor size. Conversely, decreasing the percentage results in a longer growth period and larger tumor size. This can be attributed to the presence of quiescent and necrotic regions in more rapidly growing tumors (due to p_{extrm} having increased) which are larger and cover a greater portion of the tumor. As a result, these regions can effectively limit the growth and contribute to the smaller final size. In contrast, slower-growing tumors (due to p_{extrm} having decreased) have smaller and slower-evolving quiescent and necrotic regions, allowing them to grow for a longer period and attain a larger size.

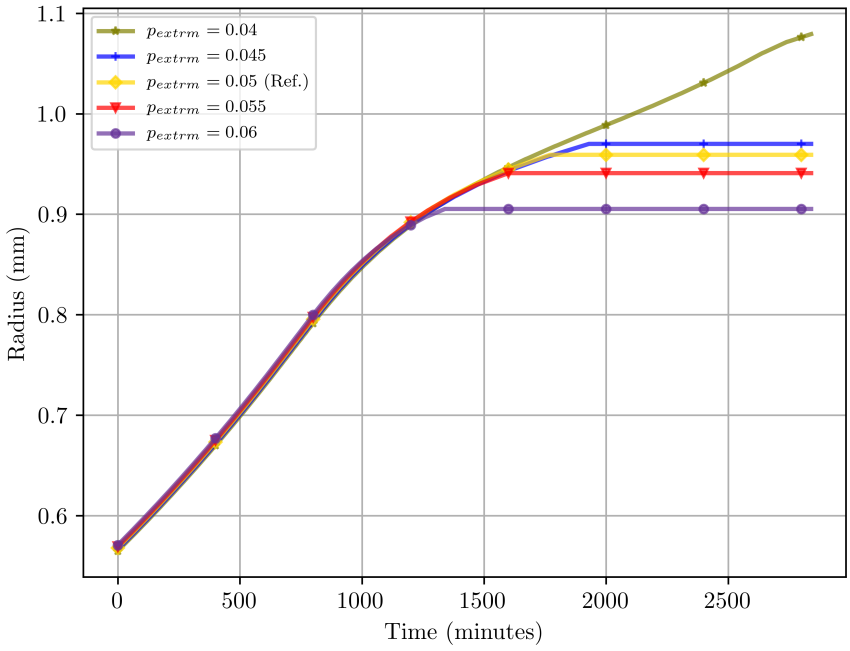

Figure 3.24: Radius vs time, altered p_{extrm}.

In the figure below, Figure 3.25, we can observe that larger percentages of extracellular matrix correspond to larger radii when the tumor is in the fully proliferating phase. Conversely,

smaller percentages of extracellular matrix result in smaller radii, as expected. It is evident that once quiescent and necrotic regions form, the growth patterns undergo a noticeable change. As mentioned earlier, a higher extracellular matrix percentage leads to larger quiescent and necrotic regions, consequently resulting in smaller increase in new radii after these regions have formed. This leads to a smaller difference between these radii and the reference radii after those regions have formed, as can be seen in Figure 3.25. On the other hand, for lower extracellular matrix percentages, the quiescent and necrotic regions are relatively small, causing the increase in new radii to remain somewhat similar after their formation. As a result, the difference in radii becomes less pronounced when comparing the radii of the sensitivity cases (i) and (ii) to the reference case radius. This is because smaller increases in radii are observed in the reference case following the formation of necrotic and quiescent regions. This trend is illustrated in Figure 3.25 by the graphs of $p_{extrm} = 0.04$ and $p_{extrm} = 0.045$ increasing.

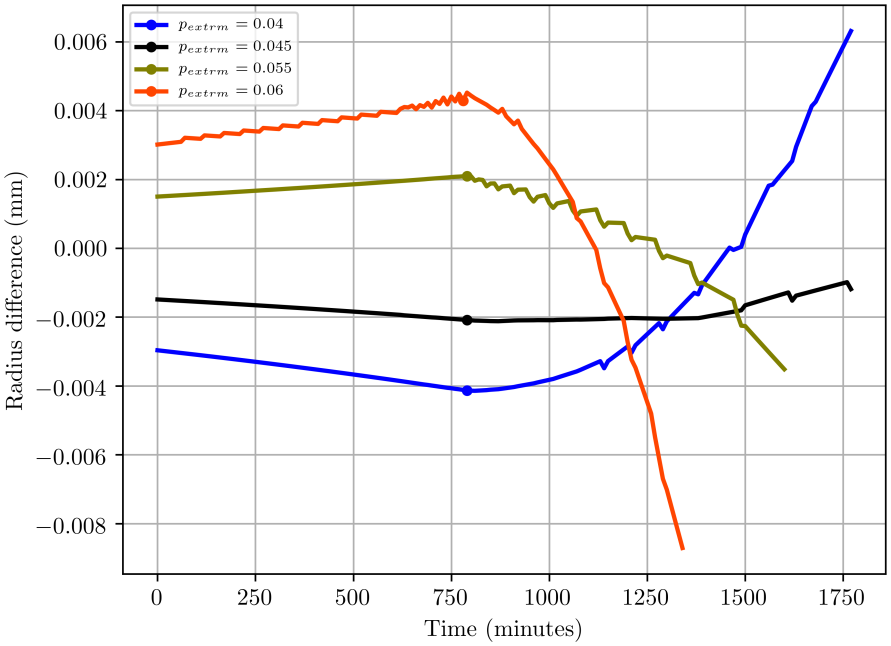

Figure 3.25: Difference in radius relative to the reference solution vs time, altered p_{extrm}. The dots mark initial formation of necrotic regions.

Chapter 4

Discussion & Conclusions

In this thesis, we have developed a mathematical model for avascular tumor growth. Additionally, we implemented the model and observed that it aligns with the established patterns of tumor evolution. Furthermore, we conducted an analysis to examine the impact of different model parameters on avascular tumor growth.

We observed that modifying the nutrient diffusion coefficient, D_N, and the diffusion coefficient associated with the internally produced/excreted growth-inhibiting factors, D_{G1}, had a substantial influence on tumor growth. Thus, it is crucial for these parameters to be accurately set in terms of their magnitude. Specifically, increasing D_N resulted in extended growth periods and larger final tumor sizes. Conversely, decreasing D_N led to a reduction in both the growth period and final tumor size. Since nutrients serve as growth-promoting factors and diffusion affects their distribution within the tumor, higher diffusion leads to more even distribution of nutrients throughout the tumor, while lower diffusion results in poor nutrient distribution, these growth trends are reasonable. On the other hand, increasing D_{G1} caused a decrease in the final tumor radius and growth period, while decreasing D_{G1} led to an increase in both the growth duration and final tumor size. Considering that $G1$ represents growth-inhibiting factors, these growth patterns align with what one would expect.

On the other hand, altering the diffusion coefficient of the externally supplied growth factors, D_{G2}, had relatively minor effects on the evolution, yet it yielded interesting observations. When D_{G2} was increased compared to the reference case, slight increases resulted in longer growth periods and larger tumor sizes. This was due to the formation of the GIF quiescent region, which is influenced by a weighted sum of G2 and G1, occurring closer to the center. As a result, a larger portion of the tumor remained in a fully proliferating state compared to the reference case. This trend persisted until D_{G2} was significantly increased, causing the G2 distribution to be so evenly spread that the GIF quiescent region extended not only close to the center but also further away, encompassing a larger portion of the tumor. Thus the growth duration and final tumor sizes from then on experienced a decreasing trend. Conversely, when D_{G2} was decreased, the GIF quiescent regions formed either as disks or annuli closer to the boundary compared to the reference case. This was because the G2 concentration was lower in the center, resulting in the GIF threshold being reached only in proximity to the boundary. Since G1, the internally produced/excreted growth-inhibiting factors, is the main contributor to reaching θ_G, the annular regions soon transformed into disk-shaped regions. Consequently,

when D_{G2} was decreased, the GIF quiescent regions occupied a larger portion of the tumor, leading to fewer proliferating cells. As a result, the growth durations were shorter and the final tumor sizes were smaller compared to the reference case. Depending on whether the initial GIF quiescent region was annulus-shaped or disk-shaped, the decrease in tumor size and growth duration did not necessarily follow a strictly decreasing pattern.

Moreover, it was observed that modifying the rate of nutrient consumption in the proliferating regions had a significant impact on tumor development. Increasing the nutrient consumption in the proliferating regions, represented by α_{pro}, led to shorter growth durations and smaller final tumor sizes, which is reasonable given the reduced presence of growth-promoting factors. Conversely, decreasing α_{pro}, indicating an increase in growth-promoting factors, resulted in longer growth periods and larger final tumor sizes. In the sensitivity cases with decreased α_{pro}, nutrient-deprived quiescent regions did not form due to the increased availability of nutrients. Furthermore, changes in the nutrient consumption within the quiescent regions, denoted as α_{qui}, exhibited similar growth tendencies as modifying α_{pro}, albeit to a lesser extent. This is reasonable because adjustments in α_{qui} do not affect growth until quiescent regions are established. Moreover, it was observed that increasing α_{qui} had a more significant impact on the growth pattern compared to decreasing α_{qui}. This can be attributed to the fact that increasing α_{qui} creates a steeper nutrient concentration gradient between proliferating and quiescent regions, causing more nutrients to be transported away from the proliferating regions. Consequently, this leads to reduced growth and a shorter growth period.

Modifications in the consumption of G1 growth-inhibitors, denoted as γ_{proqui}, also exerted a significant influence on tumor development. Increasing the consumption of G1 resulted in larger final tumor sizes, which is reasonable considering the reduced presence of growth-inhibiting factors. The reduction in growth-inhibiting factors prolonged the period of full proliferation and facilitated greater growth at each time step. However, it was observed that the growth period did not exhibit a significant alteration compared to the reference case. This can be attributed to rapidly growing tumors also experiencing more rapidly growing quiescent regions. Conversely, decreasing γ_{proqui}, indicating an increase in growth-inhibiting factors, led to shorter growth periods and smaller final radii. In the sensitivity case with the most pronounced decrease in γ_{proqui} (case (i) in Table 3.8), the GIF quiescent region actually formed earlier than the nutrient-deprived quiescent region due to the increased presence of G1. Additionally, modifications to the production/excretion of G1, represented by λ, exhibited a significant effect on the growth pattern. Decreasing λ resulted in longer growth periods and larger final tumor sizes, as expected due to the reduced presence of growth-inhibiting factors. Conversely, increasing the production/excretion of G1 led to smaller tumor sizes and growth periods. In fact, in the sensitivity case with the greatest increase in λ (case (iv) in Table 3.9), the abundance of growth-inhibiting factors caused the entire tumor to become quiescent due to high GIF concentrations before either nutrient-deprived quiescent regions or necrotic regions formed.

On the other hand, variations in the consumption rate of G2, denoted as ξ_{proqui}, had minor effects on tumor growth. Interestingly, these alterations did not consistently lead to larger or smaller final tumor sizes. Therefore, despite the small magnitude of these changes, further investigations into the influence of these factors would be valuable. When ξ_{proqui} was increased,

slightly larger tumor sizes and growth periods were observed, which is reasonable considering the reduced presence of growth-inhibiting factors. However, when ξ_{proqui} was decreased, the tumor growth pattern did not consistently exhibit a decreasing or increasing trend. A slight decrease in ξ_{proqui} resulted in larger final tumor size and growth period compared to the reference case. This can be attributed to the slight increase in G2 levels, causing the GIF quiescent region to occur closer to the center. As a result, a slightly larger portion of the tumor remained in a fully proliferating state. Notably, a more significant decrease in ξ_{proqui} led to a slightly smaller final tumor size and a longer growth period. This was due to lower consumption of G2, resulting in higher and more evenly distributed G2 concentration within the tumor. Consequently, the initial GIF quiescent region was larger compared to the reference case, leading to slower growth at each time step. Moreover, it is worth noting that the production and excretion of G1 depend on the spatial distribution within the tumor. Consequently, when the tumor exhibits slower growth, the GIF quiescent region will also grow more gradually. As a result is it is possible for the growth period to be prolonged.

Furthermore, it was observed that alterations in the supply of nutrients and G2 growth-inhibitor factors at the boundary significantly influence tumor development. This finding suggests that drugs targeting and influencing these supplies have the potential to inhibit tumor growth and hinder the transition into the vascular phase. Specifically, increasing the nutrient supply, κ, resulted in longer growth periods and larger tumor sizes, which is logical considering the increased presence of growth-promoting factors. Conversely, decreasing κ led to shorter growth periods and smaller tumor sizes, aligning with the reduced availability of growth-promoting factors. On the contrary, augmenting the supply of G2 growth-inhibitor factors, ψ, led to shorter growth periods and smaller tumor sizes, as expected due to the increased concentration of growth-inhibiting factors. In contrast, reducing ψ resulted in larger tumor sizes and longer growth periods, reflecting the decreased availability of growth-inhibiting factors.

Through the analysis of the mitotic function, it became evident that the parameters with the most significant influence on growth were ρ, which scaled the mitotic value, and η, which determined the contribution of nutrients to growth. Increasing the parameter ρ resulted in a higher production of new cells at each time step, indicating more rapid tumor growth compared to the reference case. This increased growth was accompanied by an elevation in the production/excretion of G1. Consequently, the final tumor sizes and growth periods were smaller relative to the reference case. Conversely, decreasing ρ led to a reduction in the number of new cells produced at each time step, resulting in overall smaller growth and a shorter growth duration compared to the reference case. Similarly, when the parameter η was increased, there was an increase in the production of new cells at each time step. However, as observed with increased ρ, the rapidly growing tumor also developed a rapidly evolving quiescent region, leading to smaller overall growth periods and tumor sizes compared to the reference case. On the other hand, decreasing η resulted in a lower production of cells at each time step. This prolonged the tumor's growth period and led to a larger final tumor size. However, it is important to note that the sensitivity case where η was decreased the most (case (i) in Table 3.13) had a shorter growth period and smaller final tumor size compared to the case with a lesser decrease in η. This is due to the quiescent and necrotic regions forming around the same time in both cases. Consequently, the smallest tumor, corresponding to the

sensitivity case with the smallest η value, ceased to grow sooner, as observed.

In contrast, modifying the parameters ν_1 and ν_2, which governed the influence of growth-inhibiting factors on tumor growth, had minimal effects. Increasing these parameters led to a slight decrease in the final tumor size compared to the reference case. Conversely, decreasing ν_1 and ν_2 resulted in a slight increase in the final tumor size.

Furthermore, it was observed that the composition of the extracellular matrix, specifically the percentage it comprised within the tumor, had a significant impact on tumor development. Therefore, it is crucial to select the appropriate percentage from a biological standpoint, as it plays a vital role in tumor behavior and progression. Specifically, an increase in the percentage of ECM led to accelerated tumor growth at each time step, whereas a decrease in the percentage resulted in slower growth at each time step.

During the sensitivity analysis, it was observed that alterations in parameters related to nutrient concentration and G1 concentration had the most significant influence on tumor development. Therefore, it is crucial to set these parameters to biologically accurate magnitudes to ensure that the simulated tumor development and patterns are qualitatively correct. The strong dependency on these parameters also suggests that drugs targeting and influencing these factors have the potential to inhibit tumor growth. Thus, there is a need to develop models that incorporate the influence of these factors to a greater extent, as it would be of great interest.

Furthermore, the sensitivity analysis revealed that GIF quiescent regions can appear at different locations within a tumor, resulting from the interaction of externally supplied and internally produced/excreted growth-inhibitor factors. This variability in quiescent region locations lead to different growth patterns in tumors. Therefore, there is a need to develop models that extensively investigate the effect of both internally and externally supplied growth-inhibiting factors on tumor growth patterns. Such models have the potential to provide a more comprehensive understanding of tumor growth and generate novel insights into treatments and experimental strategies.

Additionally, the sensitivity analysis revealed that the proportion of extracellular matrix (ECM) within a tumor directly impacts its growth dynamics. This highlights the significance of considering ECM composition in models for avascular tumor growth to accurately understand and predict tumor behavior. Therefore, models should more extensively include the extracellular matrix and its composition within tumors.

These findings highlight the potential benefits of developing more detailed models that comprehensively analyze the influence of these parameters. Such models have the potential to contribute to the development of experimental approaches and significantly enhance our understanding of tumor evolution.

Chapter 5

Extension model

In this chapter, we will introduce an extension model that builds upon the framework developed and analyzed in the thesis. The key modifications include the incorporation of additional equations to account for the densities of different cell types. Furthermore, the growth of the tumor will be influenced by the rates of change of these cell densities.

The following assumptions and comments are made with respect to the extension model.

- It is assumed that a tumor consists of three components. Those are, living cells (denoting both proliferating and quiescent cells), necrotic cells and the extracellular matrix, abbreviated ECM.

- Advection-diffusion type PDEs will be used to model the concentration of growth factors. The model will incorporate three growth factors. Firstly, we will consider externally supplied nutrients as growth-promoting factors. Secondly, we will account for growth-inhibitor factors that are produced by cells within the tumor during the cell cycle or excreted by necrotic cells. Lastly, we will include externally supplied growth-inhibitor factors that represent the immune system's response to the tumor.

  - An advection-diffusion equation will be formulated to represent the nutrient concentration within the tumor. The equation will not include a source term since we assume that nutrients are only externally supplied and not produced within the tumor. However, it will include a sink term to account for the consumption of nutrients by the cells. Furthermore, we will assume that the nutrient level in the surrounding area of the tumor remains fixed, indicating a constant supply of nutrients. This condition will be expressed by a positive Dirichlet boundary data.
  - A diffusion equation will be formulated to represent the growth-inhibitor factors, $G1$, produced or excreted internally by the cells. The PDE is in accordance with the one presented in [2]. The equation incorporates both source and sink terms, representing the production/excretion and consumption of $G1$ within the tumor, respectively. Moreover, we assume that these GIFs do not exist outside the tumor, which is reasonable considering they are a product of the cells specific to the tumor. Hence, we assume no transport of $G1$ across the tumor boundary. This condition will be represented by a homogeneous Neumann boundary condition.

  - We will represent the growth-inhibitor factors, $G2$, produced by the immune system in the surrounding tissue using an advection-diffusion equation. Since $G2$ is not produced within the tumor, the equation will not contain a production term. However, it will include a sink term to account for the cells consumption of $G2$. Additionally, we will assume that the concentration of $G2$ in the tissue surrounding the tumor remains constant. Therefore, the boundary supply of $G2$ will be represented by a positive Dirichlet boundary condition.

- There will be introduced a GIF threshold, denoted by θ_G, and a nutrient threshold, denoted by θ_N, which will be used to categorize the cells as proliferating, quiescent or necrotic. If the growth-inhibiting concentrations exceeds θ_G, mitosis will be inhibited and lead to cell quiescence or death, depending on the current nutrient level. Moreover, θ_N represent the minimum nutrient concentration required for cell growth. In order for a cell to have the potential to proliferate, the nutrient concentration must surpass θ_N. If the nutrient concentration falls below this threshold, the cell will become quiescent or die. Moreover, if a cell has died, it will remain dead.

- We will introduce a function to represent the mitotic rate, which denotes the rate at which a cell divides into two daughter cells.

- To model the cell densities, we will utilize diffusion-type PDEs. The model includes three distinct cell densities: the density of proliferating cells, the density of quiescent cells, and the density of necrotic cells.

  - We will formulate a diffusion equation to describe the density of proliferating cells within the tumor. This equation will include a sink term that accounts for proliferating cells transitioning into a quiescent state. Additionally, there will be two source terms, one representing the increase of proliferating cells resulting from mitosis and another representing the transition of quiescent cells back to a proliferating state.
  - The density of quiescent cells is also modeled using a diffusion PDE. The equation incorporates two sink terms, representing the decrease in quiescent cells due to their transition to a necrotic state and their transition back to a proliferating state. Additionally, there is a source term accounting for the increase in quiescent cells resulting from proliferating cells transitioning to a quiescent state.
  - We will employ a PDE to model the density of necrotic cells. Unlike the previous cell density equations, this equation does not include a sink term, as all dead cells remain in a necrotic state. Moreover, the PDE does not include a diffusion term as the cells are dead and do not exhibit molecular movements. However, it does incorporate a source term to represent the death of quiescent cells.

- In the model, we make the assumption that only living cells actively consume nutrients and growth-inhibiting factors. Necrotic cells, on the other hand, do not consume any substances but solely excrete growth-inhibiting factors.

- In the model, we neglect adhesion forces between cells, as well as between cells and the extracellular matrix (ECM). Furthermore, we disregard any constraints imposed by the surrounding geometry.

We denote the concentrations of nutrients, G1 growth-inhibiting factors, and G2 growth-inhibiting factors as u_N, u_{G1}, and u_{G2}, respectively. Additionally, we use the variables P to represent the density of proliferating cells, Q to represent the density of quiescent cells, and D to represent the density of necrotic/dead cells. The model consist of the following equations.

$$\frac{\partial u_N}{\partial t} + \nabla \cdot (-D_N \nabla u_N + \vec{c}_N u_N) = -r_N(u_N, u_{G1}, u_{G2}, P, Q) \quad \forall \vec{x} \in \Omega \tag{5.1}$$

$$u_N = \kappa \quad \forall \vec{x} \in \partial\Omega.$$

Equation (5.1) describes the temporal changes in nutrient concentration as influenced by diffusive and advective forces, as well as the consumption of nutrients by proliferating and quiescent cells. The consumption term r_N depends not only on u_N, P, and Q, but also on the concentrations of growth-inhibiting factors. This dependency arises because higher concentrations of growth-inhibiting factors lead to reduced proliferation and cell viability, resulting in a decreased demand for nutrients.

$$\frac{\partial u_{G1}}{\partial t} + \nabla \cdot (-D_{G1} \nabla u_{G1}) = -r_{G1}(u_N, u_{G1}, u_{G2}, P, Q) + S_{G1}(u_N, u_{G1}, u_{G2}, P, Q, D) \quad \forall \vec{x} \in \Omega. \tag{5.2}$$

$$\vec{\nu} \cdot (-D_{G1} \nabla u_{G1}) = 0 \quad \forall \vec{x} \in \partial\Omega.$$

Here ν denotes the outward pointing unit normal vector at the boundary. Equation (5.2) describes the changes in G1 concentration resulting from diffusive forces, as well as the production/excretion and consumption of G1. The sink term r_{G1} represents the consumption of G1 by both quiescent and proliferating cells. On the other hand, the source term S_{G1} accounts for the increase in G1 due to its production by both proliferating and quiescent cells, as well as the excretion of G1 by necrotic cells. It is important to note that both r_{G1} and S_{G1} depend on all three growth factors, as these factors influence the state of a cell and determine how much G1 it can consume and produce/excrete.

$$\frac{\partial u_{G2}}{\partial t} + \nabla \cdot (-D_{G2} \nabla u_{G2} + \vec{c}_{G2} u_{G2}) = -r_{G2}(u_N, u_{G1}, u_{G2}, P, Q) \quad \forall \vec{x} \in \Omega \tag{5.3}$$

$$u_{G2} = \psi \quad \forall \vec{x} \in \partial\Omega.$$

Equation (5.3) describes the changes in G2 concentration resulting from diffusive and advective forces, as well as the consumption of G2 by the living cells. The sink term, r_{G2}, represents the consumption of G2 by both proliferating and quiescent cells. Notably, it becomes apparent that the consumption rate depends on the current levels of all three growth factors.

The mitotic rate, the rate at which proliferating cells divide into two identical daughter cells, is denoted by $m(u_N, u_{G1}, u_{G2})$ and depends on the concentrations of growth factors.

$$\frac{\partial P}{\partial t} + \nabla \cdot (-D_P \nabla P) = -r_{P,Q}(u_N, u_{G1}, u_{G2}, P) + S_{P,m}(m, P) + S_{P,Q}(u_N, u_{G1}, u_{G2}, Q). \tag{5.4}$$

Equation (5.4) models the density of proliferating cells. It describes the changes in density resulting from diffusion forces, as well as factors that decrease or increase the number of proliferating cells. The sink term $r_{P,Q}$ represents the decrease in density due to proliferating

cells transitioning to a quiescent state. On the other hand, the source term $S_{P,Q}$ represents the increase in density resulting from quiescent cells transitioning back to a proliferating state. Additionally, the term $S_{P,m}$ denotes the increase in proliferating cells due to mitosis. Importantly, it should be noted that all the sink and source terms depend on the current concentrations of growth factors. Moreover, note that $S_{P,Q}$ depends on Q.

$$\frac{\partial Q}{\partial t} + \nabla \cdot (-D_Q \nabla Q) = r_{P,Q}(u_N, u_{G1}, u_{G2}, P) - S_{P,Q}(u_N, u_{G1}, u_{G2}, Q) - r_{Q,D}(u_N, u_{G1}, u_{G2}, Q). \tag{5.5}$$

Equation (5.5) models the density of quiescent cells. It describes the changes in density over time resulting from diffusive forces and factors that increase or decrease the amount of quiescent cells. As mentioned, the term $r_{P,Q}$ represents proliferating cells transitioning to a quiescent state, which contributes as a source term in this equation while serving as a sink term in equation (5.4). Conversely, the term $S_{P,Q}$, which represents quiescent cells transitioning back to a proliferating state, acts as a sink term in equation (5.5) while being a source term in equation (5.4). Additionally, the term $r_{Q,D}$ represents quiescent cells dying and becoming necrotic, contributing as a sink term. Furthermore, it is important to note that equation (5.5) depends on the density of proliferating cells, P, and the concentrations of all three growth factors.

$$\frac{\partial D}{\partial t} = r_{Q,D}(u_N, u_{G1}, u_{G2}, Q). \tag{5.6}$$

Equation (5.6) represents the density of necrotic cells. Since necrotic cells are dead, they do not exhibit molecular movements. Therefore, there is no diffusive term in this equation. Additionally, necrotic cells cannot transition to a quiescent or proliferating state, so there are no sink terms. However, the term $r_{Q,D}$, which represents quiescent cells transitioning to a necrotic state, is included as a source term in equation (5.6). This term accounts for the only way in which cells can become necrotic. Furthermore, note that equation (5.6) depends on the quiescent cell density, Q, and all three growth factors.

$$\frac{dV}{dt} = C \int_\Omega S_{P,m} + S_{P,Q} - r_{P,Q} - r_{Q,D}\, dx. \tag{5.7}$$

Equation (5.7) describes the change in tumor volume, where V represents the volume of the tumor. The evolution of the tumor volume is dependent on the rate of change of the cell densities, which are influenced by the increase and decrease of specific cell types. Additionally, there is a constant C, which depends on the extracellular matrix.

Upon examining the equations in the extension model, it becomes evident that they are coupled, meaning that they depend on each other. As a result, employing splitting schemes becomes necessary in order to solve the model. Two main types of splitting schemes commonly used are fully-implicit and iterative coupling [40, 41].

Fully-implicit methods involve simultaneously solving the complete system of coupled equations. These methods possess the advantage of being unconditionally stable. However, a drawback is that they are computationally expensive. On the other hand, the iterative coupling approach divides the coupled problem into sub-problems and solves them independently, utilizing only the most recent solution information from the other sub-problems. At each time

step, the sub-problems are iteratively solved, utilizing the newly computed solutions until convergence is achieved within a specified tolerance [40, 41]. By utilizing iterative methods, it is possible to employ different discretizations for the sub-problems, which proves valuable as they often represent distinct physical phenomena such as flow and mechanics [40, 41, 42]. Furthermore, if the iterative method employs the same spatial discretization as the fully-implicit method on all the sub-problems, the iterative and fully-implicit solutions should be identical at each time step once the iterative method has converged [40, 41].

Furthermore, since the concentrations of the growth factors and the cell densities likely operate on different time scales, it would be sensible to utilize multirate iterative schemes [43, 44]. Additionally, when dealing with nonlinear coupled terms, a linearization method such as the L-scheme [45, 46, 47] or the Newton method must be applied alongside a splitting scheme.

Refer to Appendix A for a straightforward coupled problem of tumor growth, which is solved using an iterative splitting scheme. The convergence rates are also presented in the appendix.

Appendix A

A straightforward coupled tumor growth problem

An iterative splitting scheme has been applied to solve a set of fully coupled equations on a dynamically evolving domain. Although the problem being addressed is simpler than the extension model presented in the thesis, it encompasses all the crucial relationships. Specifically, the problem involves a circular domain that expands at each time step, along with two fully coupled partial differential equations. These PDEs are solved using iterative coupling, implicit Euler, and finite element method at each time step.

The general PDEs used are

$$\frac{\partial u_1}{\partial t} + \nabla \cdot (-D_1 \nabla u_1 + \vec{c}_1 u_1) = F_1(u_2) \quad \forall\, \mathbf{x} \in \Omega \tag{A.1}$$

$$\frac{\partial u_2}{\partial t} + \nabla \cdot (-D_2 \nabla u_2 + \vec{c}_2 u_2) = F_2(u_1) \quad \forall\, \mathbf{x} \in \Omega \tag{A.2}$$

where all coupling terms are included in the function on the right-hand side.

In order to assess the convergence of the approximate solutions, the exact solutions for both u_1 and u_2 were selected as $u_{\text{exact}} = (1 + x^2 + 2y^2)t$. The right-hand sides of the equations were defined as $F_1 = f_1 - u_2$ and $F_2 = f_2 - u_1$, where f_1 and f_2 do not represent coupling terms. These right-hand sides were determined by substituting the exact solution into the respective PDEs and defining them as the resulting expressions. Specifically, $f_1 = (1+x^2+2y^2)(1+t)-6tD_1+2xtc_{11}+4ytc_{12}$ and $f_2 = (1+x^2+2y^2)(1+t)-6tD_2+2xtc_{21}+4ytc_{22}$. Where $D_1 = 1$, $D_2 = 2$, $\vec{c}_1 = [-1, 1]$ and $\vec{c}_2 = [2, 3]$.

For the boundary conditions, Dirichlet boundary conditions were chosen, where the boundary values are set to equal the exact solution on the boundary. In other words, the boundary conditions are specified in a way that matches the exact solution. As for the initial solutions, they were set to equal the exact solution at the initial time. Hence,

$$u_1 = u_2 = (1 + x^2 + 2y^2)t \ on\ \partial\Omega,$$

$$u_1 = u_2 = 0 \ at\ t = 0$$

The growth relation for the problem was defined as $r_{\text{new}} = r_{\text{initial}} + 0.5t$, where $r_{\text{initial}} = 1$ is the initial radius and t is the time. The circular domain was computed using the formula $A_{\text{circle}} = \pi r_{\text{new}}^2$, where r_{new} represents the updated radius at each time step. The calculations were performed using P_1-elements, which correspond to piece-wise linear functions on triangular elements. As a result, we can anticipate that the solutions will converge with second-order accuracy in terms of the L_2-norm.

To solve the problem, an iterative splitting scheme was employed using implicit Euler in time and finite element in space. At each time step, the following procedure was followed:

1. Make an initial guess for u_2.
2. Solve the PDE for u_1 using the previous solution of u_2.
3. Solve the PDE for u_2 using the newly computed solution of u_1.
4. Recalculate u_1 using the updated solution of u_2.
5. Repeat steps 2-4 until the sum of the L_2-norms of the differences between the current and previous solutions of both u_1 and u_2 is less than or equal to the tolerance of 10^{-6}. I.e., $(\|u_1 - u_{1,\text{previous}}\|_{L_2} + \|u_2 - u_{2,\text{previous}}\|_{L_2}) \leq 10^{-6}$.

This iterative process continues until the solutions converges within the specified tolerance, ensuring the accuracy of the numerical solutions for u_1 and u_2 at each time step.

Table A.1 shows the L_2-errors of the final solutions obtained. It can be observed that when the number of elements is doubled, the error decreases by a factor of approximately four for both approximate solutions. This indicates that the approximate solutions exhibit second-order convergence.

Number of elements	$\|u_{exact} - u_1\|_{L_2}$	$\|u_{exact} - u_2\|_{L_2}$
16	0.062696	0.042758
32	0.016089	0.010955
64	0.003973	0.002693
128	0.000989	0.000671

Table A.1: Convergence rates.

Bibliography

[1] International Agency for Research on Cancer Cancer Tomorrow. Estimated number of new cases from 2020 to 2040 [table]. `https://gco.iarc.fr/tomorrow/en/dataviz/tables?types=0`. Accessed on 07/10/2022.

[2] M.A.J. Chaplain. Avascular growth, angiogenesis and vascular growth in solid tumours: The mathematical modelling of the stages of tumour development. *Mathematical and Computer Modelling*, 23(6):47 – 87, 1996.

[3] National Cancer Institute. `https://www.cancer.gov/publications/dictionaries/cancer-terms/def/angiogenesis`. Accessed on 14/05/2023.

[4] T. Roose, S.J. Chapman, and P.K. Maini. Mathematical models of avascular tumor growth. *SIAM Review*, 49(2):179–208, 2007.

[5] A.C. Burton. Rate of growth of solid tumours as a problem of diffusion. *Growth*, 30(2):157–176, 1966.

[6] A. Taghibakhshi, M. Barisam, M.S. Saidi, N. Kashaninejad, and N.T. Nguyen. Three-dimensional modeling of avascular tumor growth in both static and dynamic culture platforms. *Micromachines*, 10(9):580–597, 2019.

[7] H.P. Greenspan. Models for the growth of a solid tumor by diffusion. *Studies in Applied Mathematics*, 51(4):317–340, 1972.

[8] H.M. Byrne and M.A.J. Chaplain. Free boundary value problems associated with the growth and development of multicellular spheroids. *European Journal of Applied Mathematics*, 8(6):639–658, 1997.

[9] S. Cui and A. Friedman. A free boundary problem for a singular system of differential equations: An application to a model of tumor growth. *Transactions of the American Mathematical Society*, 355(9):3537–3590, 2003.

[10] G.J. Pettet, C.P. Please, M.J. Tindall, and D.L.S. McElwain. The migration of cells in multicell tumor spheroids. *Bulletin of mathematical biology*, 63(2):231–257, 2001.

[11] J.P. Ward and J.R. King. Mathematical modelling of avascular-tumour growth. *Mathematical Medicine and Biology: A Journal of the IMA*, 14(1):39–69, 1997.

[12] J.P. Ward and J.R. King. Mathematical modelling of drug transport in tumour multicell spheroids and monolayer cultures. *Mathematical biosciences*, 181(2):177–207, 2003.

[13] J.A. Sherratt. Traveling wave solutions of a mathematical model for tumor encapsulation. *SIAM Journal on Applied Mathematics*, 60(2):392–407, 2000.

[14] J.A. Sherratt. Cellular growth control and travelling waves of cancer. *SIAM Journal on Applied Mathematics*, 53(6):1713–1730, 1993.

[15] J.A. Sherratt and M.A.J. Chaplain. A new mathematical model for avascular tumour growth. *Journal of mathematical biology*, 43(4):291–312, 2001.

[16] S. Tohya, A. Mochizuki, S. Imayama, and Y. Iwasa. On rugged shape of skin tumor (basal cell carcinoma). *Journal of theoretical biology*, 194(1):65–78, 1998.

[17] M.A.J. Chaplain, M. Ganesh, and I.G. Graham. Spatio-temporal pattern formation on spherical surfaces: numerical simulation and application to solid tumour growth. *Journal of mathematical biology*, 42:387–423, 2001.

[18] B.P. Marchant, J. Norbury, and J.A. Sherratt. Travelling wave solutions to a haptotaxis-dominated model of malignant invasion. *Nonlinearity*, 14(6):1653, 2001.

[19] J.A. Adam and S.A. Maggelakis. Mathematical models of tumor growth. iv. effects of a necrotic core. *Mathematical Biosciences*, 97(1):121–136, 1989.

[20] T.N. Hartmann. Editorial: Metabolism and cell adhesion in cancer. *Frontiers in Cell and Developmental Biology*, 10, 2022.

[21] C.J.W. Breward, H.M. Byrne, and C.E. Lewis. The role of cell-cell interactions in a two-phase model of avascular tumour growth. *Journal of Mathematical Biology*, 45:125–152, 2002.

[22] C.P. Please and G.J. Pettet. Avascular tumour dynamics and necrosis. *Mathematical Models and Methods in Applied Sciences*, 9(4):569–579, 1999.

[23] A. Logg, K.A. Mardal, and G.N. Wells. *Automated Solution of Differential Equations by the Finite Element Method. The FEniCS Book*. Springer, Heidelberg, 2012.

[24] National Cancer Institute. National cancer institute - dictionary. `https://www.cancer.gov/publications/dictionaries/cancer-terms`. Accessed on 12/09/2022.

[25] National Cancer Institute. What is cancer? `https://www.cancer.gov/about-cancer/understanding/what-is-cancer`. Accessed on 07/10/2022.

[26] J.A. Adam. A simplified mathematical model of tumor growth. *Mathematical Biosciences*, 81(2):229–244, 1986.

[27] L. Glass. Instability and mitotic patterns in tissue growth. *Journal of Dynamic Systems, Measurements, and Control*, 95(3):324–327, 1973.

[28] R.M. Shymko and L. Glass. Cellular and geometric control of tissue growth and mitotic instability. *Journal of Theoretical Biology*, 63(2):355–374, 1976.

[29] A. Fasano, A. Bertuzzi, and A. Gandolfi. *Complex Systems in Biomedicine*, chapter 3. Springer, 2006.

[30] K. Atkinson. numerical analysis. `https://www.britannica.com/science/numerical-analysis#ref235493`. Accessed on 02/11/2022.

[31] T. Sauer. *Numerical Analysis*. Pearson, Harlow, 2014.

[32] R. LeVeque. *Numerical Methods for Conservation Laws*. Birkhäuser, Berlin, 1990.

[33] S. Brenner and L. Scott. *The Mathematical Theory of Finite Element Methods*. Springer, New York, 2008.

[34] W. Cheney. *Analysis for Applied Mathematics*. Springer, New York, 2001.

[35] W. Rudin. *Principles of Mathematical Analysis*. McGraw-Hill Education, Singapore, 1976.

[36] D.H. Griffel. *Applied Functional Analysis*. Ellis Horwood Limited, Chichester, 1988.

[37] L.C. Evans. *Partial Differential Equations*. American Mathematical Society, United States of America, 2010.

[38] P. Knabner and L. Angermann. *Numerical Methods for Elliptic and Parabolic Partial Differential Equations*. Springer, New York, 2003.

[39] Komen. `https://www.komen.org/breast-cancer/diagnosis/stages-staging/tumor-size/`. Accessed on 01/05/2023.

[40] J.W. Both, M. Borregales, J.M. Nordbotten, K. Kumar, and F.A. Radu. Robust fixed stress splitting for Biot's equations in heterogeneous media. *Applied Mathematics Letters*, 68:101–108, 2017.

[41] J. Kim, H.A. Tchelepi, and R. Juanes. Stability, accuracy, and efficiency of sequential methods for coupled flow and geomechanics. *SPE Journal*, 16(2):249–262, 2011.

[42] E. Storvik, J.W. Both, K. Kundan, J.M Nordbotten, and F.A. Radu. On the optimization of the fixed-stress splitting for Biot's equations. *International Journal for Numerical Methods in Engineering*, 120(2):179–194, 2019.

[43] T. Almani, K. Kumar, A. Dogru, G. Singh, and M.F. Wheeler. Convergence analysis of multirate fixed-stress split iterative schemes for coupling flow with geomechanics. *Computer Methods in Applied Mechanics and Engineering*, 311:180–207, 2016.

[44] T. Almani, K. Kumar, G. Singh, and M.F. Wheeler. Stability of multirate explicit coupling of geomechanics with flow in poroelastic medium. *Computers & Mathematics with Applications*, 78(8):2682–2699, 2019.

[45] F. List and F.A. Radu. A study on iterative methods for solving Richards' equation. *Computational Geosciences*, 20:341–353, 2016.

[46] M. Borregales, F.A. Radu, K. Kundan, and J.M. Nordbotten. Robust iterative schemes for non-linear poromechanics. *Computational Geosciences*, 22:1021–1038, 2018.

[47] M.A.B. Reverón, K. Kundan, J.M. Nordbotten, and F.A. Radu. Iterative solvers for Biot model under small and large deformations. *Computational Geosciences*, 25:687–699, 2021.